PFC/RR-93-03

The Development of an Omegatron Plasma Ion Mass Spectrometer for Alcator C-Mod

Edward E. Thomas, Jr.

May, 1993

Plasma Fusion Center
Massachusetts Institute of Technology
Cambridge, MA 02139

This work is supported by the U.S. Department of Energy
Contract No. DE-AC02-78ET51013

THE DEVELOPMENT OF AN OMEGATRON PLASMA ION MASS SPECTROMETER FOR ALCATOR C-MOD

by

Edward E. Thomas, Jr.
B.S. Physics, Florida Institute of Technology
(1989)

Submitted to the Department of Physics
in Partial Fulfillment of the Requirements
for the Degree of

Master of Science

at the
Massachusetts Institute of Technology
May, 1993

Signature of Author _____
Department of Physics, 7 May 1993

Certified by _____
Dr. Earl Marmar, Thesis Advisor

Certified by _____
Dr. Brian LaBombard, Thesis co-Advisor

Certified by _____
Professor Boleslaw Wyslouch, Thesis Reader

Accepted by _____
Professor George Koster, Graduate Officer,
Department of Physics

The Development of An Omegatron Plasma Ion Mass Spectrometer for Alcator C-Mod

by

Edward E. Thomas, Jr.

Submitted to the Department of Physics on 7 May 1993 in partial fulfillment of the requirements for the Degree of Master of Science in Physics.

ABSTRACT

A new diagnostic device, the Omegatron Probe, has been developed to investigate relative impurity levels and impurity charge state distribution in the Alcator C-Mod Tokamak edge plasma. The Omegatron probe consists of two principal components, a "front-end" of independently biased grids, arranged in a gridded energy analyzer fashion and a large collection cavity. Particles enter the probe in a thin "ribbon" through a knife-edge slit. The grids provide a means to measure and control the parallel energy distribution of the ions. In the collection cavity, an oscillating electric field is applied perpendicularly to the ambient magnetic field. Ions whose cyclotron frequencies are resonant with this electric field oscillation will gain perpendicular energy and be collected. In this way, the probe can be operated in two modes: first, by fixing the potentials on the grids and sweeping frequencies to obtain a " Z/m spectrum" of ion species and second, by fixing the frequency and sweeping the grid potentials to obtain the distribution function of an individual impurity species.

The Omegatron probe performed successfully in tests on a Hollow Cathode Discharge (HCD) linear plasma column. It obtained measurements of $T_e \approx 5$ eV, $T_i (H^+) \approx 2.0 \pm 0.2$ eV, $n_0 \approx 9 \times 10^{15}$ m^{-3}, RMS potential fluctuation levels of $\sim 0.5 \pm 0.05\ T_e$, and obtained "Z/m" spectra for the plasma ions (H^+, H_2^+, He^+). Additional experiments confirmed the theoretical scalings of the $f/\Delta f$ resolution with the applied electric field and magnetic field strengths. The instrument yielded an absolute level of resolution, $f/\Delta f$, of appoximately 2.5 to 3 times the theoretical values. Finally, the results from the HCD are used to project operation on Alcator C-Mod.

Thesis Advisor: Dr. Earl Marmar
Title: Senior Research Scientist, M.I.T. Department of Physics

Thesis co-Advisor: Dr. Brian LaBombard
Title: Research Scientist, M.I.T. Plasma Fusion Center

Acknowledgements

There are many people that have given me support while working on this project. To all of them I extend my most heartfelt gratitude.

First of all, I have to thank Dave Gilbert, of DCM Machining, whose company did an excellent job making the Omegatron probe components. My gratitude is also extended to the Nuclear Engineering department and specifically to Professors Jeffrey Freidberg and Kevin Wenzel and to Thomas Hsu, for assistance and advice in operating the Hollow Cathode Discharge. The HCD proved an excellent platform for testing the Omegatron's capabilities.

Steve Kochan, of the Alcator engineering staff, gave me excellent advice and taught me an enormous amount about art of hardware design. Bob Childs and Tom Toland, of the Alcator vacuum shop, showed me the importance of assembling and maintaining a clean vacuum system.

Members of the Alcator physics staff gave me advice at each stage of the Omegatron's development. Yuichi Takase and Steve Golovato provided me a great deal of information for the development of the Omegatron's RF system. Bruce Lipschultz gave me useful information on edge plasma physics and on probe theory during the early stages of the Omegatron's development. Earl Marmar, my thesis advisor, gave me useful advice in analyzing the Omegatron data.

The member of the Alcator physics staff with whom I worked the closest was Brian LaBombard. Brian and Bruce were the first to introduce me to the Omegatron probe concept. From Brian, I have learned a great deal about the field of plasma physics and the peculiarities of the tokamak edge plasma. He also taught me the importance of being a careful and complete researcher. Much of the work presented in this thesis is the result of literally hundreds of hours of conversations between Brian and I.

Finally, I thank my parents and most especially my fiancée Wendy for their love and support. They have stood by me through this entire period (especially while writing my thesis) and have always been there when I need them. I dedicate this thesis to them.

OUTLINE

List of Figures

List of Tables

Chapter I: Introduction

This thesis describes the development and testing of a new type of diagnostic device for fusion experiments, the Omegatron Plasma Ion Mass Spectrometer or, simply, Omegatron Probe. This probe is designed to measure the temperature, charge state distribution, and relative levels of impurity ions in a tokamak edge plasma environment. In this chapter, the motivation for developing such a probe will be presented.

I.1 Tokamaks and Edge Plasma Physics

In recent years, the tokamak device has become the principal design used in the development of a practical, controlled fusion machine.[1] The toroidal geometry of these devices has led to enhanced energy and particle confinement while maintaining some degree of stability.[2] As the goal of the fusion program is to develop a reactor with a specified triple-product of plasma parameters, $n_{i0}T_{i0}\tau_E$, where n_{i0} is the ion number density, T_{i0} is the ion temperature, and τ_E is the energy confinement time, the tokamak confinement geometry has been very successful in approaching the desired reactor parameters. In Figure I.1, a scaling of the fusion triple-product is shown as a function of temperature with points representing the results of various fusion devices.[3]

Of particular recent interest in the fusion community, is the role of the tokamak edge plasma; the edge plasma being defined as the region of plasma that exists outside to the last closed magnetic flux surface, as shown in Figure I.2. Recent experiments have indicated that many aspects of tokamak plasma behavior, such as enhanced confinement modes (H-modes), plasma and impurity densities, and transport conditions, are controlled by the conditions in the edge plasma.[4] Therefore, it is vital to understand physical processes that occur within the edge plasma and to precisely measure those conditions.

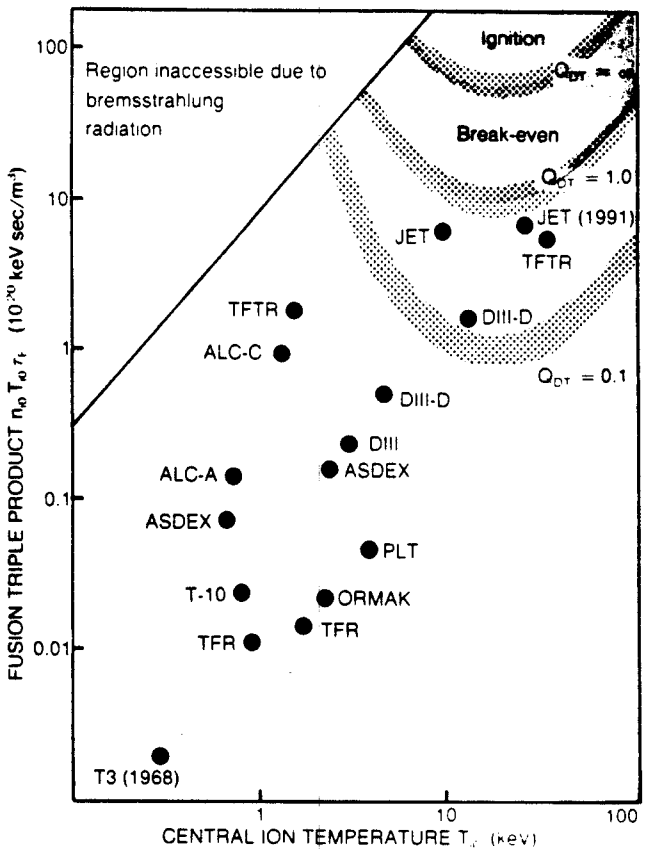

Figure I.1: Curve of Fusion Triple-Product vs. Temperature [from Reference 3]

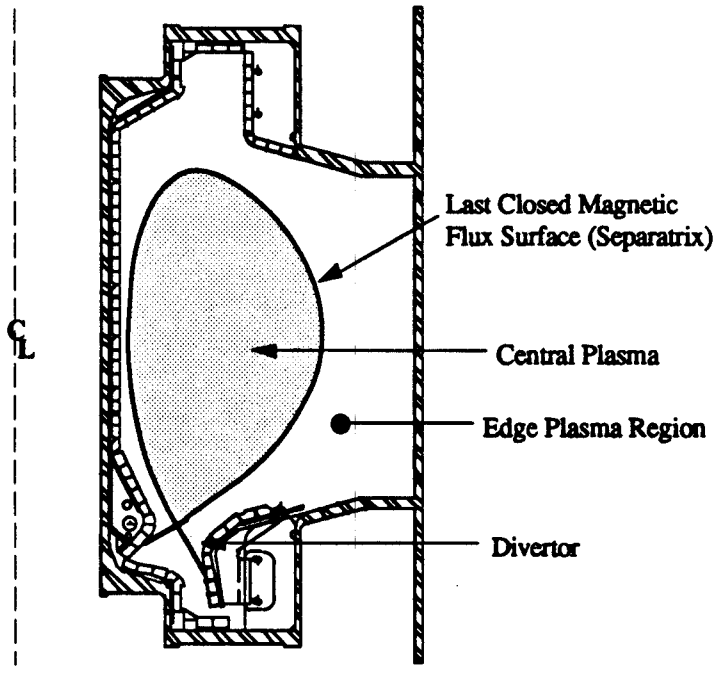

Figure I.2: Alcator C-Mod Cross-Section

I.2 Impurity Production

Since impurities play such a major role in the operation of tokamaks, it is necessary to understand the physics of their production and transport mechanisms. Impurities in tokamak hydrogen and deuterium plasmas are of two classes, low-mass (Z) impurities, such as carbon and oxygen, and high Z impurities, such as tungsten and molybdenum. It has been found, from spectroscopic measurements, that the low Z impurities can account for as much as 5 to 10 percent of the plasma density. The primary role of these impurities is enhanced radiation from the edges of the plasma, near the first wall surfaces. Additionally, the influx of these low mass impurities is linked to disruptive instabilities and can act to limit the density of stable plasma operations. The high Z impurities cause serious energy radiation from the core plasma and it is believed that concentrations of as little as 0.1 percent of the plasma density could prevent ignition.[5]

Experiments have been performed to study the transport mechanisms of impurities once they enter the plasma,[6] but the exact methods by which they are produced as well as the effectiveness of each method is still not well characterized. There are several methods of impurity production that include,[7]

> Thermal Desorption, a process by which light atoms are spontaneously emitted from a metal surface with a functional form of: $\frac{dc}{dt} = \frac{c}{\tau_0} e^{\frac{E_d}{kT}}$, where c is the concentration, E_d is the binding energy, and T is the temperature of the metal surface.
>
> Chemical Reactions, in which plasma particles react with surface atoms to produce molecules with low binding energies.
>
> Evaporation of surface material, due to a large influx of plasma energy deposited on the walls.
>
> Sputtering, a process in which high energy ions bombard the wall surfaces and, via momentum transfer, liberate surface atoms.

There is on-going research to attempt to characterize each of these process-

es and to gain insight on which of these processes will be dominant in future fusion reactors.[8,9]

I.3 Edge Plasma Diagnostics

In order to characterize the impurity production and transport, it is, of course, necessary to measure the conditions of the edge plasma. In the core plasma, only non-perturbative methods, such as interferometry, reflectometry, and Thomson scattering can be used to make measurements of plasma properties (i.e., density and temperature) since no physical probe would be able to withstand the plasma conditions of $T_i \sim 10$ to 15 keV. In the edge plasma, however, the density is $\sim 10^{16}$ to 10^{19} m^{-3}, and the ion and electron temperatures are ~10 to 100 eV, below the maximum thermal flux limit for many metals. Therefore, both non-perturbative and direct particle measurement techniques are used to obtain very detailed information on the conditions in the edge plasma.

I.3.1 Non-Perturbative Techniques

These techniques, such as interferometry, reflectometry, and emission spectroscopy are used to measure the density and temperature for the bulk plasma and for many impurity species. However, such measurements usually require multiple views through the plasma and, in the relatively thin edge plasma, it sometimes can be difficult to achieve these conditions. Additionally, density fluctuations can cause serious signal degradation for these types of measurements.[10] These methods yield observations which complement other measurement techniques used on the plasma edge.

I.3.2 Probe Techniques

Probe techniques include all those methods by which local particle measurement of the plasma takes place. For all of these types of probes, there are two major constraints. First, the measurement that is made is a local parameter of the plasma; therefore, multiple measurements at different locations or complementary data from other diagnostics has to be folded into the analysis in order to form a complete picture of edge plasma. Second, the act of inserting a probe in a plasma distorts the local plasma

conditions (i.e., a sheath forms at the probe surface), so that in order to interpret the results, a mapping must be made to relate the collected signal to conditions in the unperturbed plasma. Despite the difficulties, the use of probes is a reliable means to obtain data on the edge plasma.

A presentation will be made of some of the various types of edge plasma probes currently used in tokamaks. Each of these probes has elements that contributed to the development and design of the Omegatron probe.

I.3.2.1 Langmuir Probes

The Langmuir probe is perhaps the most basic, yet most useful, type of edge plasma probe. The probe tip is biased at some voltage and collects all particles that make it over the potential barrier. In this way, the probe is used to measure the ion saturation current (I_{sat}), the electron temperature (T_e), and the floating potential (V_f) of a plasma.[11] From that information, the electron distribution function of the plasma can be constructed. Since these probes are quite easy to design and build, arrays of Langmuir probes can be immensely useful in characterizing information like heat flows to divertor plates and first wall surfaces (as planned in Alcator C-Mod). In Figure I.3 is a typical Langmuir probe trace taken with one of the on-board probes on the Omegatron.

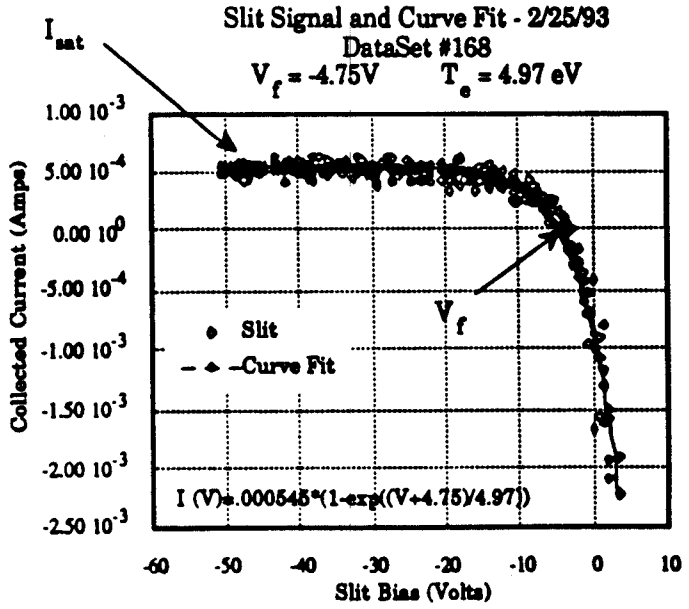

Figure I.3: Signal to Slit - Langmuir Probe from Omegatron Probe operation on the Hollow Cathode Discharge Plasma Column

I.3.2.2 Reciprocating Probes

The reciprocating probe concept is an extension of the Langmuir probe. In this probe system, multiple Langmuir probes are mounted at the tip of a pneumatically driven tube. During the course of a plasma discharge (perhaps several times), this probe tip is inserted into, and then removed from, the plasma. Unlike the fixed Langmuir probes, this probe setup can obtain density and temperature profiles through the radial extent of the edge plasma. This has been used successfully on DIII-D[12] and is expected to be used on Alcator C-Mod.[13]

I.3.2.3 Gridded Energy Analyzers

Gridded energy analyzers are an enhancement over the Langmuir probe as it allows independent analysis of ions and electrons. The typical analyzer has a thin entrance slit followed by a series of grids that act to accelerate and decelerate the incoming particles. In this way, for either electrons or ions, a temperature and a distribution function can be determined.[14] Probes of this type have been used successfully on several tokamaks including the Alcator C tokamak[15] and the DITE tokamak.[16] In Figure I.4, is a general schematic of a gridded energy analyzer arrangement.

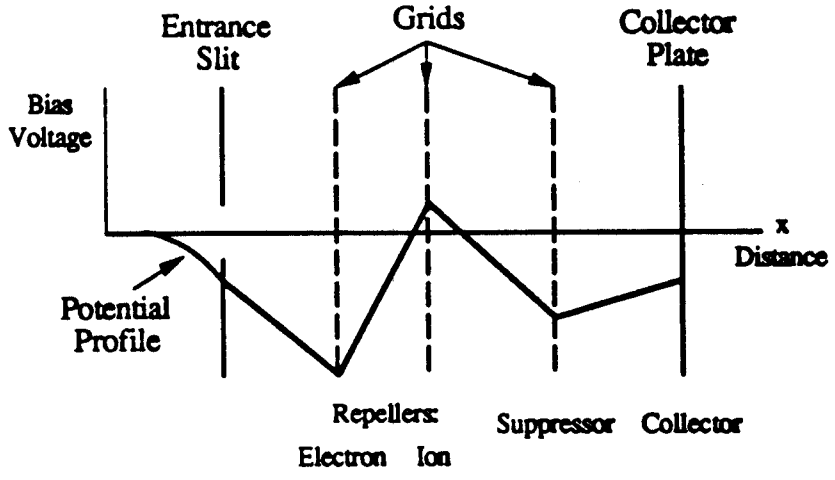

Figure I.4: Typical Schematic of a Gridded Energy Analyzer

I.1.3.4 Charged-Particle Analyzers

Charged-particle analyzers are used to obtain information on the charge state distribution of particles in a plasma. It usually consists of applying an electric field (either with a ramped amplitude or with an oscillating frequency) in a direction perpendicular to the local magnetic field. In this way, the Larmor orbit of an incoming ion is altered and, with the proper geometry, only those ion species that are resonant will be detected. It is possible to then get a spectrum of particles with different charge-to-mass, "Z/m", ratios. The difficulty with this type of analyzer comes in interpreting the overlap in particles with the same "Z/m" ratios, for example, D^+ and He^{+2}. The PIMS (Plasma Ion Mass Spectrometer) analyzer has worked very well in analyzing the edge plasma conditions in the DITE[17] and TEXTOR[18] tokamaks.

I.4 Omegatron Devices

Ever since the first Omegatron was used by Hipple, Sommer and Thomas in 1949,[19] the Omegatron device has had an illustrious history. The concept has been used to measure the Faraday constant (the product of Avagadro's number and the electron charge, a result that still holds today), used as a residual gas analyzer for vacuum systems, and recently, at UCLA, as a plasma diagnostic on the PISCES experiment. The following section gives a brief description of past applications of the Omegatron and concludes with the probe that has been developed for use on Alcator C-Mod.

I.4.1 Residual Gas Analyzer

The Omegatron was used, initially, to investigate several fundamental physical quantities such as the proton charge-to-mass ratio, the ratio of proton mass to electron mass, and the proton magnetic moment.[20] Later, during the 1950's and 1960's, the Omegatron was used extensively as a residual gas analyzer. It operated by ionizing a neutral gas and trapping the ions electrostatically in the analyzer cavity. An oscillating electric field would be applied perpendicular to a weak magnetic field and those particles in resonance would be collected. In this way a "Z/m" spectrum of the gases in the chamber could be obtained.[21,22] A typical design of these early Omegatrons is

shown in Figure I.5.[23]

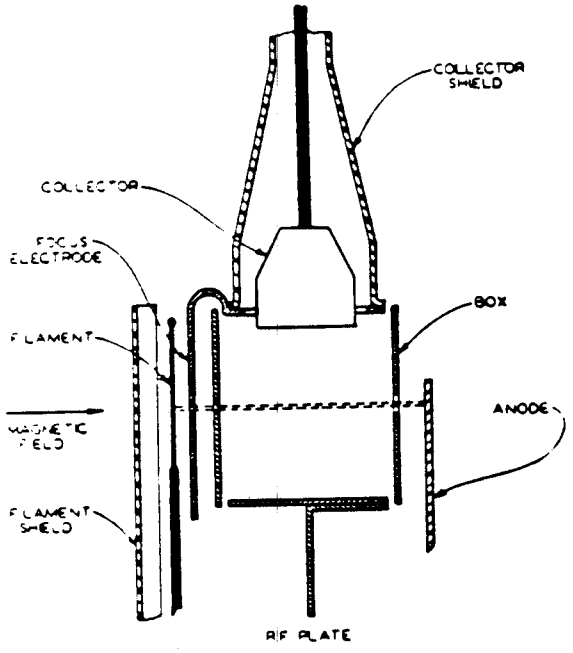

Figure I.5: Schematic of Omegatron Cross-Section
[from Reference 23]

I.4.2 Plasma Diagnostics

Recently, the Omegatron has been rediscovered for use as a plasma diagnostic. In the first Omegatron plasma application, the Omegatron was used to evaluate the different ion species that populated the plasma on the PISCES linear plasma column at UCLA.[24] The success of the probe in obtaining "Z/m" spectra for the plasma column indicated that the Omegatron probe concept could become a valuable asset in diagnosing the plasma conditions in other plasma devices. It is from this starting point that the Omegatron Plasma Ion Mass Spectrometer for Alcator C-Mod was developed.

I.4.3 Omegatron Plasma Ion Mass Spectrometer

The Omegatron Probe that has been developed for use on Alcator C-Mod (or just C-Mod) is a hybrid probe in that it combines elements of the gridded-energy analyzer, Langmuir probe, and, of course, the classic Omegatron arrangement. It is the first Omegatron design that is specifi-

cally intended for operation in the environment of a tokamak device.

The Omegatron experiments described here were not performed on Alcator C-Mod, since C-Mod was not operating at that time. However, the exact probe operated successfully in a linear plasma column device, the Hollow Cathode Discharge (HCD), that is operated by the M.I.T. Nuclear Engineering Department. The results presented in this thesis are from the initial operation of the Omegatron Probe in the HCD. There a two sets of results that are presented: first, an analysis of the performance of the probe as an Omegatron spectrometer to compare the probe's performance with the theoretical predictions; and second, a critical assessment of the probe's operation so as to scale the results from these tests on the HCD to operation on Alcator C-Mod.

I.5 Alcator C-Mod

For completeness, a brief overview is now presented on the Alcator C-Mod tokamak. C-Mod is the third in the series of Alcator tokamaks (after Alcator's A and C) to be built at the Massachusetts Institute of Technology; a schematic of the C-Mod cross-section is shown in Figure I.2. The Alcator tokamaks are high-magnetic field, high performance fusion experiments designed to explore many issues of tokamak particle and energy transport and confinement, fusion reactor technologies, and understanding basic plasma physics. The basic design parameters for Alcator C-Mod are listed in Table I.1.[25] Alcator C-Mod has ten horizontal and twenty vertical ports (ten each on the top and bottom) through which experiments can access the main plasma. The Omegatron probe is designed to enter C-Mod via one of the top vertical ports and reside behind the limiter surfaces.

Table I.1: Alcator C-Mod Design Parameters

Major Radius	R =	0.665 m
Minor Radius	a =	0.210 m
Toroidal Field	B_T =	9 T
Plasma Current	I_P =	3 MA
Elongation	κ =	1.8 (typical)
Flat-top Duration		~1 sec (@ 9 T) ~7 sec (@ 5 T)
Peak Plasma Densities	n_0	$\sim 10^{20} - 10^{21}$ m^{-3}
Peak Plasma Temperatures		~ 4 - 8 keV

The following chapters of this thesis present a theoretical description for the operation of the Omegatron probe, an overview of the design and construction of the probe, and, a presentation and analysis of the data from the first experimental runs.

[1] Wesson, J., Tokamaks, Oxford University Press, New York, 1987.

[2] Freidberg, J.P., Ideal Magnetohydrodynamics, Plenum Press, New York, 1987.

[3] Cordey, J.G., R.J. Goldston, and R.R. Parker, "Progress Towards a Tokamak Fusion Reactor", Physics Today, Vol. 45, No. 1, (1992).

[4] Stangeby, P.C. and G.M. McCracken, "Review Paper: Plasma Boundary Phenomena in Tokamaks", Nuclear Fusion, Vol. 30, No. 7, (1990).

[5] McCracken, G.M., and P.E. Stott, "Review Paper: Plasma-Surface Interactions in Tokamaks", Nuclear Fusion, Vol. 19, No. 7, (1979).

[6] Marmar, E.S., et. al., "Impurity Injection Experiments on the Alcator C Tokamak", Nuclear Fusion, Vol. 22, No. 12, (1982).

[7] McCracken, G.M., and P.E. Stott, "Review Paper: Plasma-Surface Interactions in Tokamaks", Nuclear Fusion, Vol. 19, No. 7, (1979).

[8] Fussmann, G., et. al., "Sputtering Flux Measurements in the ASDEX Divertor", Max Planck Institute for Plasma Physics Report, IPP III/153, October, 1989.

[9] Stamp, M.F., et. al., "Particle Influx Measurements in JET Helium Plasmas using a Multichannel Visible Spectrometer", Journal of Nuclear Materials, 162-164, (1989).

[10] Stott, P.E., "Measurements at the Plasma Edge", Proceedings of Diagnostics for Contemporary Fusion Experiments, Bologna, 1991.

[11] Lipschultz, B., et. al., "Electric Probes in Plasmas", Journal of Vacuum Science and Technology A, Vol. 4, No. 3, 1986.

[12] Watkins, J.G., et. al., "Scrape-Off Layer Measurements in DIII-D", Journal of Nuclear Materials, 196-198, (1992).

[13] Weaver, J. , " The Development of a Reciprocating Langmuir Probe System for Alcator C-Mod", B.S. Thesis, Massachusetts Institute of Technology, 1992.

[14] Hutchinson, I.H., Principles of Plasma Diagnostics, Cambridge University Press, 1987.

[15] Wan, A.S., et.al. "Janus, a Bidirectional, Multifunctional Plasma Diagnostic", Review of Scientific Instruments, Vol. 57, No. 8, (1986).

[16] Matthews, G.F., "The Measurement of Ion Temperature in Tokamak Edge Plasma", Ph.d. Thesis, University of Oxford, 1985.

[17] Matthews, G.F., "Plasma Ion Mass Spectrometry in the Boundary of the DITE Tokamak", Plasma Physics and Controlled Fusion, Vol. 31, No. 5, (1989).

[18] Matthews, G.F., "Plasma Ion Mass Spectrometry in the TEXTOR Boundary", Journal of Nuclear Materials, 196-198, (1992).

[19] Sommer, H., H.A. Thomas, and J.A. Hipple, "A Precise Method of Determining the Faraday by Magnetic Resonance", Physical Review, Vol. 76 (1949).

[20] Sommer, H., H.A. Thomas, and J.A. Hipple, "The Measurement of e/M by Cyclotron Resonance", Physical Review, Vol. 82, No. 5, (1951).

[21] Averina, et. al., "Omegatron Mass-Spectrometer for Analysis of the Composition of Residual Gases in High-Vacuum Systems", Translated from Pribory i Tekhnika Ékspermenta, No. 2, March-April, (1964).

[22] Batrakov, B.P. and P.M. Kobzev, "Omegatron for High-Vacuum", Translated from Pribory i Tekhnika Ékspermenta, No. 4, July-August, (1963).

[23] Wagener, J.S., and P.T. Marth, "Analysis of Gases at Very Low Pressures by Using the Omegatron Spectrometer", Journal of Applied Physics, Vol. 28, No. 9, (1957).

[24] Wang, E.Y., et. al., "An Omegatron Mass Spectrometer for Plasma Ion Species Analysis", Review of Scientific Instruments, Vol. 61, No. 8, (1990).

[25] Hutchinson, I.H. "The Physics and Engineering of Alcator C-Mod", M.I.T. Plasma Fusion Center Research Report, PFC/RR-88-11, August, 1988.

Chapter II: Omegatron Probe Theory

Much of the original theoretical work on the Omegatron probe was performed in the early 1950's by H. Sommer, H. A. Thomas, and J. A. Hipple.[1] Later, theoretical refinements were made to model the trajectories of ions in the Omegatron probe by others.[2,3] In order to understand and interpret the data collected by the Alcator C-Mod Omegatron probe, a slightly modified Omegatron theoretical model was developed to describe the probe operation. Much of the new theoretical work presented in this chapter is the result of numerous, lengthy discussions with Dr. Brian LaBombard.[4]

The motivation for developing this new model was two-fold: first, some estimate of the expected particle flux was needed so as to properly design the current collection electronics; and, second, some constraints were needed to develop the probe hardware. The model makes key predictions about the Omegatron's operation. It generates an I-V (current versus voltage) characteristic curve for the expected signal while operating near a resonance peak and defines the operating space in which the Omegatron should function. In this chapter, a discussion of the theoretical model of the Omegatron probe operation is presented.

II.1 Ideal Omegatron Theory

The basic theory describing the operation of the Omegatron is quite elementary. An oscillating electric field (of the form: $\mathbf{E} = \mathbf{E}_0 \sin(\omega t)\,\mathbf{x}$) is applied perpendicular to a magnetic field (of the form: $\mathbf{B} = \mathbf{B}_0\,\mathbf{z}$). For resonant frequencies, this causes an increase in the radius of a particle's gyro-orbit as perpendicular energy is delivered to it. As long as the particle remain in the region where this oscillating electric field exists, its gyro-radius will continue to expand until it is collected on one of the RF/Collector plates. Figure II.1 demonstrates this effect. R_0 is defined to be the distance from the centerline of the Omegatron to the RF/Collector plates.

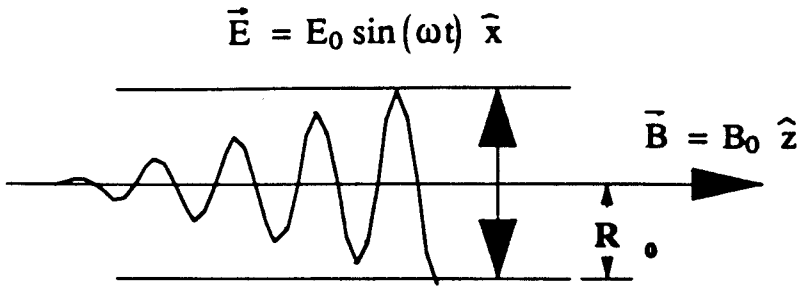

Figure II.1: Orientation of Magnetic Field and Oscillating Electric Field

II.1.1 Particle Orbits

In general, in the presence of a magnetic field, a charged particle's gyro-frequency (or cyclotron frequency) is given by, [5]

$$\omega_c = \frac{qB}{m} \tag{2.1}$$

and the particle travels in a helical path with a radius (the Larmor radius)

$$r_L = \frac{mv_\perp}{qB} \tag{2.2}$$

where: $v_\perp \approx v_{th\perp} = \sqrt{(2T_\perp/m)}$.

However, in the presence of an oscillating electric field (as described above), the radius of the gyro-orbit changes approximately as,[6]

$$r_\varepsilon = \left(\frac{E_0}{B\varepsilon}\right) \sin\left(\frac{\varepsilon t}{2}\right), \quad \text{where: } \varepsilon = |\omega - \omega_c| \tag{2.3}$$

It should be noted that the key assumption in this equation is that particles have no significant Larmor radius when they enter this RF field region. The effect of having some initial gyro-radius has been modeled as a phase difference with respect to the applied electric field.[7,8] For particles in the Omegatron probe, the envelope of their gyro-orbits, r_p, will, on average, be: $r_p \approx r_\varepsilon + 2r_L$. However, for the conditions in Alcator C-Mod, except for the most massive ions, the ions of interest will have relatively small initial gyro-radii so that $r_p \approx r_\varepsilon$. For example, using a singly charged, 10 eV molybdenum ion (molybdenum is of interest since it is the primary plasma facing material on the limiter surfaces and likely to be the most massive el-

ement expected to be detected by the Omegatron), the diameter of its Larmor orbit ($2r_L$) is ~ 1.49 mm; which is approximately 50% of the RF/Collector plate spacing. This means that even molybdenum must still have its gyro-radius increased in order to be collected. From this information, it is a reasonable assumption to use equation 2.3 to model the ion behavior in the Omegatron. This assumption will be used throughout the remainder of this analysis.

II.1.2 Resonant Particles

At resonance, when $\varepsilon \rightarrow 0$, there is a linear increase in the particle orbit in time,

$$r(t) = \frac{E_0 t}{2B}$$

or

$$t_{collection} = \frac{2R_0 B}{E_0} \qquad (2.4)$$

where, $R_0 \equiv$ distance from Omegatron centerline to the RF/collector plates. From this, it can be concluded that for some fixed value for R_0, there is a collection time ($t_{collection}$ or t_{coll}) that is independent of species. It also implies that some control must be maintained over the resonant particles' parallel velocity so that they spend enough time within the RF cavity to be collected. This will be addressed in section II.2.

II.1.3 Far Off-Resonance Particles

There are two classes of particles that are present for cases when $\varepsilon \neq 0$. The first occurs when $\varepsilon >> 0$; this is the case of off-resonant particles. Under these conditions, the radius of the particle's orbit will undulate, undergoing a series of maxima and minima at frequency $\varepsilon/2$ (as described by equation 2.3). These particles will pass through the RF cavity and be collected on the end collector plate. The second class of particles is in a regime where certain non-zero values of ε lead to values of $r_\varepsilon \approx R_0$; implying particle collection. This case of near-resonance determines the Omegatron

"Z/m" resolution.

II.1.4 Near-Resonance Particles and Resolution

This near-resonance regime of particles occurs in a window near $\varepsilon \approx 0$. A critical value of ε (say, ε') is defined such that for $\varepsilon \leq \varepsilon'$, non-resonant particles have the possibility of reaching the RF/Collector Plates,

$$\varepsilon' \equiv \frac{E_0}{BR_0}. \tag{2.5}$$

Sommer, Hipple and Thomas used the value, ε' to define the Omegatron resolution as (refer to Figure II.2),[9,10]

$$\text{Resolution} \equiv \frac{f}{\Delta f} = \frac{\omega_c}{2\varepsilon'} = \frac{qR_0B^2}{2mE_0}. \tag{2.6}$$

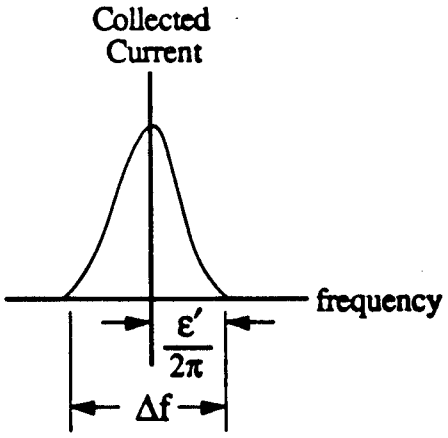

Figure II.2: Resolution Criterion

It follows that the frequency width at the base of the resonance peak, Δf, is

$$\Delta f = \frac{E_0}{\pi R_0 B}. \tag{2.7}$$

It should be noted, that this is a non-standard method of defining the resolution and frequency width of a resonance peak. Typically, in optical spectroscopy, the resolution is defined in terms of the Full Width at Half-Maximum (FWHM). However, this is the definition that has been adopted

for use with Omegatron probes and will be used throughout this analysis.

For the Alcator C-Mod Omegatron conditions: $E_0 \sim 90$V/cm, B ~ 6T, and $R_0 \approx 2.89$ mm, gives a frequency width of ~ 150 kHz. However, the operating frequency range of the probe, looking at ions from singly charged hydrogen to singly charged molybdenum is, in the Radio Frequency (RF) range of, ~950 kHz to ~92 MHz with resolutions of 576 to 6, respectively.

II.2 Mapping the Distribution Function

As stated in section II.1.2, some control must be maintained over the parallel energy of the particles so that resonant particles reside in the RF electric field long enough to be collected. The Omegatron (or any probe) in the plasma perturbs the local plasma conditions. This is manifested primarily in the formation of a sheath at the surface of the probe; a small region in which a potential barrier forms in order to maintain an equal flux of electrons and ions to the probe surface.[11] Under the assumption that the temperature of the ions is comparable to the electrons (as is typical in the edge plasma), a negative sheath is formed (see Figure II.5). Consequently, as the ions drift towards the probe, they are accelerated through the sheath.[12] As a result, the ion entrance velocity is large enough that, if left unaltered, the ions would simply pass through the probe in a time $t < t_{coll}$.

In order to control the parallel ion velocity in the Omegatron, a series of grids is used in a gridded energy analyzer fashion (see Figure II.3). The arrangement of the grids is based upon work done with the Janus probe on Alcator C.[13] Ions are decelerated by the potentials applied to the grids and are allowed to drift slowly into the RF cavity region. However, since this process of deceleration changes the parallel distribution of the particles, a careful mapping must be performed to properly relate the flux of particles collected in the probe to the distribution in the main plasma. The objective of performing this mapping is to estimate the flux of particles to the RF/Collector plates as a function of the bias voltages on the grids, while looking at a particular resonant species.

It is assumed that the ions in the plasma have a Maxwellian parallel velocity distribution. The Omegatron will be sensitive only to a half-Maxwellian (as shown in Figure II.4); specifically, those particles that are

traveling towards the probe. As an ion enters the knife-edge slit, it will encounter the series of biases that are applied to the grids. There are two critical potential differences experienced by the ions as they pass through the grids. This is shown in Figure II.5.

$\Delta\phi_{max} \equiv$ Most positive potential in the grid system

$\Delta\phi_{collector} \equiv$ Bias on RF/Collector plates (shown in Figure II.5)

where, $\phi_{plasma} \equiv 0$.

If the frequency of the applied electric field is set at the cyclotron frequency of some ion species, the maximum flux possible to the RF/Collector plates, assuming one hundred percent particle transmission through the entrance slit and grids, can be modeled as,

$$\Gamma = n_0 \left(\frac{m}{2\pi kT}\right)^{\frac{1}{2}} \int_{v_{min}}^{v_{max}} v_{\|} e^{-\frac{mv_{\|}^2}{2kT}} \, dv_{\|} \tag{2.8}$$

where, n_0, is the plasma density just in front of the entrance slit to the probe. It is now necessary to determine the limits of integration, v_{max} and v_{min}.

II.2.1. Finding v_{max}

For v_{max}, there are two limits on the maximum parallel kinetic energy for which particles can be collected. First, for a fixed t_{coll} and RF cavity size (length, x, and RF plate spacing, $2R_0$), there is a maximum velocity, v_g (based upon geometrical factors), for which particles will remain in the RF Cavity for sufficient time to be collected.

$$v_g = \frac{x}{t_{coll}} = \frac{xE_0}{2R_0B_0} \tag{2.9}$$

Second, the final potential that the particle experiences determines the final kinetic energy. Therefore, the term, v_{max} (the upper limit of integration), can be determined from,

$$\frac{1}{2}mv_{max}^2 = \frac{1}{2}mv_g^2 + Ze\Delta\phi_{coll}$$

or

$$v_{max} = \sqrt{v_g^2 + \frac{2Ze\Delta\phi_{coll}}{m}} \quad . \qquad (2.10)$$

II.2.2 Finding v_{min}

Likewise, v_{min} is determined by the potential difference $\Delta\phi_{max}$, which defines the minimum energy that a particle must have in order to be collected.

$$v_{min}^2 = \frac{2Ze\Delta\phi_{max}}{m} \qquad \text{for } \Delta\phi_{max} > 0$$
$$= 0 \qquad \text{for } \Delta\phi_{max} \le 0 \qquad (2.11)$$

Shown in Figure II.6 are different configurations for $\Delta\phi_{max}$ and $\Delta\phi_{collector}$ and the regions of the distribution function in the main plasma that the probe is sensitive to under each configuration.

II.2.3 Computing the Flux at Resonance

With the expressions for v_{max} and v_{min} above, it is now possible to solve the integral in equation 2.8. Since the expressions for v_{max} and v_{min} are functions of the value of $\Delta\phi_{max}$ and $\Delta\phi_{collector}$, it is expected that the value for the flux, Γ, will also be a function of those. The results of the integration are as follows.

$\phi_{plasma} \equiv 0$

For $\Delta\phi_{max} \le -\frac{mv_g^2}{2eZ}$: $\Rightarrow \Gamma = 0$.

For $-\frac{mv_g^2}{2eZ} < \Delta\phi_{max} < 0$:

$$\Gamma = n_0\left(\frac{kT}{2\pi m}\right)^{\frac{1}{2}}\left[1 - e^{-\frac{m}{2kT}\left(v_g^2 + \frac{2eZ\Delta\phi_{collect}}{m}\right)}\right] \qquad (2.12)$$

And, for the case: $\Delta\phi_{collect} < -\frac{mv_g^2}{2eZ} \Rightarrow \Gamma = 0$.

For $\Delta\phi_{max} > 0$:

$$\Gamma = n_0 \left(\frac{kT}{2\pi m}\right)^{\frac{1}{2}} \left[e^{-\left(\frac{eZ\Delta\phi_{max}}{kT}\right)} - e^{-\frac{m}{2kT}\left(v_g^2 + \frac{2eZ\Delta\phi_{collect}}{m}\right)} \right]$$

And, for the case in which: $\Delta\phi_{collect} < \Delta\phi_{max} - \frac{mv_g^2}{2eZ} \Rightarrow \Gamma = 0$

Using the dimensions of the probe (as listed in Table II.1), it is possible to estimate the level of ion current that should be appearing on the RF/Collector plates. Figure II.7 shows the estimated current for a typical bias scenario on the grids.

TABLE II.1: Omegatron Probe Dimensions

Plasma Conditions	Probe Dimensions
$B_{tor} \approx 6$ Tesla	Slit: 1cm x 20μm
$T_e \sim 15$eV	RF/Collector Plate: x = 4.06cm
$T_i \sim 10$ eV	Plate Separation: $2R_0 = 5.78$mm
$n_0 \sim 10^{12}$ cm^{-3}	RF Amplitude: $E_0 \approx 90$ V/cm
	Transmission: ~ 5%

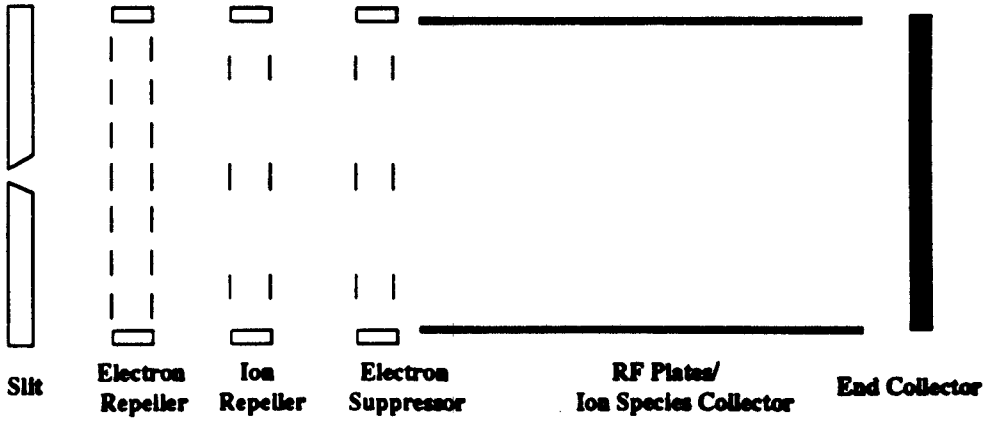

Figure II.3: Arrangement of Probe Components

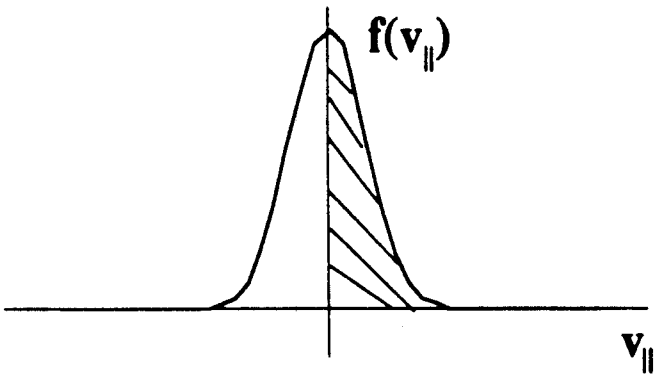

Figure II.4: Probe is sensitive to a half-Maxwellian.

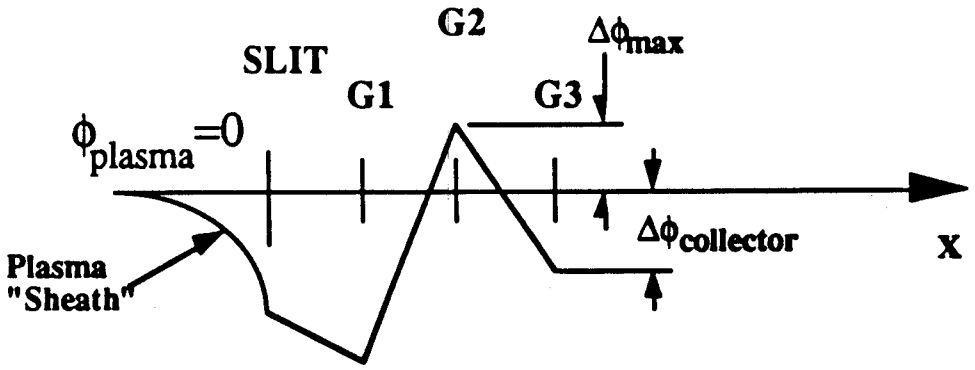

Figure II.5: Typical Potential Profile experienced by Ions as they pass through the grids.

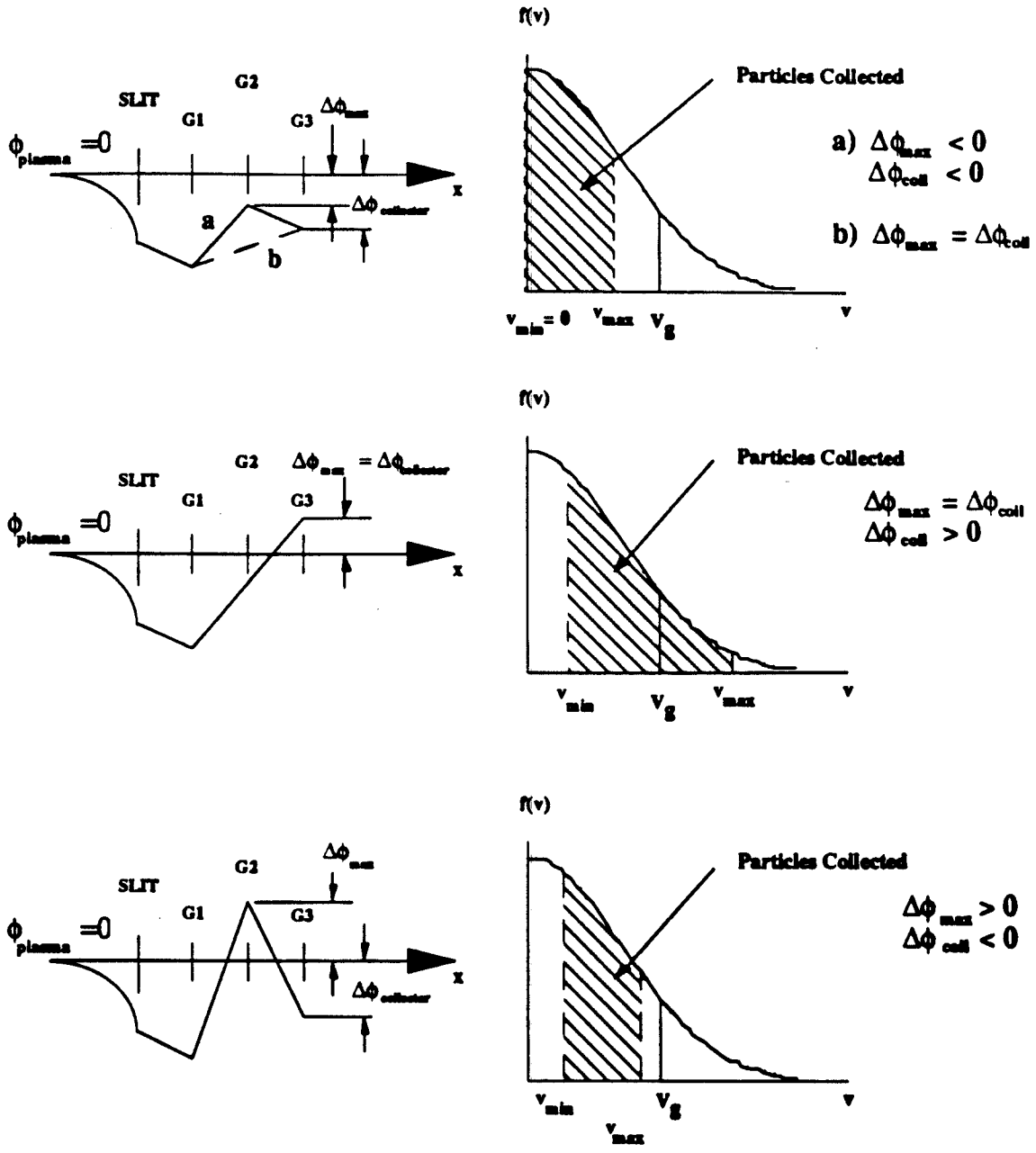

Figure II.6: Mapping of Conditions on $\Delta\phi_{max}$ to Conditions in Main Plasma

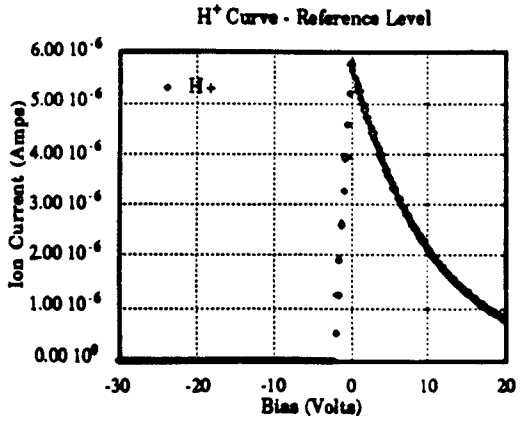

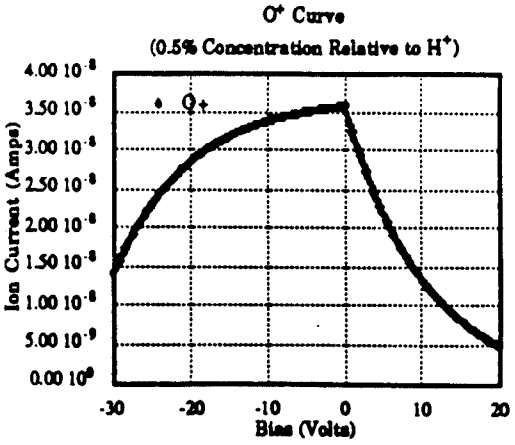

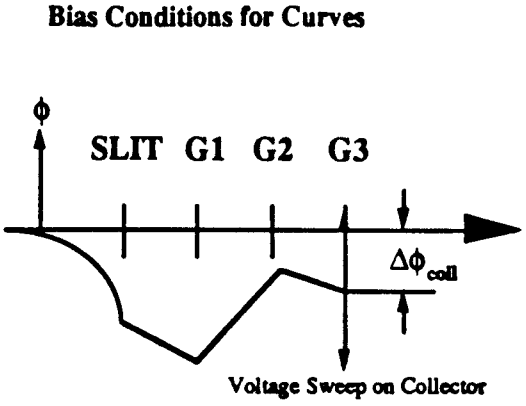

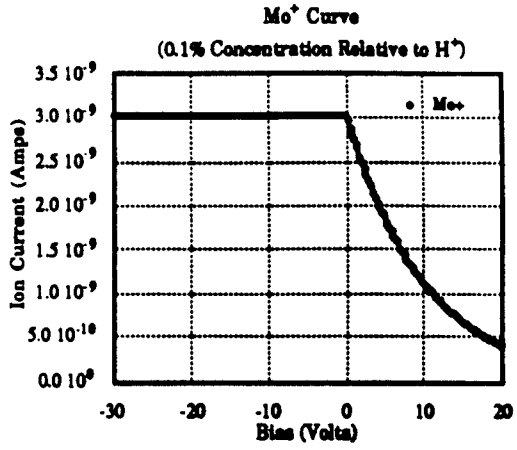

Conditions For Model:	**B = 6 T**	**RF Amplitude ~ 90 V/cm**
	T_i = 10 eV	**T_e = 15 eV**
	n = 10^{18} m^{-3}	**Transmission = 5%**

Figure II.7: Estimated Collected Ion Current

II.3 Modifications due to Plasma Potential Fluctuations

All of the previous analysis for the estimated current was based upon the assumption that the probe was able to collect particles in such a fashion as to be insensitive to plasma fluctuations. In practice, this may be accomplished by electrically biasing each component in the Omegatron relative to the slit potential, which is allowed to electrically float. However, a situation may arise when it becomes difficult to achieve this floating condition. It then becomes necessary to develop some modification to the collected flux model to account for perturbations in the plasma potential.

II.3.1 Modeling the Fluctuations

In Figure II.8 is shown a schematic for the effect of the fluctuation on the values of $\Delta\phi_{max}$ and $\Delta\phi_{collector}$. Although it is the plasma potential that is actually fluctuating, for computing purposes, it is convenient (and equivalent) to consider the grid bias as fluctuating and the plasma potential fixed at zero. The fluctuating potential appears as an instantaneous change in the grid bias, relative to their time-averaged values, and is defined to be some function of time represented by $\phi_f(t)$.

There are newly defined potentials:

$$\Delta\phi_c(t) = \Delta\phi_{collector} - \phi_f(t)$$
$$\Delta\phi_m(t) = \Delta\phi_{max} - \phi_f(t) \qquad (2.13)$$

which are the new, relative values of the biases on the grids as a result of a plasma fluctuation. These time dependent variables are then used to calculate the flux.

It is now necessary to describe the fluctuation, ϕ_f, itself. A typical approach to modeling plasma potential fluctuations is to assume some Gaussian probability distribution about the mean level, ϕ_{po} as shown in Figure II.9. The term, $P(\phi_f)$, is the probability that the fluctuation has some level ϕ_f. This probability function acts to spread the energy distribution of particles collected by the probe and causes broadening of the current-voltage (I-V) characteristic and a distortion of the position and level of the maxi-

mum collected signal. From the above information, it is now possible to compute the new value of the flux, Γ.

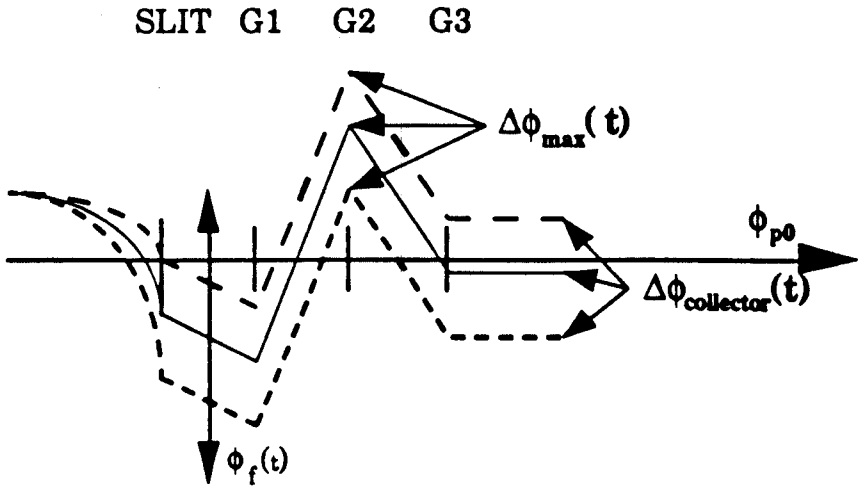

Figure II.8: Potential Profiles Experienced by Ions as a Result of Fluctuations.

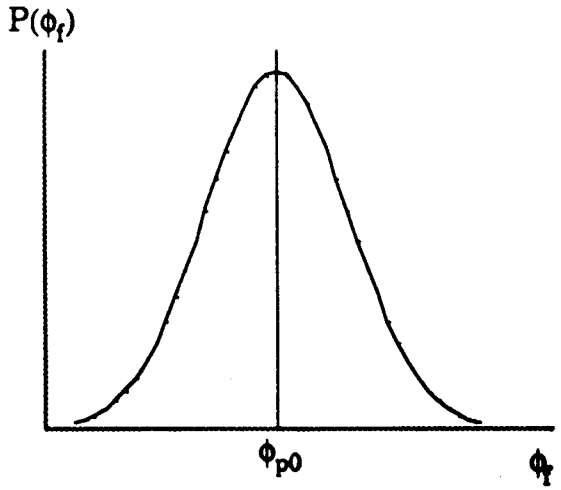

Figure II.9: Gaussian Probability Distribution of Plasma Potential Fluctuations about the Mean Level, ϕ_{p0}.

II.3.2 Computing the Flux with Fluctuations

First, it is necessary to make use of the substitutions for $\Delta\phi_{max}$ and $\Delta\phi_{collector}$ as defined by equations 2.13. Similar to the analysis in section

II.2, the value of ϕ_{p0} is taken to be zero. The new value of the collected flux is then defined as,

$$\Gamma(\Delta\phi_{max},\Delta\phi_{collector}) = \int_{-\infty}^{\infty} \Gamma(\Delta\phi_m(t),\Delta\phi_c(t))\ P(\phi_f)\ d\phi_f \tag{2.14}$$

where, the Gaussian weighting function, $P(\phi_f)$, is defined as,

$$P(\phi_f) = N e^{-\alpha^2 \phi_f^2}$$

$$\int_{-\infty}^{\infty} P(\phi_f)\ d\phi_f = 1$$

$$\left\langle \phi_f^2 \right\rangle = (\gamma T_e)^2 = \int_{-\infty}^{\infty} P(\phi_f)\ \phi_f^2\ d\phi_f ; \quad \text{where } \gamma = \text{constant} \tag{2.15}$$

In the last equation in 2.15, there is a relationship that expresses the RMS fluctuation level, ϕ_f, as proportional to the electron temperature, T_e. With this relationship on T_e, it is now possible to evaluate the constants N and α; this is shown in equation 2.16.

$$N = \frac{1}{\sqrt{2\pi}\,\gamma T_e} \quad \text{and} \quad \alpha = \frac{1}{\sqrt{2}\,\gamma T_e} \tag{2.16}$$

Measurements in the edge plasma of TEXT (the Texas EXperimental Tokamak) shows values of $\gamma \sim 0.1$ to $0.2\ T_e$.[14] In Figure II.10, the same conditions that were used to calculate the flux in Figure II.7 are considered, with the inclusion of a 20% relative fluctuation level. As expected, the peak signal is shifted, by as much as 5 to 7 volts, and there is a clear indication of a broadening in the collected current signal. From these results, it is clear that plasma fluctuations can have a serious effect on the collected flux to the Omegatron probe; therefore, it is imperative that in analyzing the probe's data, a proper accounting must be made as to how well the probe was able to electronically compensate for plasma fluctuations.

II.4 Theoretical Results

The above results have some direct consequences on the physical design and operation of the Omegatron probe. First, the model indicates that the Omegatron will be a low current system; the signals collected for the primary plasma species will be on the order of a few microamperes, and, the current level for the impurity species will tend to be on the order of tens of nanoamperes. These results are consistent, in terms of absolute current levels, with the experimental results from other mass spectrometer and gridded energy analyzer plasma probes.[15,16,17] Second, the model indicates that the current collected is also dependent upon the geometry of the probe; specifically, the ratio of length of the RF cavity to RF/Collector Plate spacing (x/R_0). Therefore careful consideration is to be made when laying out the dimensions of the Omegatron. However, the third, and perhaps most significant result, is that there does not appear to be any truly insurmountable problem in designing such a probe. Although the parameters and constraints of probe operation may be difficult in practice, they are not impossible to achieve.

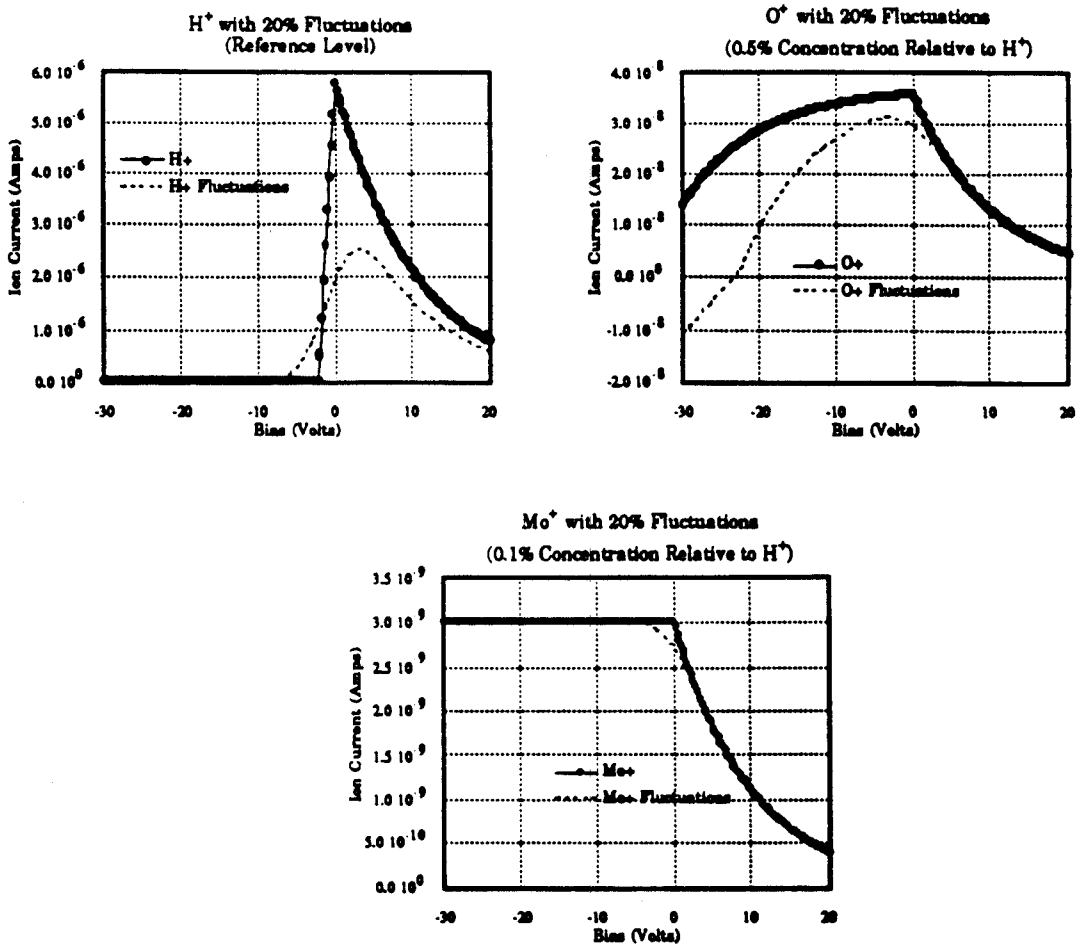

Conditions For Model:

$B = 6\ T$	RF Amplitude ~ 90 V/cm
$T_i = 10\ eV$	$T_e = 15\ eV$
$n = 10^{18}\ m^{-3}$	Transmission = 5%
$\gamma = 0.20$	

Figure II.10: Estimated Collected Ion Current with a Normalized 20% Plasma Potential Fluctuation Level

[1] Sommer, H., H.A. Thomas, and J.A. Hipple, "The Measurement of e/M by Cyclotron Resonance", Physical Review, Vol. 82, No. 5 (1951).

[2] Berry, C., "Ion Trajectories in the Omegatron", Journal of Applied Physics, Vol. 25, No. 1 (1954).

[3] Brubaker, W. and G.D. Perkins, "Influence of Magnetic and Electric Field Distribution on the Operation of the Omegatron", Review of Scientific Instruments, Vol. 27, No. 9 (1956).

[4] LaBombard, B., Private Communications on Omegatron Electronics and Omegatron Probe Theory, 1991-1993.

[5] Brillouin, L., "A Theorem of Larmor and Its Importance for Electrons in Magnetic Fields", Physical Review, Vol. 67, No. 7/8 (1945).

[6] Sommer, H., H.A. Thomas, and J.A. Hipple, "The Measurement of e/M by Cyclotron Resonance", Physical Review, Vol. 82, No. 5 (1951).

[7] Berry, C., "Ion Trajectories in the Omegatron", Journal of Applied Physics, Vol. 25, No. 1 (1954).

[8] Brubaker, W. and G.D. Perkins, "Influence of Magnetic and Electric Field Distribution on the Operation of the Omegatron", Review of Scientific Instruments, Vol. 27, No. 9 (1956).

[9] Sommer, H., H.A. Thomas, and J.A. Hipple, "The Measurement of e/M by Cyclotron Resonance", Physical Review, Vol. 82, No. 5 (1951).

[10] Wang, E.Y., et. al., "An Omegatron mass spectrometer for plasma ion species analysis", Review of Scientific Instruments, Vol. 61, No. 8 (1990).

[11] Chen, F.F., Introduction to Plasma Physics, Plenum Press, New York, 1974.

[12] B. Lipschultz, et.al., "Electric Probes in Plasmas", Journal of Vacuum Science and Technology A, Vol. 4, No. 3 (1986).

[13] Wan, A.S. "Ion and Electron Parameters in the Alcator C Tokamak Scrape-Off Region", Ph.D. Thesis, Massachusetts Institute of Technology, 1986.

[14] Wooten, A.J., et.al.,"Fluctuations and Anomalous Transport in Tokamaks", Fusion Research Center Report, #340, The University of Texas at Austin, 1989.

[15] Pitts, R.A., "Ion Energy, Sheath Potential and Secondary Electron Emission in the Tokamak Edge", Ph.D. Thesis, University of London, 1990.

[16] Matthews, G.F., "Plasma Ion Mass Spectrometry in the Boundary of the DITE Tokamak", Plasma Physics and Controlled Fusion, Vol. 31, No. 5 (1989).

[17] Wan, A.S., et.al."Janus, a Bidirectional, Multifunctional Plasma Diagnostic", Review of Scientific Instruments, Vol. 57, No. 8 (1986).

Chapter III: Probe Hardware and Electronics

The development of the Omegatron device was an iterative process. It involved the simultaneous development of the theory, probe hardware, and probe electronics. Each of these areas of the Omegatron's development had to be balanced so as to allow creative feedback. In the end, a fairly simple and modular design was adopted for the probe; the design allows for fairly easy interface between the hardware and the electronics, and facilitates rapid disassembly and reassembly when repairs are needed.

In developing the probe, several constraints were placed at the beginning of development. These included:

- The probe had to enter the Alcator C-Mod (or C-Mod) vacuum vessel through a vertical port with a 3 inch diameter through hole and be aligned to a typical magnetic flux surface.

- The length of the RF/Collector plates had to be as long as possible so as to maximize the length of time the particles would be in the oscillating electric field.

- The plasma facing surface of the probe would have to be able to withstand both large thermal shocks and thermal cycling (the typical plasma shot would last from 1 to 7 seconds at intervals of 15 to 20 minutes)

- The electronics would have to be a fast time-response, low current (< 1 nanoampere) circuitry that was fairly insensitive to high frequency plasma potential fluctuations and capable of rejecting common mode voltages of hundreds of volts.

These, along with several, more minor constraints, impacted greatly on the final design of the Omegatron probe. This chapter is divided into two major sections: first, is a discussion of the various probe components and their overall contribution to the Omegatron's operation and, second, is a discussion of the circuitry used by the Omegatron components and the on-board Langmuir probes.

III.1 Omegatron External Components

The Omegatron probe is assembled from three major external compo-

nents: a) the Heat Shell, which is the main plasma facing surface of the probe assembly; b) the Shield Box, which provides a housing for the grids, the RF/Collector Plates, and the End Collector; and c) the Patch Panel, which provides the interface point between the probe components and the electronics. In this section each of these components will be discussed.

III.1.1 Heat Shell

The Heat Shell is the primary plasma facing component of the Omegatron probe. It is a hollowed-out disk of molybdenum that is a nominal 2.80 inches in diameter and 0.588 inches high (see Figure III.1, below, and Figure III.6).

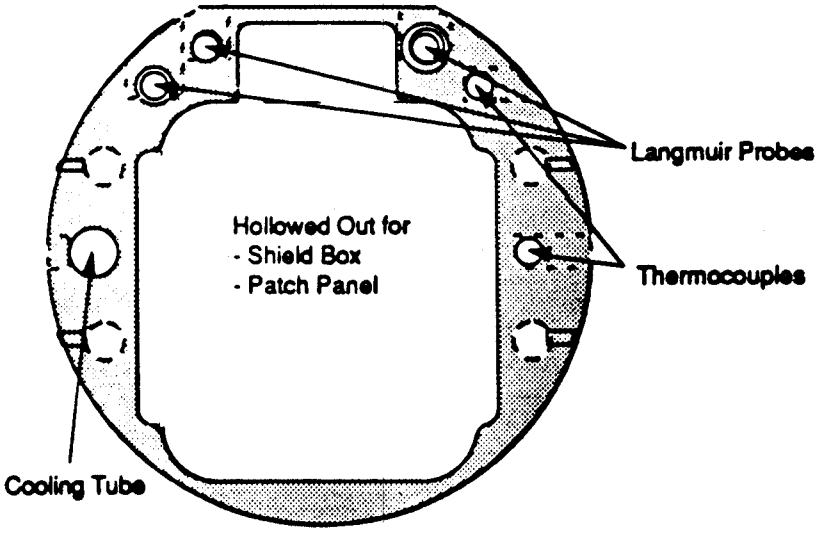

Figure III.1: Omegatron Heat Shell - Top View (1:1)

Of the many considerations that went into the design of the Heat Shell, the two primary concerns were that the Shell be able to fit through the 3.0 inch diameter vertical port on Alcator C-Mod and that the probe would be able to withstand the heat flux from the plasma.

The major constraint to the design of all of the Omegatron components was the passing of the Omegatron through the vertical port. It placed an immediate size restriction on the probe hardware and some ingenuity was required in order to facilitate the integration of all of the probe components. In addition to this, since the probe had to be aligned to a particular magnet-

ic flux surface, there was very little freedom in the orientation of the probe. A more detailed description of the probe orientation will be presented in Section III.3.2.

The second major concern regarding the Heat Shell was the amount of heating that would take place during a plasma discharge. This was motivated by a concern about surface melting on the probe. Additionally, the in situ RF load resistors rapidly begin to lose their power handling ability above 100°C. It is therefore necessary to estimate the temperature rise of the Heat Shell.

For some typical Alcator C-Mod discharge, the plasma conditions in the edge plasma should be: particle density, $n_o \approx 10^{18}$ m^{-3}, electron temperature, $T_e = 20$ eV, and primary ion species, Hydrogen, $m_i = m_{H+}$. The ion saturation current density of the plasma under these conditions will be,[1]

$$J_{sati} = 0.61\, e\, n_0 \left(\frac{kT_e}{m_i}\right)^{\frac{1}{2}} \approx 4.27 \times 10^3 \frac{A}{m^2}. \qquad (3.1)$$

This current density corresponds to a heat flux, q, to the probe surface of,

$$q = \gamma T_e J_{sati} \approx 5.97 \times 10^5 \frac{J}{m^2 \cdot sec.} \qquad (3.2)$$

For a 3 second heat pulse, there is a heat flow of $q' = 1.8 \times 10^6$ J/m^2 to the probe surface. For a given material, the temperature rise due to an amount of heat, Q, is,[2]

$$\Delta T = \frac{Q}{m\, c_p} = \frac{q' A_{sur}}{\rho\, V\, c_p} \qquad (3.3)$$

where, A_{sur} is the surface area upon which the heat impinges, V is the volume, c_p is the heat capacity of the material. For the calculation for the Omegatron, A_{sur}, is the area of the flat face of the Omegatron which is ~1.21 $\times 10^{-3}$ m^2, the volume of the hollowed out shell is ~4.2 $\times 10^{-5}$ m^3. From the CRC Handbook of Chemistry and Physics,[3] the density of molybdenum is, $\rho = 1.02 \times 10^4$ kg/m^3, and the heat capacity is, $c_p = 250$ $J\text{-}kg^{-1}\text{-}K^{-1}$. This information gives of a temperature rise of $\Delta T = 20.3°$ C during a discharge.

This analysis shows that there is not a very large temperature rise during a given discharge. However, with repeated discharges, the temper-

ature may rise above 100°C. Because of this, a dry nitrogen system has been designed to facilitate the cooling of the probe between discharges.

III.1.2 Shield Box

The Shield Box provides the housing for all of the internal components of the Omegatron, except for the Langmuir probes and the thermocouples. Made of copper, it is electrically isolated from the Heat Shell by a series of 0.020 inch mica sheets. The Omegatron circuitry is extremely sensitive to currents on the probe components, including displacement currents from stray capacitance between components. In order to reduce the effect of this stray capacitive coupling, the entire Shield Box is biased at the slit potential; therefore, all internal components see the same external potential and, hence, experience no displacement currents. Figure III.2 has a diagram of the Shield Box with the internal components labeled.

The Shield Box was designed to fit inside the Heat Shield pocket with roughly 0.020 inches of clearance on all sides. It is 2.31 inches long by 1.80 inches at its widest point by 0.413 inches high. The front section holds the grids and the slit, the next section is a hollow cavity (the RF Cavity) for the RF/Collector Plates, and the back section holds the End Collector.

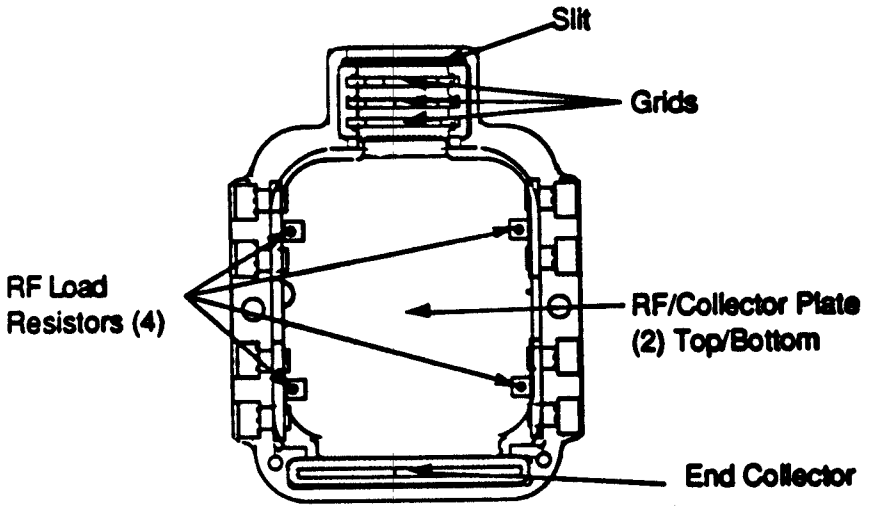

Figure III.2: Shield Box and Internal Components (1:1 Scale)

III.1.3 Patch Panel

The Patch Panel is designed to hold all of the SMA-type feedthrough bulkhead connectors for the Omegatron. It is made of aluminum and has 0.004 inch hardcoat for electrical insulation. Unlike flame-spray coating or other types of coatings, this hardcoat penetrates (about half the thickness of the coating, in this case 0.002 inches) into the surface of the material coated; this makes a stronger bond to the base material and increases the insulating ability.[4] The Patch Panel is designed to have exactly the same footprint as the Shield Box. When assembled, a thin copper plate is placed between the Patch Panel and the Shield Box, which acts to completely enclose all the components in the Shield Box, and the entire assembly is placed in the Heat Shell and held in place with a large spring.

Each SMA connector is locked in place by a matching hexagonal pattern on the underside of the Patch Panel (see Figure III.3). From the bulkhead underside, a 0.040 inch diameter wire is used to deliver the signal to each probe component. From the bulkhead topside, standard 0.080 inch or 0.141 inch co-axial SMA semi-rigid cable is used to get to the vacuum feedthrough flange.

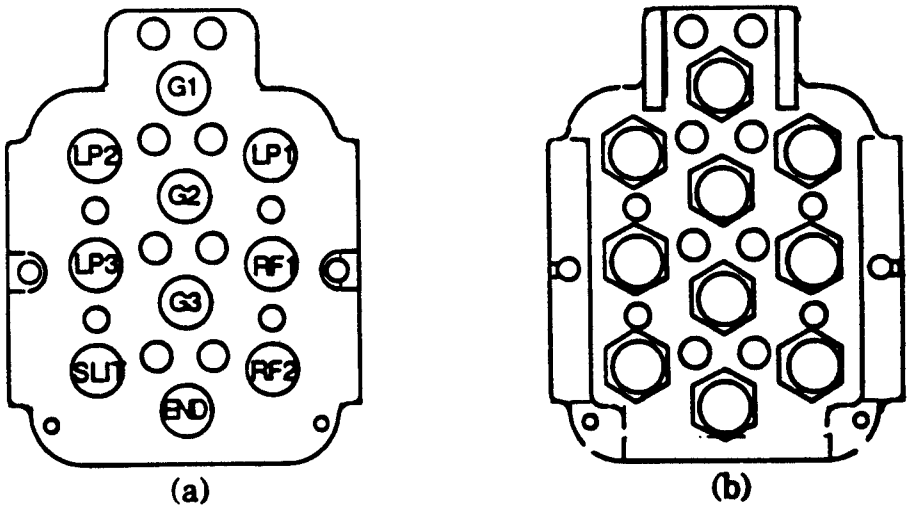

Figure III.3: Patch Panel Views (1:1 Scale) - (a) Top Side (b) Under Side

III.2 Omegatron Internal Components

The primary Omegatron probe components, all of which lie inside the Shield Box, are the entrance, knife-edge slit, the grids, the RF/Collector (or just RF) plates, and the end collector; the layout of these components is shown in Figure III.2. The electronics that drives each of these components not only allows for independent biasing of each, but also allows for signal detection on each component. In this way, a complete accounting of the particles that enter the slit can be performed.

Much of the layout of the slit and grid assembly was based upon work done by Dr. Alan Wan on the Janus probe, a gridded energy analyzer probe which was used successfully on Alcator C.[5,6] Through extensive communication with Dr. Wan, detailed design sketches of Janus were obtained, and several of that probe's design concepts for the slit and grid layout were incorporated into the Omegatron probe.[7]

The other "internal" components are the Langmuir probes and the thermocouples, which, although not directly part of the Omegatron probe, provide vital information for the Omegatron's operation and for data analysis. Each of these components is discussed in detail in the following sections.

III.2.1 Knife-Edge Slit

The entrance slit is a four-piece construction made from tungsten which was electron-beam welded using a stainless steel braze (see Figure III.4). As demonstrated by Monte-Carlo simulations by Dr. Wan, the use of a 45° knife-edge arrangement for the slit will enhance the particle flux through the slit, as compared to a straight edge slit. This is due to the fact that particles are traveling along spiral paths and, by making the slit angled, there is a larger class of particles whose velocity components are suitable for passage through the slit.

The designed dimensions of the slit are 1 cm long by 25 microns wide, while the actual area exposed to plasma is roughly a rectangular oval, with length 0.5 inches, width 0.10 inches, and 0.050 inch radius rounded ends; this is shown in Figure III.6. In actuality, a great deal of difficulty was en-

countered in trying to electron-beam weld the slit. The slit used on the Omegatron for the HCD experiment was roughly triangular, 1 cm height, with a 25 micron base; this corresponds to approximately half the area of the original design value. At a future time, a redesign of the slit will be necessary to ensure reliable assembly.

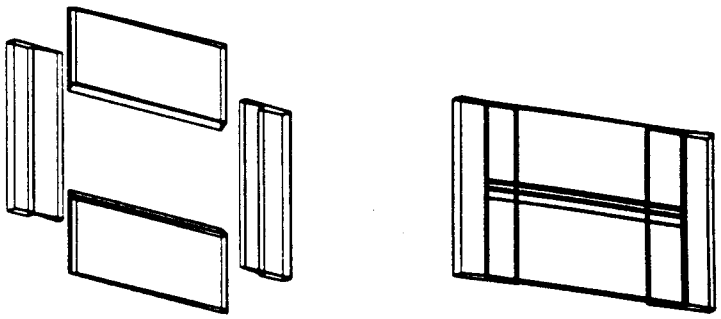

(a) (b)

Figure III.4: Slit Views - (a) Exploded View (b) Assembly

The current on the slit is handled similarly to the current on the Langmuir probes due to the expected high currents (possibly as high as a few milliamperes). In fact, during probe operations, the slit was biased identically to the Langmuir probes in order to obtain the density and temperature of the plasma at the entrance to the probe.

III.2.2 Grids

The front-end grids are actually two tungsten meshes that are spot-welded on either side of a stainless steel frame. The first grid is made from 250 line/inch meshes. The next two grids are each made from 150 line/inch meshes. Each grid has a line weight of 0.001 inches. Each grid is electrically isolated from the Shield Box and has its spacing fixed by the combination of a ceramic comb and some mica sheets, as shown in Figure III.5.

The spacing between the grids is set by the combs to be 0.050 inches. Not shown in Figure III.5 are the mica strips that are placed on top of the grid holders to insulate them from the cover plate that is placed between the Shield Box and the Patch Panel.

The grids, RF/Collector plates, and the End Collector all use customized Omegatron circuit boards. These boards allow real-time detection of signals ranging from ~ 500 pA to 10 μA.

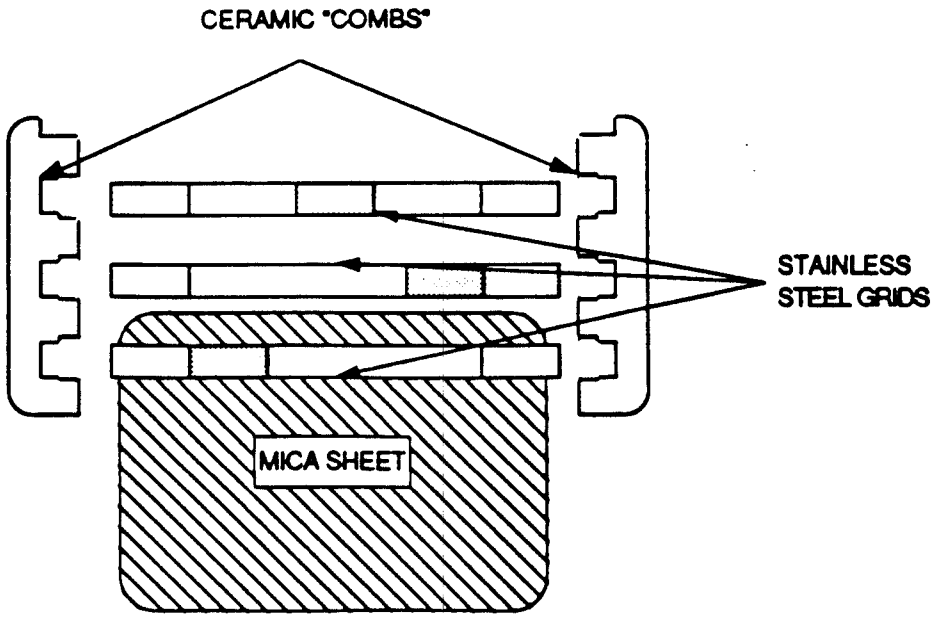

Figure III.5: Top View of Grid/Ceramic Assembly (4:1 Scale)

III.2.3 RF/Collector Plates

The RF/Collector plates are a pair of 0.032 inch thick, parallel stainless steel plates. They are separated by a distance $2R_0$, where R_0 is determined from the desired resolution of the Omegatron (refer to equation 2.7). For a frequency width, Δf ~150 KHz, this sets $2R_0 = 5.78$ mm = 0.228 inches. This was fortunate since the RF load resistors, which are needed to absorb a launched RF power of up to 40 Watts, have a width of ~0.22 inches and could be installed directly onto the RF Plates. When completely assembled, the RF/Collector plates effectively float on the leads of the RF load resistors, and were completely electrically isolated from all other components.

III.2.4 End Collector

The End Collector is the simplest of the Omegatron internal components. It is simply a stainless steel plate, 1.15 inches wide by 0.310 inches high, that is used to collect the particles that make it through the RF cavity.

In this way it is possible to complete the particle accounting in the Omegatron.

III.2.5 Langmuir Probes

There are three on-board Langmuir probes, housed in the Heat Shell, that measure the local density and electron temperature conditions at the Omegatron. These probes are all made from molybdenum rod ranging from 0.107 inches to 0.120 inches in diameter. The difference in the diameters is to allow all three probes to have the same projected area, allowing for a ±9° variation in the total magnetic field at the location of the Omegatron. In this way, data from the Langmuir probes can be analyzed directly, without having to make corrections for area effects. In Figure III.6, the locations of the Langmuir probes in the Heat Shell are shown. Langmuir probe, LP1, is the furthest in the plasma, LP2, is coplanar with the slit, and LP3 is the furthest removed from the plasma.

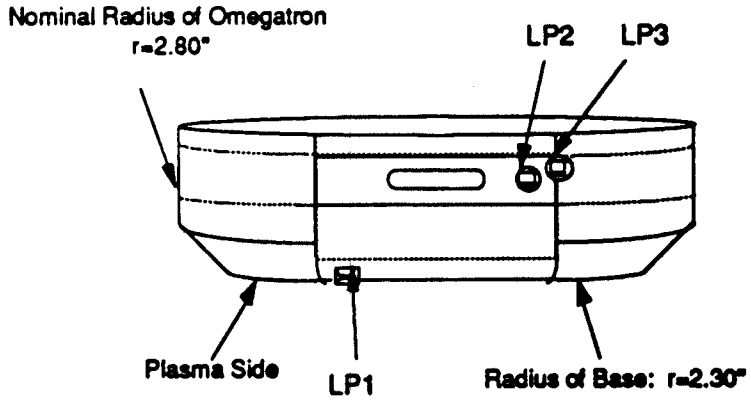

Figure III.6: 3-D View of Omegatron Probe with Langmuir Probes

The main purpose for having three Langmuir probes to have definitive information on the variation of the plasma density and temperature at the Omegatron surface. In this way, an accurate accounting can be made of the flux of particles entering the analyzer. A typical Langmuir probe trace can be modeled, near the ion saturation current, as

$$I(V) = I_0 [\, 1 - \exp \{e(V-V_f)/T_e\} \,] \qquad (3.4)$$

where the ion saturation current, I_0, is

$$I_0 = -eJ_{sat} \approx -0.61\, e\, A_{probe}\, n_0 \left(\frac{T_e}{m_i}\right)^{\frac{1}{2}}. \qquad (3.5)$$

It is then possible to find the value of T_e, the electron temperature, by taking the slope of the curve $\ln|I-I_0|$ versus V.[8] The key limitation of this model is its validity only in non-magnetized plasmas. For the magnetized case, modifications must be made to account for the fact that the source of particles to the probe is not free-streaming ions, but rather ions that have diffused across the magnetic field lines to the particular flux surface on which the probe resides. The main difference in the final result occurs in the coefficient in front of equation 3.5; 0.61 goes to 0.49. For the HCD runs, the local magnetic field around the Omegatron is approximately 1400 Gauss; under these conditions, the ions in the plasma, relative to the probe size, are virtually unmagnetized. Therefore, that is the assumption that will be used for the Langmuir probe analysis.

III.2.6 Thermocouples

There are two thermocouples in the Omegatron Heat Shell that monitor the temperature of the probe at all times; one is at the front, near the slit, and the other is near the RF/Collector Plates, as shown in Figure III.1. The thermocouples used are Type K, a Chromel and Alumel junction.

In operations on the HCD plasma column, the thermocouples were of considerable importance since the Omegatron was exposed to a steady-state plasma for up to three hours and it was necessary to have constant monitoring of the probe temperature. By using a water-cooled copper plate as a mounting for the Omegatron probe assembly, the temperature of the Omegatron was maintained at 20°C to 25°C during plasma operations.

III.3 Omegatron Probe Assembly

The Omegatron Probe is, ultimately, designed for use on Alcator C-Mod. However, it was decided to test the operation of the probe on another plasma source; additionally, C-Mod was shut down during the time when the Omegatron was tested. The Hollow Cathode Discharge (HCD) plasma column proved to be the ideal environment in which to test the probe; it is

essentially a table-top plasma source that can be run steady-state for extended periods.

III.3.1 Hollow Cathode Discharge Setup

The Hollow Cathode Discharge (HCD) is a linear plasma device that is operated by the M.I.T. Nuclear Engineering Department and is used as part of an instructional laboratory course.[9] The HCD produces a plasma column, approximately 1 meter long and 1 to 2 centimeters in diameter. The vacuum chamber is composed of 4-, 5-, and 6-way NW160 crosses (with approximately 7 inch flange diameter). Gas is fed through a hollow tantalum tube, the cathode, which is at one end of the chamber. After breakdown, the plasma column extends from the tip of the cathode to a water-cooled copper disk, the anode, at the other end of the chamber (see the schematic in Figure III.7). A nominal seleniodal magnetic field, produced by 5 copper coil magnets, of around 600 to 800 Gauss is maintained along the axis of the chamber. For the Omegatron experiments, an additional power supply was added to independently drive the two magnets around the Omegatron port. The local magnetic field at the location of the Omegatron ranged from 1300 to 1400 Gauss under normal operations.

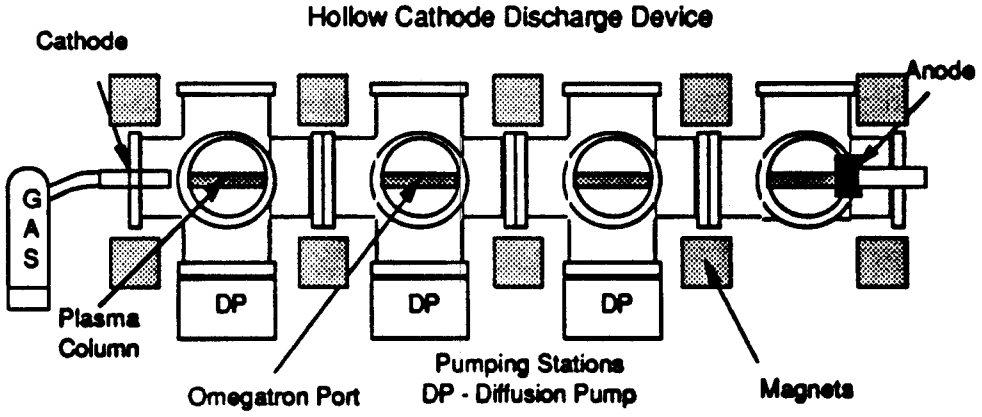

Figure III.7: Schematic of Hollow Cathode Discharge Device

Other key parameters for operation on the HCD are listed below in Table III.1.

Table III.1 - Operating Parameters for HCD

Gas:	Hydrogen/Argon or Hydrogen/Helium
Magnetic Field:	~ 1400 Gauss (at Omegatron location)
Base Pressure:	~ 8×10^{-6} Torr
Fill Pressure:	~ 5×10^{-4} Torr
Nominal Discharge:	12A/30V - 3.6 kW
Pulse Length:	Continuous
Density (at probe):	~ 10^{15} - 10^{16} m^{-3}
Electron Temperature:	~ 5 - 10 eV
Ion Temperature:	~ 1 - 5 eV

Under these conditions, in order to obtain Omegatron mode results, the frequency range of the applied RF electric field was reduced to a range of 30 kHz to 2.5 MHz. Since the magnetic field in the HCD was roughly a factor of 50 less than for Alcator C-Mod (~0.14 Tesla compared to 6 Tesla), the amplitude of the applied RF electric field was reduced from ~90 V/cm (50 V peak-to-peak across the RF plates) to ~2 V/cm (1 V peak-to-peak) to maintain approximately the same frequency width of ~ 150 kHz. However, this limited the probe to run fairly "low mass" plasmas since the resonance frequencies were so low. During the experiment, the Omegatron successfully resolved the peaks of H^+ (at 2 MHz), H_2^+ (at 1 MHz), and He^+ (at 500 kHz); most other suspected ion species, such as oxygen, nitrogen, and argon (which was used initiate the breakdown), have low enough frequencies to be indistinguishable and/or had sufficiently large Larmor radii to be effectively non-magnetized inside the Omegatron RF cavity.

Except for operating in this different magnetic field regime and the use of active water-cooling instead of a dry nitrogen cooling system, the Omegatron probe used on the HCD is identical to the probe designed for Alcator C-Mod. The goal of this HCD experiment was to verify the theoretical calculations for the resolving power of the Omegatron, by measuring the scaling of the resolution with the electric field amplitude and magnetic field strength, and then to extrapolate the results to operation on Alcator C-Mod.

III.3.2 Alcator C-Mod Setup

The Omegatron probe is designed to operate through one of Alcator C-Mod's ten vertical ports, specifically, the port designated F-Top. The vertical port is a teardrop shape that has a 3.0 inch diameter clearance at one end, as shown in Figure III.8. The Omegatron is inserted through the port, riding at the end of a 2-7/8 inch support tube, and is placed behind the limiter plates. A linear translation drive is then responsible for moving the probe vertically (up to 5 inches) into a fixed position for a given plasma discharge.

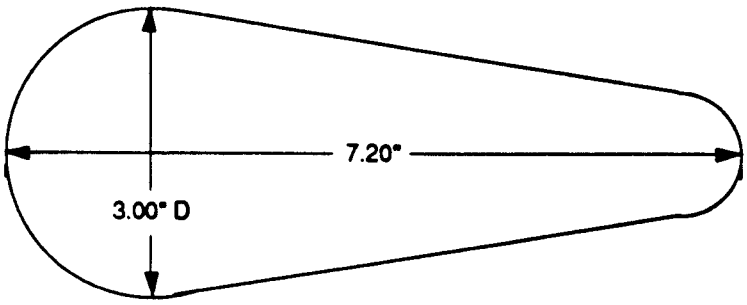

Figure III.8: Alcator C-Mod Vertical Port Footprint (1/2 Scale)

The plasma conditions the Omegatron will experience in C-Mod, will be considerably different from those present in the HCD. A review of the relevant plasma parameters is listed below in Table III.2.

Table III.2 - Operating Parameters for Alcator C-Mod

Gas:	Hydrogen, Deuterium, Helium (^{4}He, ^{3}He)
Magnets:	~4 to 6 Tesla (at Omegatron location)
Base Pressure:	~ 10^{-8} Torr
Fill Pressure:	~ 10^{-4} - 10^{-5} Torr
Pulse Length:	1- to 7- second plasma flat-top
Density (at probe):	~ 10^{18} - 10^{19} m^{-3}
Ion Temperature:	~10 - 50 eV
Electron Temperature:	~10 - 50 eV

As the probe is not intended to move in other than the vertical direction, its axis has to be aligned to the magnetic field of Alcator C-Mod. Using the results from the magnetohydrodynamic (MHD) equilibrium code developed for C-Mod allowed the selection of two angles that the Omegatron

would be aligned to; $\theta = 37^{\circ}$, the toroidal angle, and $\phi = 9^{\circ}$, the poloidal angle, with an allowed misalignment of $\pm 7^{\circ}$ on θ and $\pm 3^{\circ}$ on ϕ.[10] In Figure III.9, that geometry is demonstrated.

Finally, in Figure III.10, is a scaled schematic showing the alignment of the Omegatron probe in a cross-section of the Alcator C-Mod vacuum vessel. Here, the Omegatron is shown aligned to a magnetic flux surface for a diverted plasma shot, a typical mode under which the Omegatron will operate.

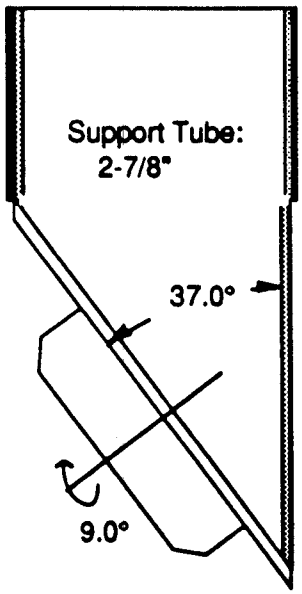

Figure III.9: Alignment of Omegatron to Alcator C-Mod Magnetic Field

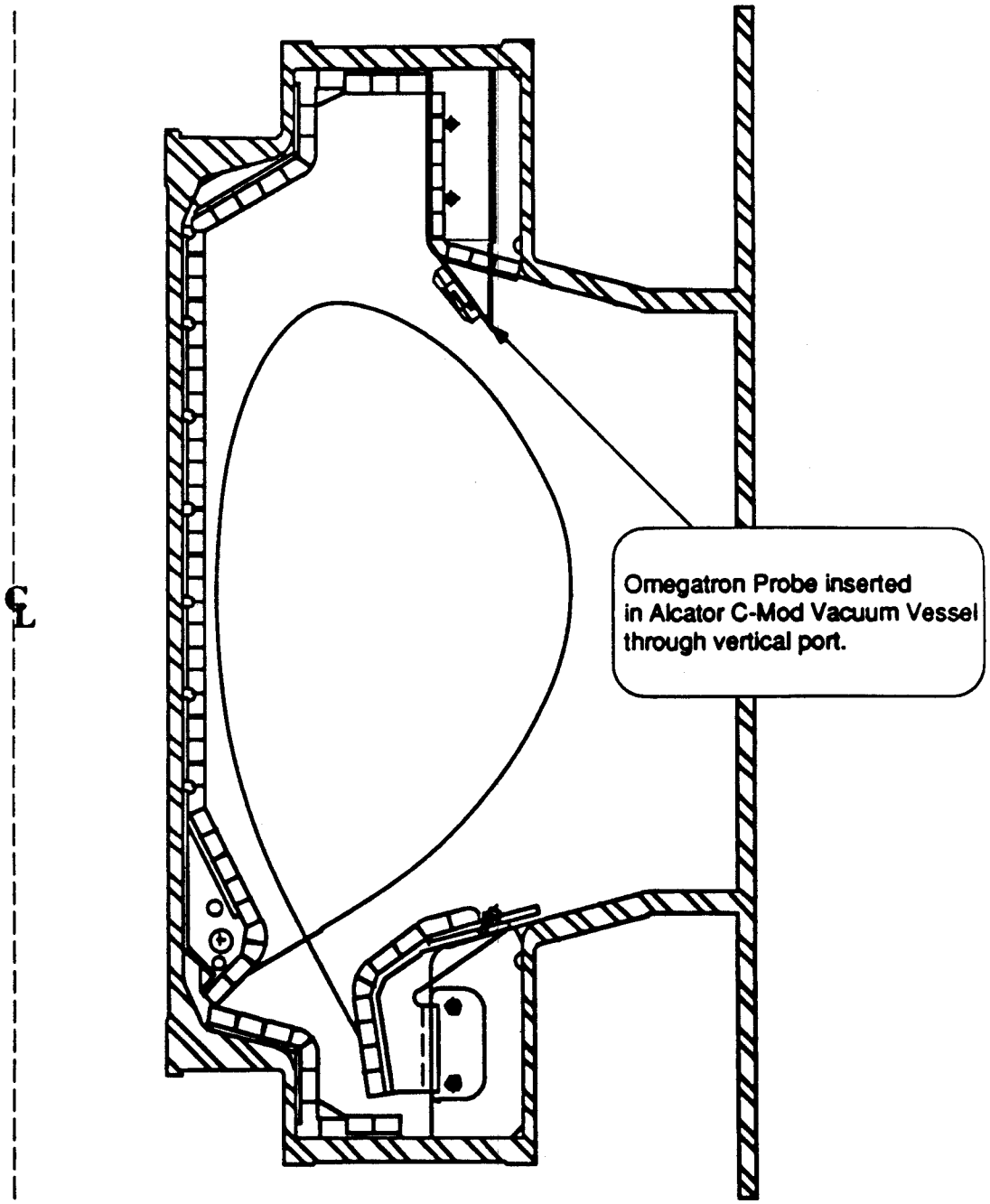

Figure III.10: Alcator C-Mod Vacuum Vessel with Omegatron Probe

III.4 Omegatron Electronics

The Omegatron electronics were perhaps the most time-consuming, yet, most valuable component of the probe's development. From work performed with similar types of edge plasma analyzers,[11,12] the expected current level to be detected by the Omegatron is on the order of a nanoampere or less. Therefore, the circuitry had to be robust enough to collect such small, real-time signals on top of voltage fluctuations with a nominal 5 kHz bandwidth.

Similarly, the circuitry for the Langmuir probes also had fairly strict constraints. Those circuits had to handle very large currents, possibly up to 10 A, without saturating while in electron collection mode, and still be able to resolve the micro-ampere level ion saturation currents. Each of these circuits is reviewed below.

III.4.1 Omegatron Boards

The Omegatron boards are basically low current ammeters. The boards have a nominal 5 kHz bandwidth and can resolve from ~800 pA to a maximum detectable current of 10 μA. The boards are limited at this current because their output voltage is 5 volts, the limit allowed for the computerized CAMAC data collection system. With additional pre-input filtering, the bandwidth is reduced, but the signal to noise ratio is improved. On the HCD, with a 10 millisecond pre-filter the minimum detectable signal was ~ 500 pA. The basic layout for the operation of the circuitry is shown in the block diagram, Figure III.11. For a detailed schematic, refer to Appendix A.

The circuit works in two main stages. First, some desired programmed waveform is placed in the V/40 input and mixed with some direct V signal input. The V/40 input is usually some ramp or waveform to be applied to the particular grid. The V input is some unknown input, such as the signal on the slit or the combined signal on previous components, that it is necessary to float on top of to reduce capacitive coupling effects. These signals are mixed and are monitored, and sent as reference potential (i.e., the separated ground plane), for the signal on the particular component.

The next stage involves the signal arriving from a grid or a collector

plate. The actual current signal is converted to a voltage by V/I = 10^6. The "virtual" signal is just a capacitor network designed to compensate for the capacitive coupling between the various probe components. The two signals are looked at differentially through a balanced network that includes some first stage amplification. The signals are then low pass filtered, at 5 kHz, by 7 pole Bessel filters, and then sent to a final stage of amplification. In the end, the output signal voltage, V_{out} corresponds to a current,

$$I = \frac{2\,V_{out}}{10^6\,(Gain)}. \qquad (3.6)$$

The gain is the final amplification performed by the chosen output channel of the circuit, either 1, 10 or 100.

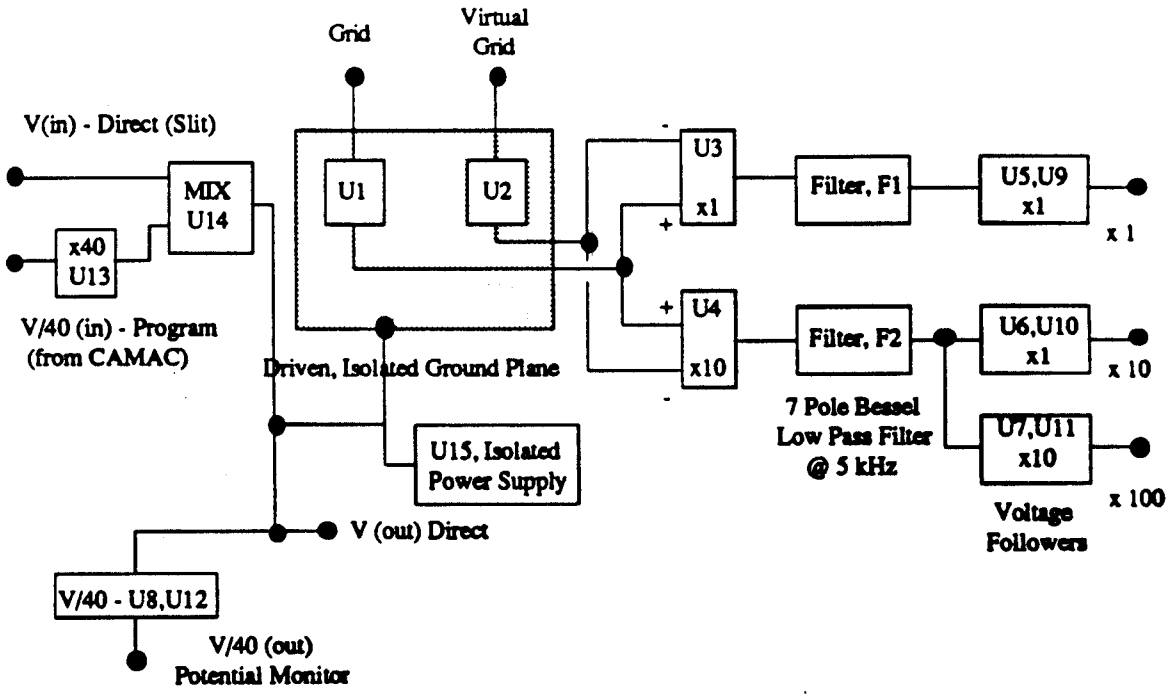

Figure III.11: Omegatron Circuit Block Diagram

III.4.2 RF/Collector Plate Electronics

Of particular interest is the method by which signals from the RF plates are collected. The original idea was to have a sinusoidal RF wave launched by a signal generator, then amplified, and sent to the RF plates via a transformer. The transformer would be a 2:1 center-tapped output.

The signal to the RF/Collector plates would travel down a pair of identical, 50Ω coaxial cables and terminate on the RF load resistors (4 - 400Ω resistors in parallel) which act as a 100Ω load. The current collected would be seen at the center-tap of the transformer secondary, which should be a node for the RF, provided the system were completely symmetric; a schematic for this system is shown in Figure III.12.

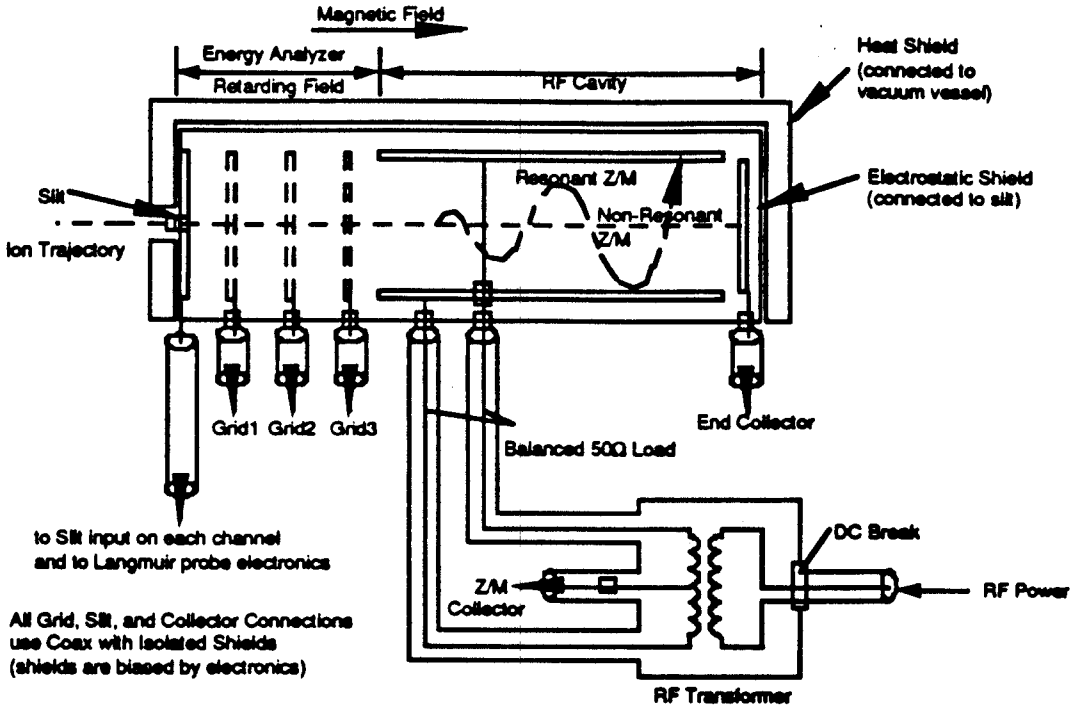

Figure III.12: Signal Collection on Omegatron Components

However, during actual testing, it was discovered that there exists both resistive and capacitive coupling between the primary and secondary leads of the transformer. This appears as a combination of a DC offset and some leakage current. A remedy for this situation was to place a 1:1 transformer before the input to the RF transformer. The secondary of this 1:1 transformer, and the primary of the RF transformer were then allowed to float to whatever potential was necessary to compensate for the resistive coupling. However, the capacitive coupling remains, and, is in some ways worse, as there is the additional capacitance due to the 1:1 transformer.

A proposal for a more permanent solution to this problem is being considered. It would involve first feeding the RF power into a 2:1 transformer.

The secondary of this system would then feed into the primary of a center-tapped 1:1 transformer. This center tap would be at the same potential as the RF Plates. The secondary of the 1:1 transformer would then supply the RF power to the RF plates. It too would be center-tapped, and the collected current would be detected at that point. Placing both center taps of the 1:1 transformer at the same potential should eliminate the major source of noise in the system, the leakage current due to capacitive coupling. The schematic for this design is shown, below, in Figure III.13.

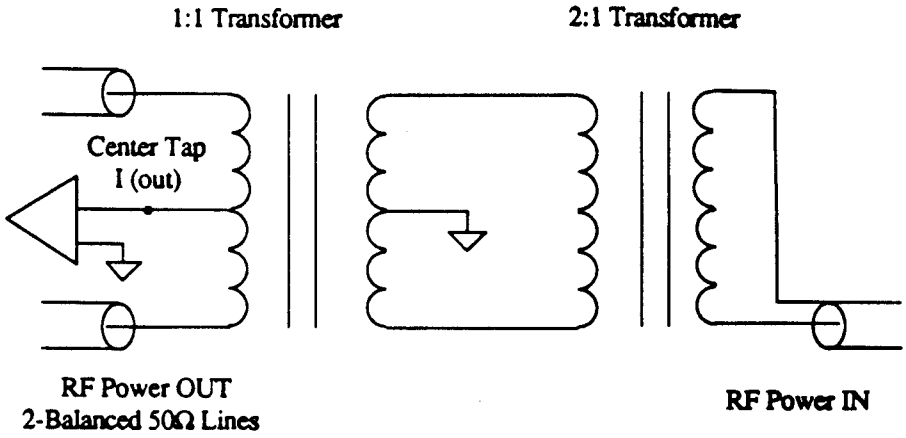

Figure III.13: Revised RF Power Transformer Setup

III.4.3 Langmuir Probe Boards

The electronics that are used as the Langmuir probe circuitry were originally designed by Dr. Brian LaBombard for the Alcator C-Mod Flush Mount Probes; these are an array of Langmuir probes that will look at the heat and particle flux to the walls of Alcator C-Mod. The use of this circuitry for the Omegatron experiment on the HCD was their first in-plasma operation. The basic layout of the Langmuir probe circuit is shown in the schematic in Figure III.14; the full circuit diagram is in Appendix A.

The probe is programmed with some waveform, common to all the Langmuir probes in the system, with the Sweep inputs, A and B. The black box of the circuit is basically a set of TTL controls that places a limit on the current to be collected. A set of relays changes the value of the measurement resistor from 1/2 Ω up to 200 Ω; this corresponds to a maximum allowable current of up to 10A with the 1/2 Ω resistor. The circuit is designed

to have a very large bandwidth ~1 MHz; consequently, a capacitive compensation network was included to mirror the capacitance on the Langmuir probe case and cabling. Additionally, to prevent the circuit from damage due to very large currents, a current monitor was built to look at the collected current. Once an over-current condition is met, this monitor will disconnect the probe. The probe remains in this over-current state for up to 90 seconds before reactivating the circuit. In operations on the HCD, the circuitry responded excellently. There was a slight problem with the offset of the signal due to the fact that the boards had not been completely tuned.

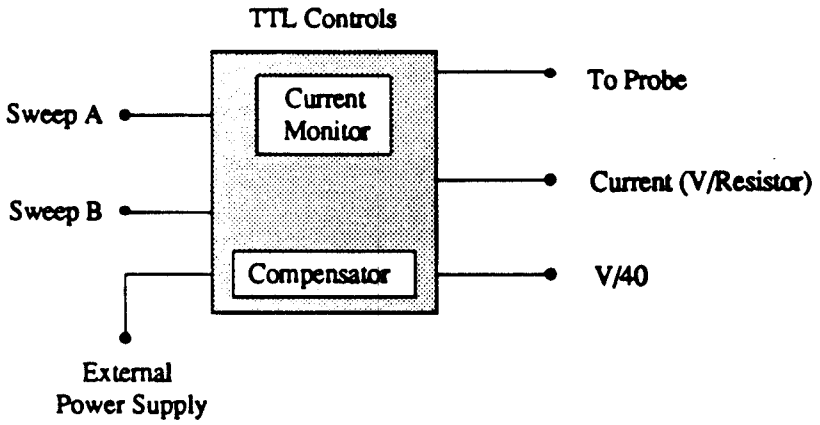

Figure III.14: Langmuir Probe Schematic

[1] Hutchinson, I.H., Principles of Plasma Diagnostics, Cambridge University Press, 1987.

[2] Sears, F.W., M.W. Zemansky, H.D. Young, University Physics, 6th Edition, Addison-Wesley Publishing, Reading, MA, 1984.

[3] Weast, R., ed., CRC Handbook of Chemistry and Physics, 70th Edition, 1989-1990, CRC Press, Boca Raton, FL, 1990.

[4] Sanford Process Corporation, Company Literature, "Technical Bulletin No. 102", Natick, MA.

[5] Wan, A.S., et.al. "Janus, a Bidirectional, Multifunctional Plasma Diagnostic", Review of Scientific Instruments, Vol. 57, No. 8 (1986).

[6] Wan, A.S. "Ion and Electron Parameters in the Alcator C Tokamak Scrape-Off Region", Ph.D. Thesis, Massachusetts Institute of Technology, 1986.

[7] Wan, A.S., Private Communications on Gridded Energy Analyzer Designs, 1992.

[8] Hutchinson, I.H., Principles of Plasma Diagnostics, Cambridge University Press, 1987.

[9] Hsu, T.C., "The NED Hollow Cathode Discharge Machine", Course Notes for Plasma Laboratory Course 22.69, Nuclear Engineering Department, Massachusetts Institute of Technology, 1992.

[10] Hakkarainen, P., "Standard MHD Equilibria Code for Alcator C-Mod", M.I.T. Plasma Fusion Center, 1990.

[11] Wan, A.S., et.al."Janus, a Bidirectional, Multifunctional Plasma Diagnostic", Review of Scientific Instruments, Vol. 57, No. 8 (1986).

[12] Pitts, R.A., "Ion Energy, Sheath Potential, and Secondary Electron Emission in the Tokamak Edge", PH.D. Thesis, University of London, 1990.

Chapter IV: Omegatron Data Analysis

In this chapter, a presentation and analysis will be made of the data taken by the Omegatron Probe while operating on the Hollow Cathode Discharge Plasma Chamber (HCD).[1] First, a description of the Omegatron experimental setup will be made. Next, a presentation will be made of data taken while the probe operated in Omegatron Mode; that is, while the probe collected resonant particles on the RF/Collector plates. Finally, data is presented that characterizes the total operation of the probe. In this way, issues such as probe transmission, space charge limitations, and scalings of the results to Alcator C-Mod can be addressed.

IV.1 Experimental Setup

The setup of the Omegatron on the HCD was rather straightforward. The probe was positioned on the second cross (labeled "Omegatron Port" in Figure III.7) of the HCD vacuum chamber. It was aligned so that the flat of the probe, and hence the entrance slit, faced the cathode. The slit was displaced approximately 4 cm from the center of the plasma column. This arrangement is shown in Figure IV.1. The primary reason for displacing the probe from the main plasma column was to prevent the probe temperature from exceeding 100°C (as described in section III.1.1).

The three key elements in running the HCD for the Omegatron experiment are the gas feed system, the magnet system and the data acquisition system. These systems were responsible for controlling the discharge conditions and monitoring the performance of the Omegatron probe. Each of these system is discussed briefly so as to provide a complete overview of the Omegatron experimental setup.

IV.1.1 Gas Feed

Gases were introduced into the HCD by injection through the biased hollow cathode (see Figure III.7). Each gas was fed from a separate gas bottle and mixed via a set of flow meters. When pulsed with a burst of a high voltage RF signal (~ 1000 V), the gas mixture would then break-down and a plasma would form.

Due to the relatively poor Omegatron resolution (as compared to C-Mod), that the theory predicts for the HCD, it was decided that in order detect any resonance peaks with the Omegatron, relatively low mass plasma ions would have to be used (refer to Table IV.1).

Table IV.1: Omegatron Mode of Alcator C-Mod vs. HCD

Parameter (at Omegatron)	Alcator C-Mod	HCD
Magnetic Field	~ 6 T	~ 0.14 T
Electric Field	~ 90 V/cm	~ 1.5 V/cm
RF Plate Spacing	5.78 mm	5.78 mm
Resolving Frequency	~ 165 kHz	~ 122 kHz
Gas: H^+ (m=1)	f_c = 92 MHz / (f/Δf) ~550	f_c = 2.1 MHz / (f/Δf) ~17
Gas: He^+ (m=4)	f_c = 23 MHz / (f/Δf) ~137	f_c = 0.53 MHz / (f/Δf) ~4
Gas: N^+ (m=14)	f_c = 6.6 MHz / (f/Δf) ~39	f_c = 150 kHz / (f/Δf) ~1.2

From the theory, any particles more massive than ~m=14, would not be detectable in a frequency sweep. In practice, however, there is also a finite noise floor due to both plasma noise and Johnson noise in the circuitry. Therefore no signals were detectable beyond the He^+ resonance.

In running the HCD, three gas feed bottles were used: Argon, which was used to start the discharge as it forms a plasma very easily; Hydrogen, used as the primary species of interest (H^+ and H_2^+); Helium, as a second, impurity species in the Hydrogen discharge. In practice, once the plasma was started, the Argon flow would be reduced and then either the Hydrogen or Helium would then be added. It was discovered that a very small flow of Argon had to remain in the gas flow in order to maintain the discharge. However, due to the Argon's large Larmor radius ($r_{L\text{-}Ar} \approx 7$ mm $> 2R_0$), it should appear as a background signal to all of the Omegatron mode measurements. For most of the HCD operations, the plasmas used were either a Hydrogen/Argon mix or a Hydrogen/Helium/Argon mix.

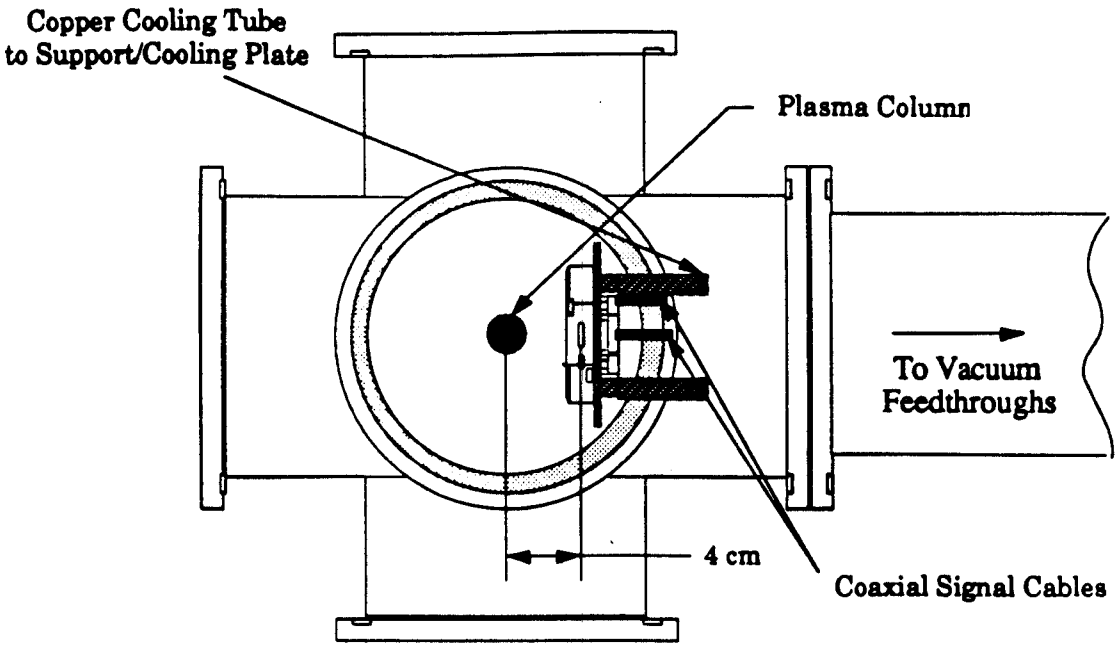

Figure IV.1: Arrangement of Omegatron in HCD Vacuum Chamber
(View: Looking Towards Anode End of Chamber)

IV.1.2 Magnets

In order to increase the resolution of the Omegatron, an additional power supply was added to the HCD magnet system (refer to Figure III.7). This increased the field strength around the Omegatron from the nominal 600 Gauss to ~ 1400 Gauss. In Figure IV.2, a mapping is shown of the measured magnetic field strength around the Omegatron.

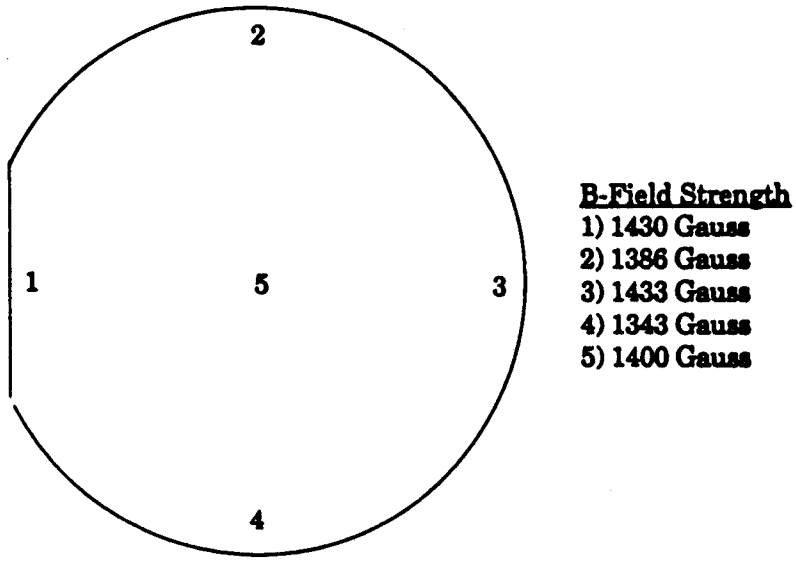

Figure IV.2: Magnetic Field Map at Omegatron Surface

Although there is a ripple in the strength of the magnetic field, it did not significantly affect the resonance conditions in the RF cavity.

IV.1.3 Data Acquisition

The data for the experiment was taken on a Hewlett-Packard, HP Vectra personal computer using the Hewlett-Packard data acquisition package, PC Instruments.[2] A front end user program was written so as to control the acquisition hardware and to create a text-based output file of the data. The procedure for taking data was to record x- (sweep voltage) and y- (current signal) signal for a single probe element (e.g., the slit, grid, RF plate, etc.) and output the data. For a single shot or dataset, the conditions on the probe would be established, and data would be taken from the relevant components.

IV.2 Omegatron Mode Data

In Omegatron mode, the RF/Collector plates had an oscillating electric field applied to them so as to "spin-up" resonant particles. There was a rather small window in which to achieve this mode of operation. It required the following characteristics:

- The slit bias must be greater than the floating potential ($V_d > V_{fl}$) so as to allow some electrons into the probe to neutralize an ion space charge barrier between the Entrance Slit and Grid 1.

- Voltages on Grids 1,2, and 3 are equal and less than 0 V ($V_{GR} \equiv V_{G1} = V_{G2} = V_{G3} < 0$ V); where 0 V corresponds to the HCD vacuum chamber ground, which was typically a few volts more negative than the local floating potential.

- The bias on the RF plates (V_{RF}) was set to be more positive than the slit, typically near to the plasma potential, $V_{SL} < V_{RF} \leq V_{Plasma}$.

- The bias on the End Collector (C/R) has to remain more negative than that of the RF Plates, $V_{C/R} \leq V_{RF}$.

However, once these characteristics were known, it became quite easy to reproduce the conditions to obtain this mode of operation.

Listed in Table IV.2, are the relevant conditions that were used in making measurements during Omegatron Mode operations (see also Figure I V.3).

Table IV.2: Omegatron Mode Operating Parameters

Bias Voltages	
SL	Grounded (0 V)
G1=G2=G3	~ -13 V to -14 V
RF	~ 5.9 V
C/R	~ -0.8 V
RF Sweep	
30 kHz to 2.5 MHz	Nominal 4.0 V peak-to-peak RF Amplitude (2.6 V @ 2 MHz)
Vacuum	
Base Pressure	$p_0 \sim 8 \times 10^{-6}$ Torr
Gas	
Hydrogen/Argon Hydrogen/Helium/Argon	Fill Pressure: ~ 5×10^{-4} Torr
Discharge Conditions	
Plasma (Typical)	12-16 Amps @ 115-130 Volts (2-3 kW input)
Magnets	
Omegatron Magnets (2/3)	Current: 75-80 A / 1300 -1400 Gauss
Chamber Magnets (1/4/5)	Current: 35-40 A/ 600 - 700 Gauss

G1,G2,G3 - Grids 1,2,3; RF - RF Plates; C/R - End Collector; SL - Slit

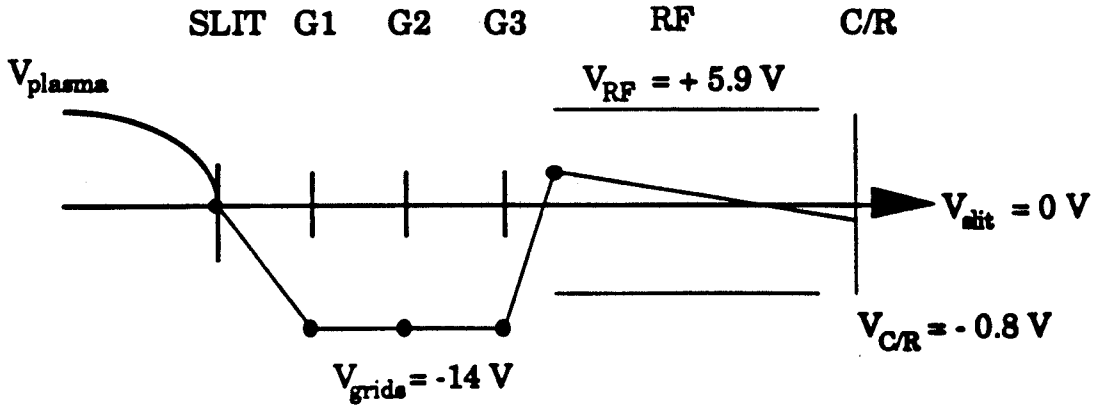

Figure IV.3: Bias Conditions in Omegatron Mode

IV.2.1 Frequency Scan Results

The Omegatron Frequency Scan consisted of looking at the currents collected on the RF/Collector plates and the End Collector while the frequency of the applied electric field was varying from ~ 30 kHz to ~ 3 MHz and the amplitude was fixed at a nominal ~7 V/cm input across the RF Plates (at the low frequency end). Due to the limitations of the signal generator used for this experiment, there was a roughly linear decrease in the amplitude of the applied RF voltage as a function of the frequency. This is shown in Figure IV.4, where there are two photographs (taken on an oscilloscope in X-Y mode) of the signals collected for a Hydrogen/Argon discharge. The x-axis represents the frequency, and the y-axis is the signal. In both photographs, the bottom-most signal is that of the applied RF voltage.

In Figure IV.4 (a), a clear resonance, the H^+ line, is observed at some frequency and appears simultaneously as an increase in the collected current to the RF plates and a decrease in current to the End Collector Additionally, in Figure IV.4 (b), a second resonance, possibly the H_2^+ line, appears to be forming when the two signals are subtracted. Unfortunately, this method of subtracting the End Collector signal from the RF Plate signal can only be performed on the oscilloscope since the data acquisition hardware was only set up to look at a single probe channel at a time.

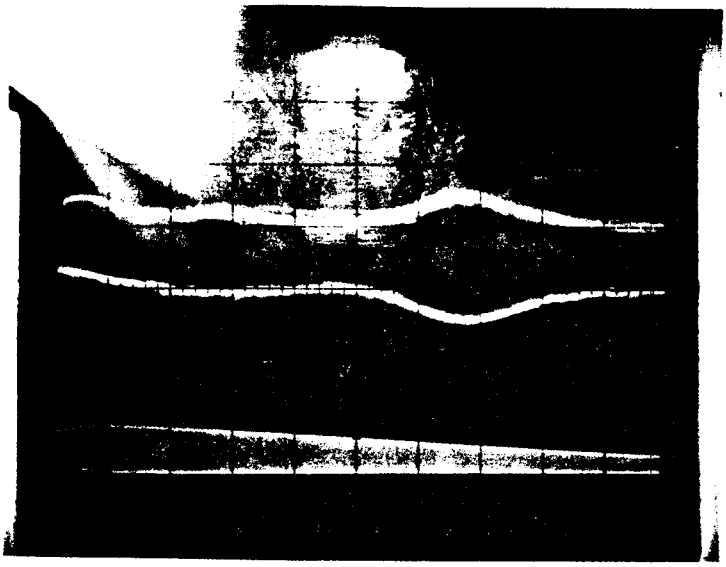

1/28/93 - 2:00 pm

Hydrogen/Argon

Signal 1: RF - 2 nA/Div
Signal 2: C/R - 2 nA/Div

Signal 3: RF Amplitude
- 4V/Div

Figure IV.4 (a) - Omegatron Signals from Oscilloscope -
RF, C/R, RF Amplitude

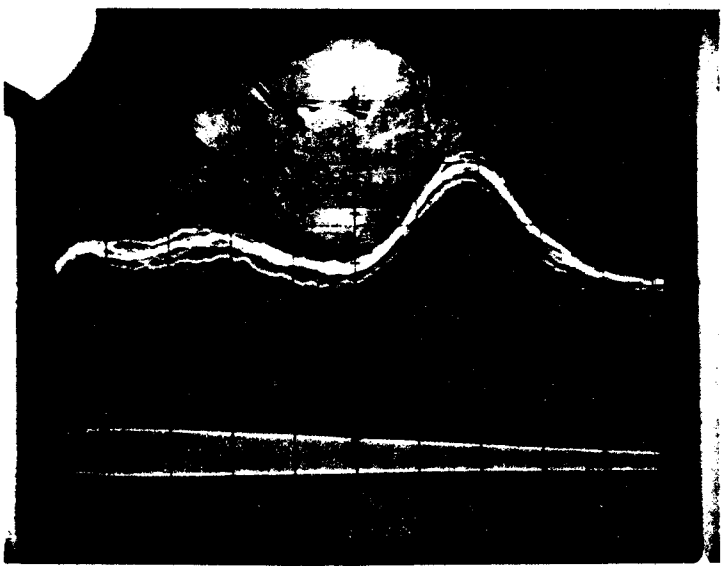

1/28/93 - 2:08 pm

Hydrogen/Argon

Signal 1: (RF - C/R)
- 1 nA/Div

Signal 2: RF Amplitude
- 4V/Div

Figure IV.4 (b) - Omegatron Signals from Oscilloscope -
(RF - C/R), RF Amplitude

In the following figures are shown some typical, processed, Omegatron mode data taken during the course of the experiment. The discharge gases are listed on each curve and all of the data was taken when the magnets were ~ 1350 to 1400 Gauss. The x-axis is frequency (Hertz), the y-axis is collected current (Amps).

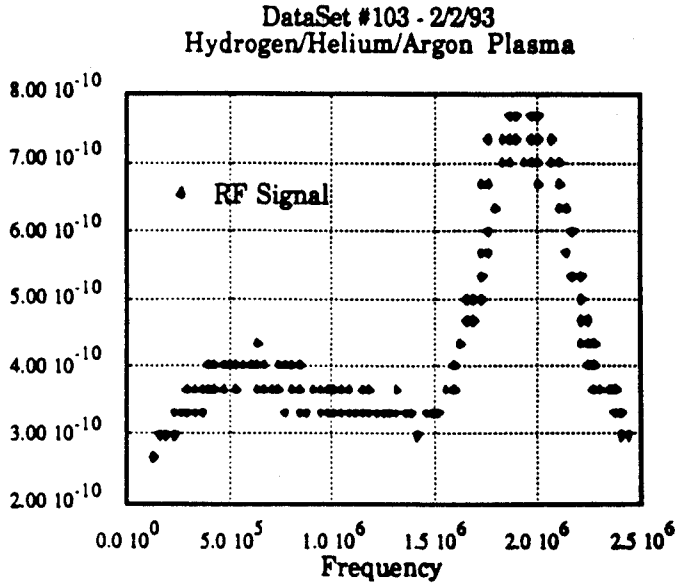

Figure IV.5 (a): Omegatron Signals - He^+/H_2^+ (~750 kHz) and H^+ (2 MHz)

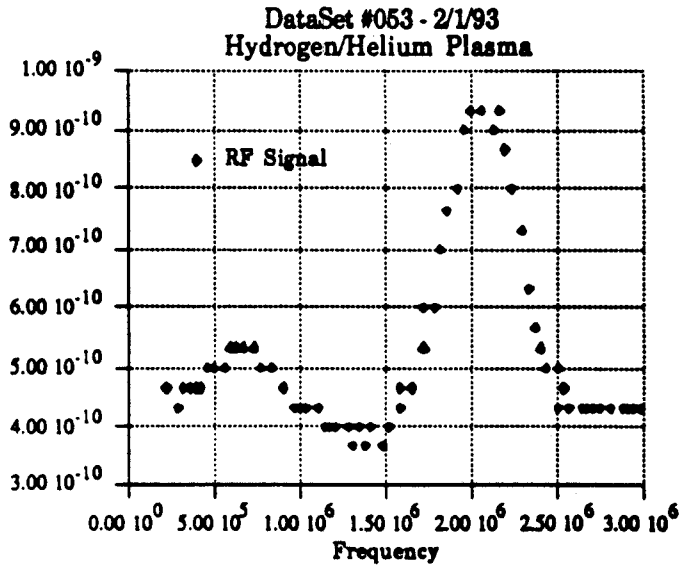

Figure IV.5 (b): Omegatron Signals - H^+ (2 MHz)

In Figure IV.5 (a), a peak is clearly observed at ~ 2 MHz, which correctly corresponds to the H^+ resonance in a 1400 Gauss magnetic field. The second peak (~ 750 kHz), may be due to the overlap of the He^+ (~ 500 kHz) and the H_2^+ (~ 1 MHz) resonances. In Figure IV.5 (b), the H^+ resonance peak is again clearly observed. However, there is an additional feature that appears at ~ 750 kHz. The plasma conditions for Dataset #053 did not include Helium gas. That feature may be some overlapping resonance with the H_2^+ resonance (possibly, H_3^+ formed in the discharge), but there is not enough information in the "Z/m" spectra to verify this. Nevertheless, the feature does appear in many of the Omegatron Mode datasets.

IV.2.2 RF Amplitude Sweep

Once the probe was able to reproduce Omegatron mode without much difficulty, it was necessary to characterize the performance of the probe by comparing the measured frequency width, Δf, to the theoretical value. From equation 2.7, the frequency width of a resonance peak, measured from the base of the peak (see Figure II.2), is,

$$\Delta f = \frac{E_0}{\pi R_0 B}. \qquad (4.1)$$

Therefore, for fixed magnetic field, B, a curve can be generated for the theoretical Δf as a function of the applied RF field amplitude, E_0.

Ideally, measurement of Δf should occur at the base of a resonance peak, but due to the presence of other resonances, it is difficult to make such a measurement. Therefore, the data for Δf was taken at the location of the full width at half-maximum (FWHM). But, for very broad resonances, even determining the FWHM becomes difficult. Figure IV.6 shows a typical broadening of the Omegatron resonance peak with increasing E/B. From Figure IV.6, it is expected that the measured value of Δf (using the FWHM technique) will be consistently smaller than the true value of Δf. Observations of typical Omegatron resonance peaks (as in Figure IV.5) indicates that the value for Δf at the base of a resonance peak will be roughly twice the measured Δf at the FWHM.

$$\Delta f\,(\text{Base}) \approx 2 \times \Delta f\,(\text{FWHM}) \qquad (4.2)$$

The scaling in equation 4.2 will be used to estimate the Δf (Base) in the

Omegatron resolution experiments.

Additionally, as the resonance gets broader, the peak will begin to become truncated as all the possible particles that can be collected, are collected, causing difficulty in determining the location of the FWHM. This effect slightly alters the slope of the curve relating Δf to the applied electric field amplitude or magnetic field strength. Consequently, the analysis of the Omegatron resolution data focus more on the scaling of the measured and theoretical values of frequency width, Δf, with the applied electric field amplitude and magnetic field strength and less on the absolute level of Δf.

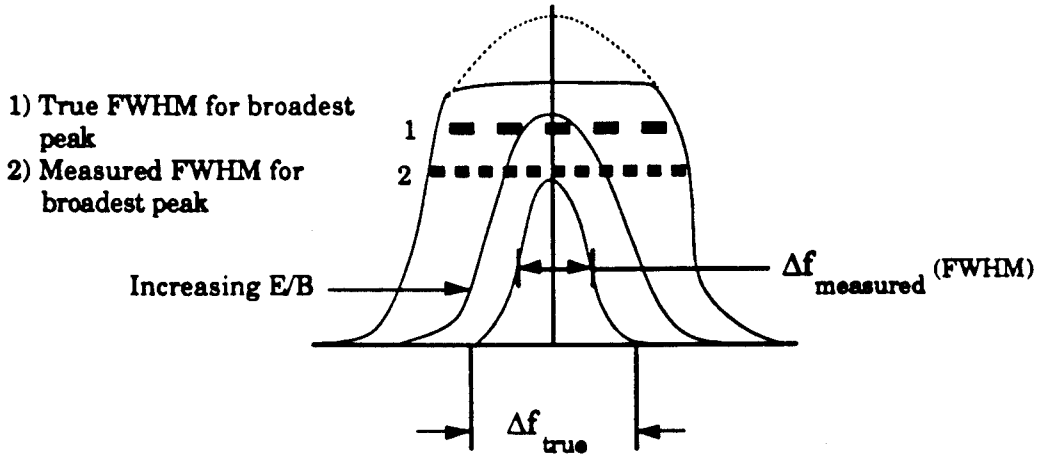

Figure IV.6: Effect of Peak Broadening on Omegatron Resolution Measurements

In the experiment performed on the HCD, a magnetic field of ~ 1350 Gauss was applied at the Omegatron location. The input peak RF voltage to the RF/Collector plates was varied from V = 1 V to 10 V at 1 V intervals. The H^+ peak was observed and Δf was measured at roughly the FWHM. The theoretical Δf was calculated from,

$$\Delta f = \frac{(0.65)*V}{2\pi R_0^2 B} \qquad (4.3)$$

where, $E_0 = (0.65*V)/(2*R_0)$. The factor of 0.65 comes from the fact that the applied RF voltage (as a function of the frequency) droops, and at ~ 2 MHz, the amplitude is about 65% of the input.

There are two figures shown for this RF Amplitude Sweep. The first, Figure IV.6, shows some of the data from for the individual RF scans. The second, Figure IV.7, shows the experimental value (Δf recorded at FWHM

and scaled to the base according to equation 4.2) and theoretical value of the frequency width, Δf, as a function of the input RF amplitude. At low RF amplitudes, a well-defined peak can be seen, but at higher amplitudes, the peaks become considerably broader. These datasets were taken with plasma conditions of, $T_e \approx 4.1$ eV, and a number density, $n_0 \approx 3 \times 10^{15}$ m^{-3} for a Hydrogen/Argon discharge, as measured with the Slit - Langmuir probe.

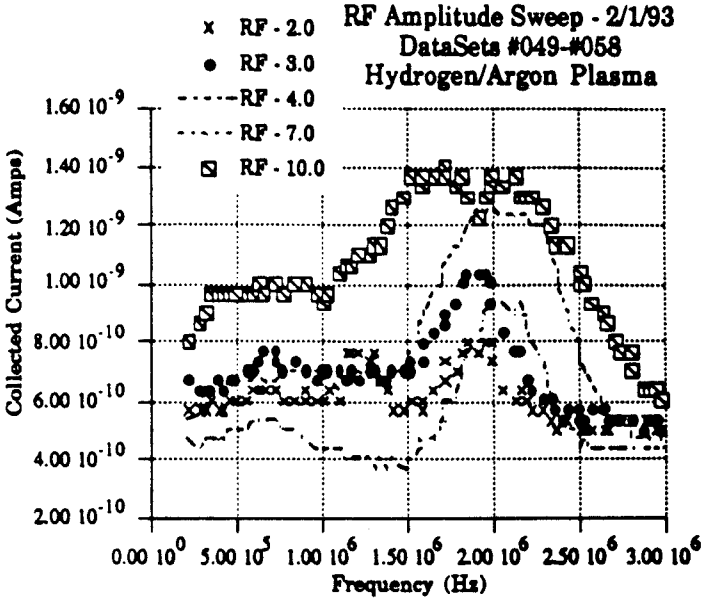

Figure IV.7: RF Amplitude Sweep - Signals on RF/Collector Plates

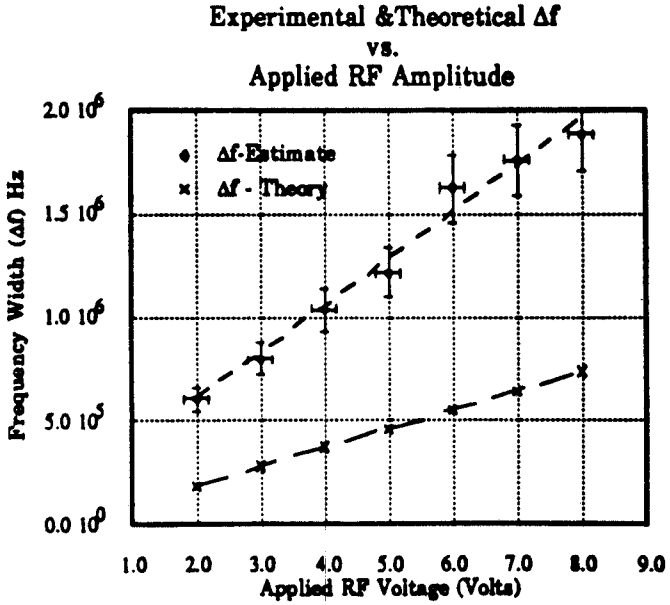

Figure IV.8: Resolution Results from RF Amplitude Sweep

As can be seen from the data in Figures IV.7 and IV.8, the resolution of the Omegatron scales similarly to the theoretical predictions. The widening of the frequency width can be clearly observed and, it scales linearly with increasing RF electric field amplitude, as indicated in equations 4.1 and 4.3. In the comparison between the absolute level of the theoretical and the experimental results, there appears to be some offset by a factor of ~ 2.5 to 3 in the two scalings for the resolution. The Omegatron experimental results give a higher value for Δf. This is may be due to some instrumental broadening of the resonance peak due to asymmetries in the applied RF electric field and geometrical deviations in the parallel alignment of the RF/Collector plates. Another contribution may be due to finite ion Larmor radius effects which can lead to higher non-resonant ion collection, and therefore, a larger value of Δf. Additionally, Wang at UCLA has reported that fairly high fill pressures (~3-5 x 10^{-4} Torr, corresponding to a neutral density ~1.5 x 10^{19} m^{-3}), similar to conditions that were present in the HCD, can contribute to broaden Δf.[3] Nevertheless, as a function of the RF amplitude, the Omegatron resolution scales as predicted theoretically.

IV.2.3 Magnetic Field Sweep

The second experiment performed in Omegatron mode was a magnetic field sweep. In this case, the current to Magnets 2 and 3, the magnets that surround the Omegatron, was varied to produce a shift in the resonance frequency location. In this way, the frequency width as a function of magnetic field strength could be examined and compared to the theoretical value, as described by equation 4.1. This experiment is vital in determining how the results from the HCD experiment can be scaled to the Alcator C-Mod environment.

There is some difficulty in performing the analysis since the amplitude of the RF electric field is not constant as a function of frequency. However, this effect can be modeled easily if it is assumed that the amplitude varies linearly with frequency. In the experiment, the current in the magnets was varied from 45 Amps to 70 Amps, at intervals of 5 Amps, and then a final reading was taken at the maximum available current to the magnets, 76 Amps. In Figure IV.9, a graph is shown of some spectra taken

during this magnetic field sweep. In it, the motion of the H^+ resonance peak can be seen shifting from ~ 2 MHz at a magnet current of 76 Amps, to lower frequencies at currents of 60 Amps and 45 Amps.

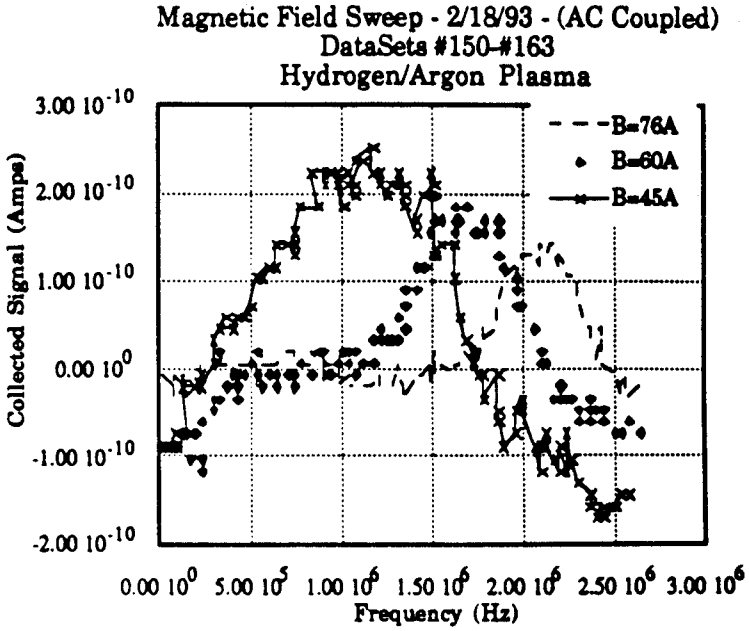

Figure IV.9: Magnetic Field Sweep Data

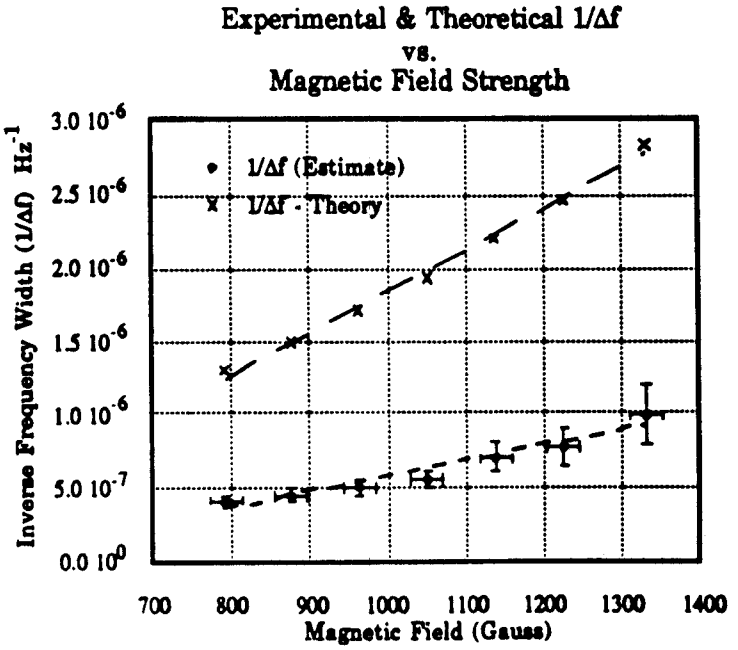

Figure IV.10: Resolution Results from Magnetic Field Sweep

The results of the Magnetic Field sweep were similar to those from the RF Amplitude sweep; the magnitude of the measured Δf was larger than the theoretical prediction, but the scaling of $1/\Delta f$, as a function of magnetic field strength, was close to the expected linear result. The similarity of the results for the scaling of the resolving frequency in both tests support the idea that the conditions that lead to the offset between the experimental and theoretical values for Δf are due to the same effects; geometrical and field (magnetic and electric) asymmetries and finite Larmor radius effects. Nevertheless, there is still generally a good scaling, i.e., a linear relationship, between the value of Δf ($1/\Delta f$) and the electric (magnetic) field strength and a difference inthe absolute levels by a factor of ~ 2.5 to 3.

I V.3 Probe Characterization

A presentation is made of the data used to characterize various elements of the total probe performance. These include capacitive coupling between components, space charge effects in the probe, and transmission characteristics of the probe components. Understanding the role of each of these characteristics, especially the space charge effects, is essential in scaling the performance of the Omegatron probe from the HCD to Alcator C-Mod.

I V.3.1 Capacitive Coupling

Due to the tight spacing of the Omegatron internal components, stray capacitive coupling will exist between these components. This stray capacitive coupling can occur when the potential on one component is changed while the potential on the other components is held fixed causing a displacement current to flow. This displacement current (I_L) is described by equation 4.4,[4]

$$I_L = C \frac{dV}{dt} \qquad (4.4)$$

where, I_L = leakage current, C = capacitance, dV/dt = changing voltage.

Since the Entrance Slit and the Shield Box are electrically connected, and the Shield Box surrounds all of the Omegatron internal components, the slit will be capacitively coupled to all of the internal components. In order to determine the magnitude of this coupling, experiments were performed that varied the potential on the slit while measuring the displacement current on each probe component. A value of the capacitance between the slit and the probe component, C, was obtained by utilizing equation 4.4. It is important to know the value of the capacitance when trying to detect very small currents while ramping the potentials on a given probe component.

These capacitive coupling experiments were performed while obtaining baseline measurements for the transmission data. Without a discharge, the voltage on the slit was ramped with a triangular wave. The signal on each component was then recorded; a flat signal indicated a voltage change with a constant slope; i.e., dV/dt = constant, as shown in Figure IV.11. When the offset was subtracted, the result yielded the capacitance, C, between the slit and the probe component.

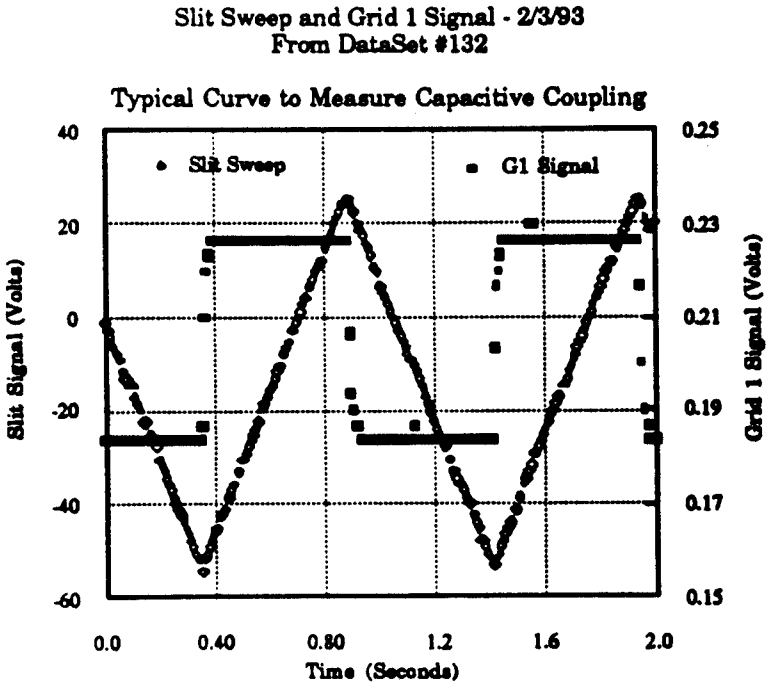

Figure IV.11: Capacitive Coupling Measurements

The final results for the capacitive coupling of the slit to the probe compo-

nents is listed in Table IV.3.

Table IV.3: Capacitive Coupling to Slit

Component	Capacitance
Grid 1	2.6 pF
Grid 2	4.0 pF
Grid 3	4.0 pF
RF/Collector Plates	29 pF
End Collector	7.0 pF

These results indicate that there is appreciable capacitive coupling between the slit and the other probe components. However, the effect of this capacitance will be experienced only if the probe components are swept in potential or if the slit is electrically floating while the other components are held at fixed potential. For typical Omegatron Mode operations, the probe will operate with both the slit and the grids held at fixed potentials or the slit will be electrically floating and all other components are biased relative to the slit; in both cases, capacitive coupling should not be a concern.

IV.3.2 Space Charge Effects

Of all of the challenges that were encountered in getting the Omegatron probe operational, the effect of space charge was perhaps the most difficult to overcome. In fact, space charge effects appear to be a dominant feature in all modes of the probe's operation. Much effort was spent characterizing the space charge effects in two regions of the probe, between the entrance slit and the first grid, and in the RF cavity. Before examining each of these cases, an analysis must be made of the physical processes that lead to the development of a space charge current limit.

IV.3.2.1 Physics of Space Charge Current Limits

As a means of definition, space charge effects become significant when the self-potential due to a number of charged particles flattens the slope of a potential difference maintained between two biased probe components. This is shown in Figure IV.12 for developing an ion space charge current limit.

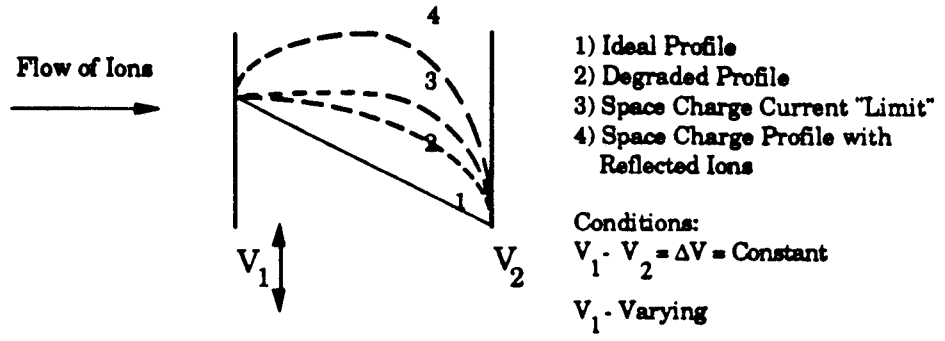

Figure IV.12: Space Charge Conditions

Assuming that a Maxwellian population of ions exists to the left of component (1), as the bias on the left component (1) is made more negative, the number of ions entering the region between components 1 and 2 increases. As the density increases (and hence the amount of positive charge), this modifies the potential profile between components 1 and 2. This continues until the potential profile becomes flat and then, eventually, peaking, restricting the flow of ions to the right by reflecting most of them back to the left.

Poisson's equation,[5]

$$\nabla^2\phi = \frac{\rho}{\varepsilon_0} = \frac{e\, n_0}{\varepsilon_0}\,, \qquad (4.5)$$

shows that as the density of the ions, n_0, increases, then the value of the self-potential will also increase; however, this increase in the self-potential will cause the ions to remain in this region for a longer time, hence, increasing the density. Consequently, the problem of space charge becomes a self-consistent problem. Attempts have been made to model the space charge problem,[6,7] however, all of these models tend to solve the problem in only one- or two- dimensions. The complete, three-dimensional problem is extremely difficult to formulate and solve. Nevertheless, this qualitative discussion serves as a good basis for examining the space charge effects in the Omegatron probe.

IV.3.2.2 Entrance Slit and Grids

The discovery of space charge problems in the probe came as a result of

trying to determine the transmission characteristics of the probe. Consequently, much of the analysis presented will be based upon data that is also used to determine the transmission of the probe.

One of the inherent difficulties with this analysis is the fact that any collected signal is the sum of two signals, an ion component and an electron component. The focus of much of the following work is on trying to unfold these two signals from a single curve. Additionally, the electrons and ions have different transmission ratios (α and β, respectively) through the entrance slit, which further complicates matters. The result is that the signal collected on any probe component is,

$$I_{col} = \beta I^{+} + \alpha I^{-} \qquad (4.6)$$

where, I^{+} is the ion current and I^{-} is the electron current (here it is assumed that I^{-} is negative).[8]

For the space charge characteristics in the front end of the probe (i.e., the grids and slit), the data from the "relative transmission" test will be examined.

In this relative transmission test, a triangular wave ramp was applied to the slit and, all other components were fixed at the lab ground (0 V). The current collected on each component was then examined (see Figure IV.13).

As can be seen in the data in Figure IV.13, there is considerable hysteresis in the collected signal, which is a clear indication that some space charge limited current had been established in the probe. Also, since the grids were all grounded, this data contains information for both ions and electrons. Several qualitative observations, based upon models for the ion and electron current collected by the probe, can be made to explain the results of this experiment.

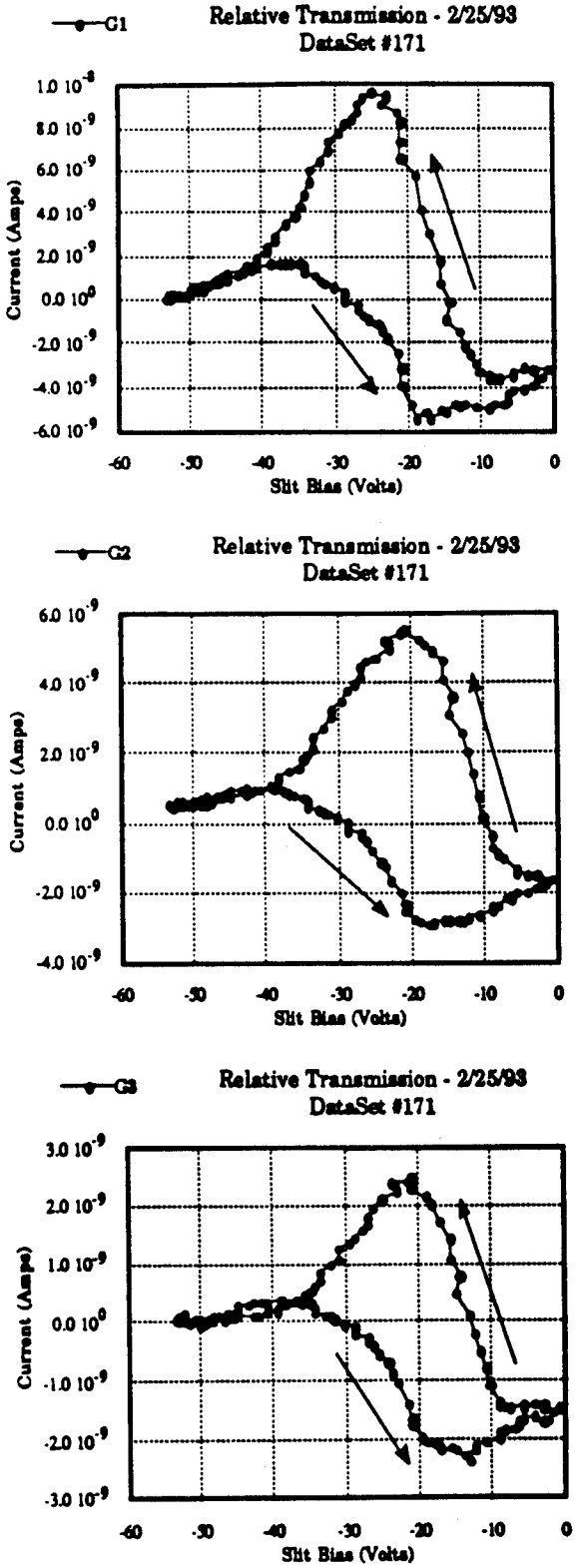

Figure IV.13: Relative Transmission Data

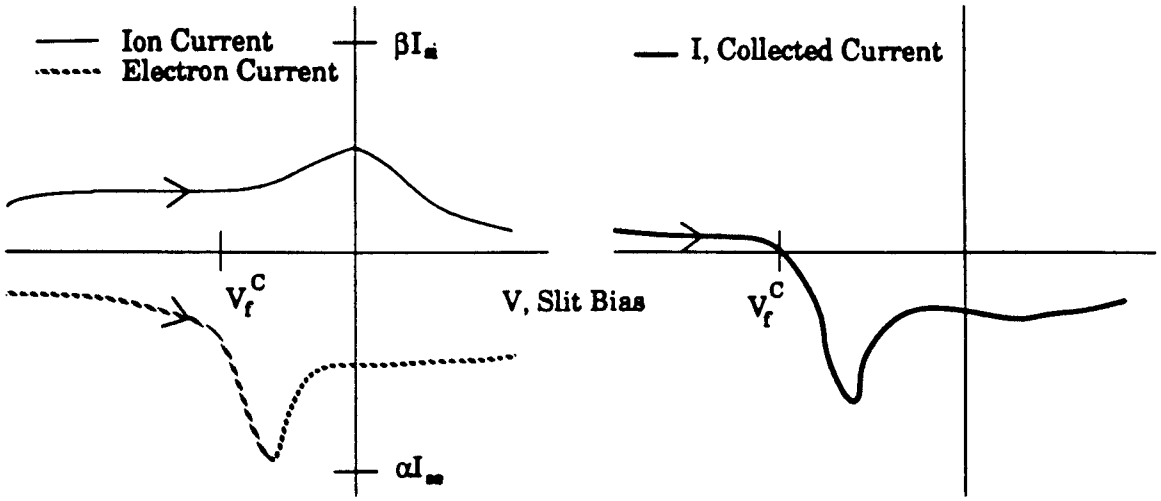

Figure IV.14: Collected Current on Probe Components accounting for Space Charge Limits - Positive Going Slit Bias

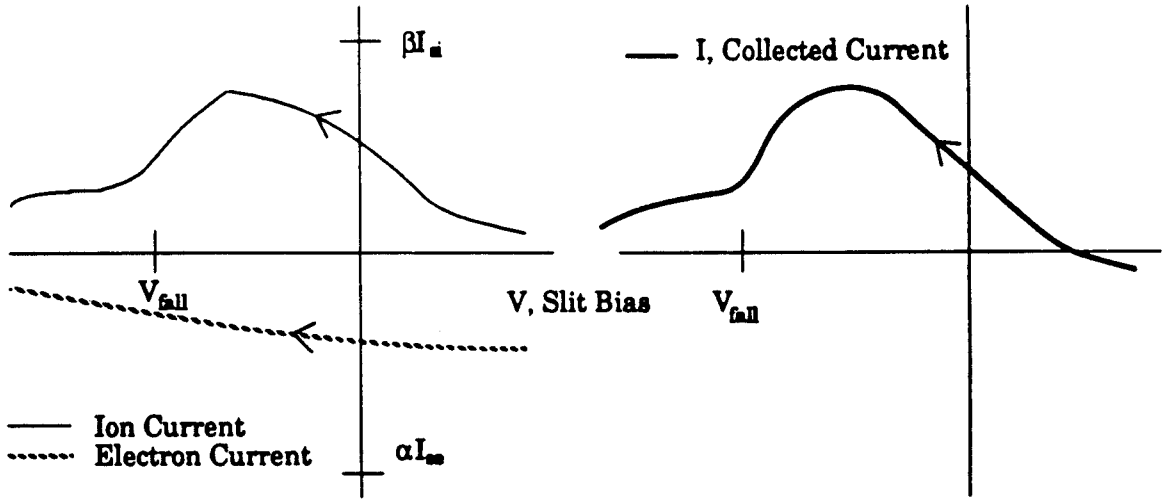

Figure IV.15: Collected Current on Probe Components accounting for Space Charge Limits - Negative Going Slit Bias

First, consider the electron signal as the slit bias is increasing positively, as shown in Figure IV.14. The electron flux starts out small, but begins to increase. As the floating potential on the probe component is achieved, V_f^C, there is a rapid, exponential increase in the electron flux, but this is quickly cut off as the electron space charge current limit is reached. The electron flux in the analyzer fails to reach the electron saturation limit in the analyzer (the label αI_{se}, is the electron saturation current multiplied by the transmission of electrons, α, through the slit; this is the maximum

electron flux to the probe component). Once the slit bias reaches very positive values, the density of electrons near the slit becomes so large that the space charge barrier begins to reflect a significant portion of the incident electron flux, reducing the electron current to the probe component. Furthermore, the potential barrier at the slit is at its maximum height to repel the electrons.

For the ion current to the probe, much depends upon the availability of electrons to neutralize the ion space charge barrier. At large negative biases on the slit, a similar effect as described above for the electrons occurs: a large ion space charge cloud forms and repels a significant portion of the ion population, reducing the ion current. As the slit is biased more positively (but still less than 0 V), the ion flux is space charge limited, but more electrons can enter the probe. Near V_f^C, enough electrons can enter the probe so as to neutralize the ion space charge. As the electrons become space charge limited, the ions can freely enter the analyzer, and hence, the ion component of the signal increases. However, once the slit bias becomes positive, the ion population decreases.

Now, as the slit starts out at a positive bias and is biased increasingly negative, the electron current does not retrace, but begins to fall further. This is due to the fact that the large electron space charge (which was established at the most positive bias) is maintained throughout much of the return path. Eventually, the space charge barrier will collapse. This occurs at the point, labeled V_{fall}; although V_{fall} may appear at a different location than where the space charge current limit was established.

For the ions, however, the situation is somewhat different. As the slit is biased negatively, more ions are drawn to the probe component. However, since the electron flux is space charge limited, the ion signal continues to grow, possibly getting close to the point, βI_{si}, the maximum ion flux into the analyzer (the product of the ion transmission factor through the slit and ion saturation current). Once the slit bias reaches the point at which the electrons are no longer space charge limited, V_{fall}, the ion component of the current rapidly decreases and the probe re-enters a condition of ion space charge limit.

These effects can be seen from the data taken for the ion and electron

transmission tests. In these runs, the probe components were biased very negatively (positively) to collect only ions (electrons). For the data taken on Grid 1, as shown in Figure IV.16, the features described above can be observed. Again, it is impossible to separate the ion and electron components, but by biasing the probe to repel one of the two species, it is possible to recover many of the key features.

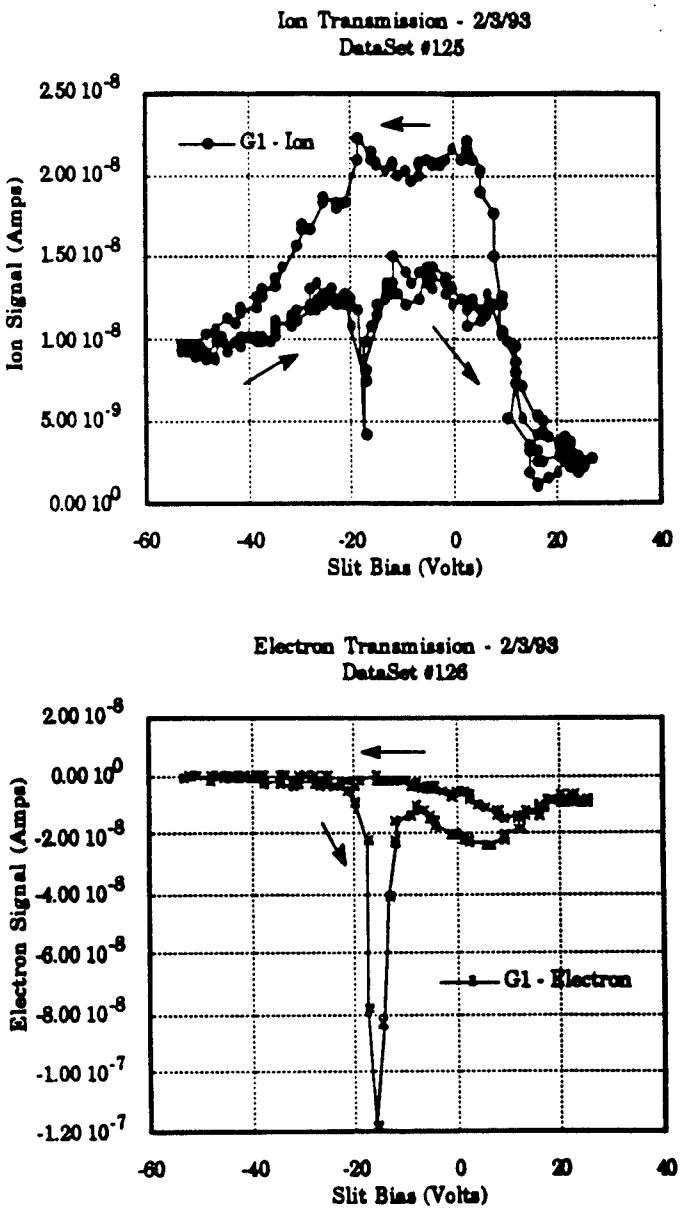

Figure IV.16: Ion and Electron Transmission Data

IV.3.2.3 RF Cavity

Characterizing the effects of space charge in the RF Cavity proved to be a far easier task than for the front end of the probe. From the design, it was expected that this region of the probe would be most likely to experience some space charge effects since it is basically a large, hollow region. Again, a qualitative description of the space charge effects will be used to describe this region.

Once particles have gotten past the front end of the probe, there is typically around one hundred nanoamperes of current available for the rest of the system. Assuming the particles are columnated by the slit, it is possible to obtain a rough estimate of the density of ions in the probe, and from this, the Debye length, λ_D.[9]

$$n = \frac{J}{e\,v} = \frac{J}{e\sqrt{\frac{2T_{||}}{m}}}$$

and

$$\lambda_D\,(cm) = 743\sqrt{\frac{T_{||}\,(eV)}{n\,(cm^{-3})}} \qquad (4.7)$$

where, J = current density and $T_{||}$ = parallel energy. Using, J ~ [75 nA/(2*Slit Length*R_{Larmor})] ≈ 0.004 A/m^2 and $T_{||}$ ~ 2.5 eV, yields results of n ≈ 1.07 x 10^6 c m^{-3}, and λ_D ≈ 1.17 cm.

When the ions reach the RF cavity (whose dimensions are 4.06 cm long x 5.78 mm high), the parallel scale length of the RF cavity, L_{RF}, is considerably larger than the ion Debye length, $L_{RF} > \lambda_D$. Consequently, an ion space charge limited condition will exist. This is apparent as the bias on the RF/Collector plates is varied while the biases on Grids 3 and the End Collector are held fixed, corresponding to Omegatron Mode collection, V_{G3} = -14.7 V and $V_{C/R}$ = -3.3 V.

In Figure IV.17, the plots of the collected current on Grid 3, the RF/Collector Plates, and the End Collector are shown as functions of the bias on the RF plates. It is expected that as the RF plates are biased negatively, they should collect more ions, Grid 3 collection should stay roughly

constant and the End Collector should collect fewer ions. However, the observed data presents a different result.

[It should be noted that because of the low magnetic field in the HCD, a negative bias on the RF/Collector Plates of a few volts, is sufficient to impart ions with a large enough Larmor radius to be collected. For this reason, in Omegatron Mode, the RF/Collector Plates are biased slightly positive (~ 5.9 Volts, as shown in Table IV.2).]

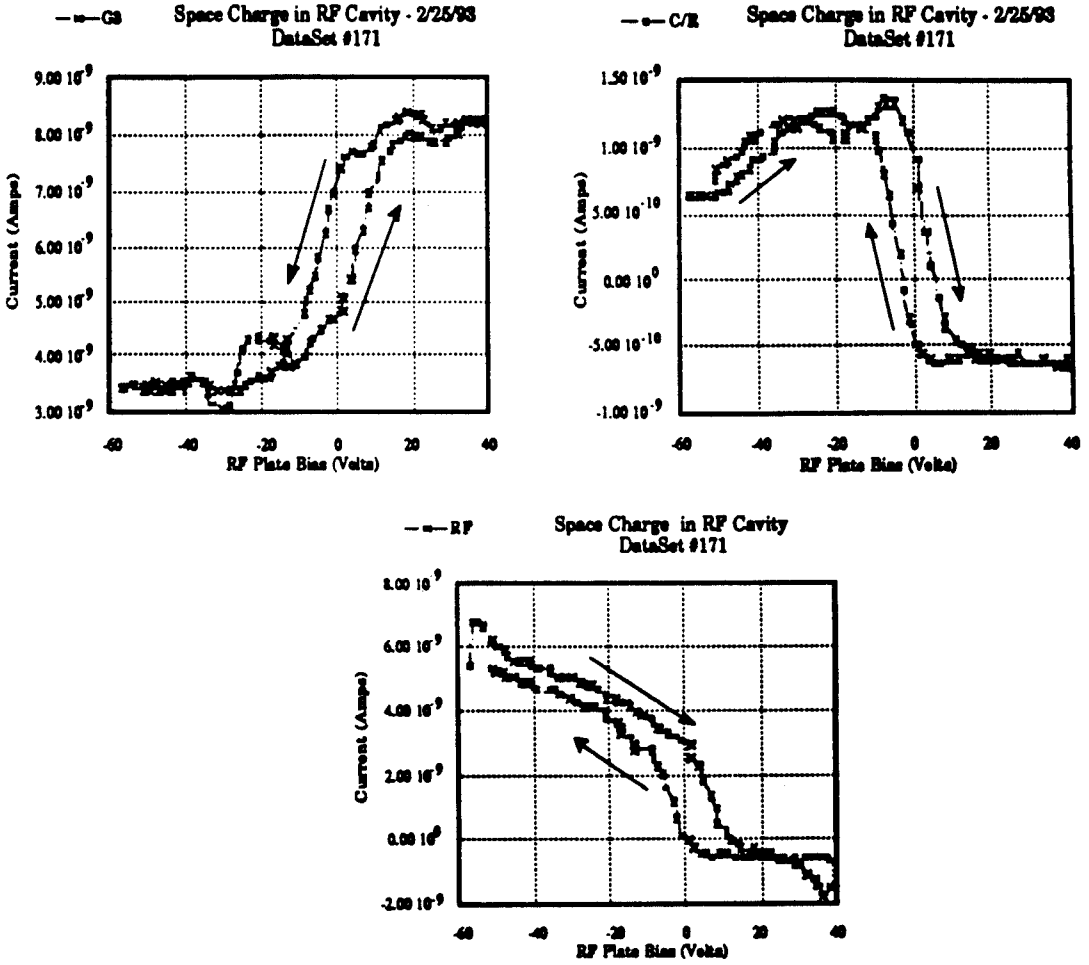

Figure IV.17: Space Charge Characteristics in Omegatron RF Cavity

The End Collector (C/R) shows a marked increase, followed by a slow decrease, in the collected signal with decreasing bias. Grid 3 shows a significant decrease in its signal. This may be explained by the presence of a large ion space charge cloud between Grid 3 and the RF Plates. As the RF

plates are biased more negatively, they will draw more particles away from the cloud and reduce the space charge barrier. But this will also allow more particles to flow through the RF cavity and get to the End Collector, hence both components will experience an increased ion signal. At the same time, since the space charge barrier is being reduced, fewer particles will be reflected away from the RF cavity, back towards Grid 3, and so its signal level will be reduced. Once the RF bias becomes negative enough (around $V_{RF} \approx -5$ to 0 Volts) to dissipate the space charge problem, then the End Collector signal will be reduced since ions entering the RF cavity will be preferentially attracted to the RF plates. Similar to the previous arguments describing hysteresis effects, it is observed that a space charge current limit is established at the most positive RF Plate biases. The retrace shows the characteristic delayed reset indicating the removal of the space charge cloud.

This completes the characterization of the space charge limits in the Omegatron probe. It is clear that space charge problems can perturb the distribution function of particles entering the probe as well as reduce the detectable signal level. This may affect operations on Alcator C-Mod, but there are several competing factors. First, the density will be considerably higher in the C-Mod edge plasma, ~ 10^{18} to 10^{19} m^{-3}, which will reduce the Debye length, but increase the overall available signal level. Also, the higher magnetic field (by a factor of at least 50) will force the particles to be more columnated, and much the higher ion temperatures, ~ 10 to 50 eV, will act to alter the Debye length. In the end, it is difficult to estimate how "bad" the space charge problems will be when the Omegatron is operating on Alcator C-Mod. As a final comment, it is known from work using the Janus gridded energy analyzer[19] probe on Alcator C, upon whose grid design the Omegatron is based, that space charge problems were not significant in its operations; this gives some hope that operations on C-Mod will give similar performance.

I V.3.3 Slit Transmission

As demonstrated in the previous sections, unfolding the individual ion and electron current signals can be a rather daunting task. This compli-

cates the determination of the ion and electron transmission characteristics of the Omegatron. Further, the presence of space charge limitations adds to the difficulty in assigning a precise value or meaning to the transmission.

A model is presented for determining the relative ion to electron transmission ratio, and, an estimate will be made for the individual values of ion and electron transmission in the Omegatron.

IV.3.3.1 Relative Ion and Electron Transmission Through the Slit

The relative transmission experiment was vital in determining the ratio of ion to electron transmission (β/α, as defined in equation 4.6) through the slit. Following the method described by Guy Matthews in his Doctoral Thesis,[11] the slit was ramped with a triangular wave and all other probe components were grounded to the lab ground (0 V). The curves for the data collected for this experiment are shown in Figure IV.13.

Using equation 4.6, it is possible to determine the ratio of β/α when the collected signal on a component, $I_{col} = \beta I^+ + \alpha I^-$ approaches zero; that is, when the probe component is at its floating potential. If the ion and electron currents to the slit are modeled as Langmuir probe currents,[12, 13] then,

$$I^+ = I_{si} \equiv I_0$$
$$I^- = I_0 \exp[\,(V - V_f^S)/T_e\,] \qquad (4.8)$$

where, V_f^S is the floating potential of the slit and, V is the bias voltage on the slit.

When the floating potential of the component is achieved, $V = V_f^C$, the ion to electron transmission ratio becomes,

$$\beta/\alpha = \exp[\,(V_f^C - V_f^S)/T_e\,]. \qquad (4.8)$$

From the data taken, it is observed that the floating potential for the grids occurs at roughly the same point for all grids, $V_f^C = -29.0 \pm 0.5$ V. This yields two pieces of useful information: first, the value of the floating potential of the probe components, and second, since all grids have the same floating potential, that the transmission of electrons and ions is roughly equal through each grid. Using the slit as a Langmuir probe, gives the

electron temperature, slit floating potential, and density of particles just outside the Omegatron entrance (as shown in Figure IV.18).

Using the measured values of $V_f^S \approx -4.75$ V and $T_e \approx 4.97$ eV, gives an estimate for the value of $\beta/\alpha \approx 0.0076$; this implies that the ion transmission through the slit is ~ 0.76% of the electron transmission. Again, this is not an absolute measure of the transmission since the individual transmissions of the electrons and ions is still unknown, rather, it gives the weighting of the ion signal relative to the electron signal.

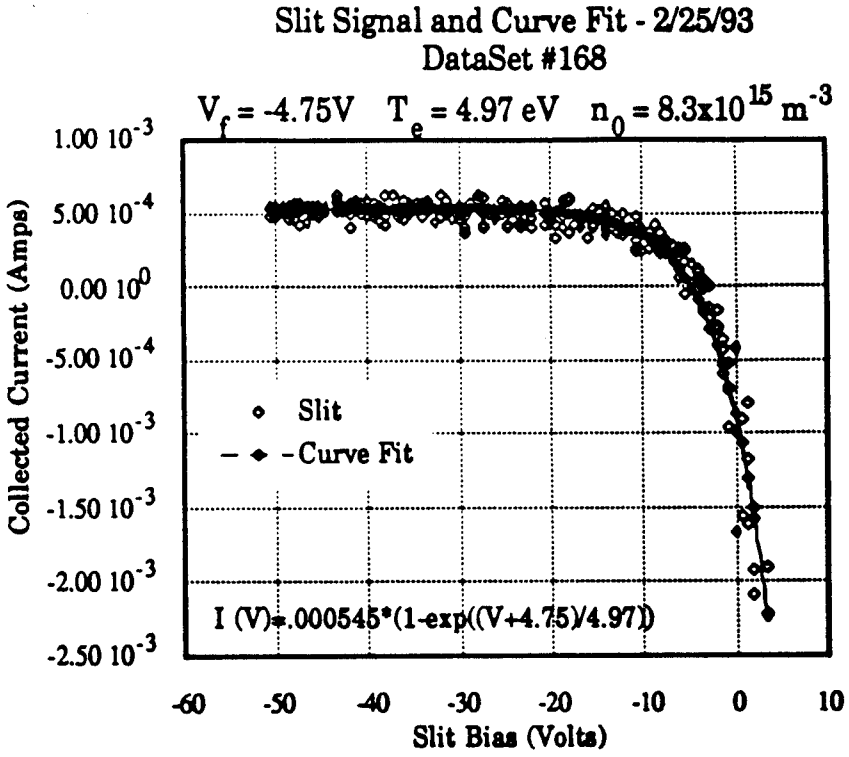

Figure IV.18: Slit - Langmuir Probe Data

Using this information, an attempt will made to compute the absolute level of the electron and ion transmission through the entrance slit under the assumption that the relative transmission ratio remains constant at all slit biases.

IV.3.3.2 Ion and Electron Transmission Through the Slit

For the same plasma conditions as the slit data (Figure IV.18) and

relative transmission data (Figure IV.13), an electron transmission dataset was also taken; see Figure IV.19 for typical curves from this dataset. This setup maintains the same triangular bias waveform that is applied to the slit, however, the probe components are biased progressively more positively, so as to repel the ion population; those biases are listed in Table IV.4. The objective is to record the electron current on each component, at the same bias voltage on the slit, and compare these values to the total flux of electrons to the slit to get the electron transmission through the slit.

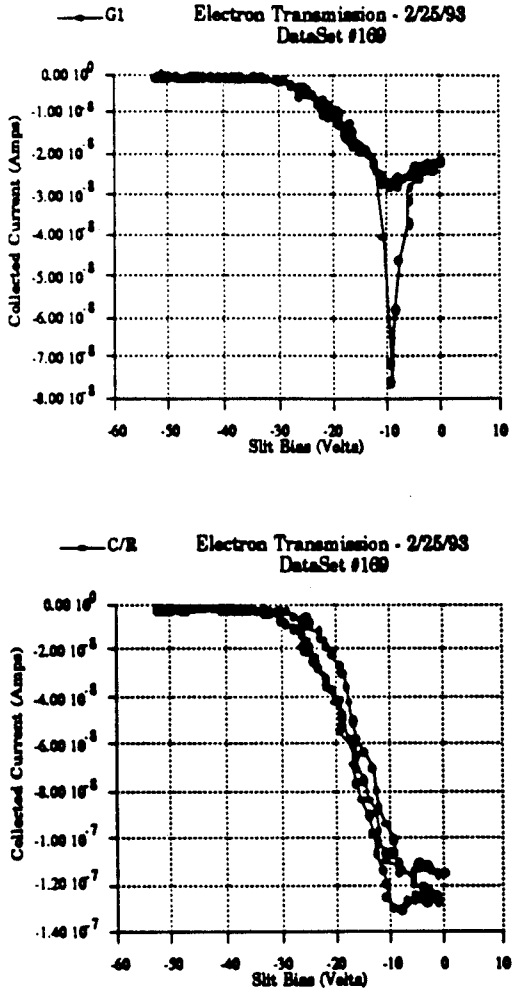

Figure IV.19: Electron Transmission Data

The first step is to select an observation point where it is established that there is a significant electron flux, and, the electrons are not space charge limited. This would be a point along the positive going part of the

current signal that was between the floating potential and the maximum electron signal. The observation point used for the calculations is at V = -20 V. At this point, the data in Figure IV.18 gives a maximum electron current through the slit of ~ -103 nA and a maximum ion current of ~ 2.1 μA; where the maximum current, I_{max} is,

$$I_{max} = I_{Aperture} \text{ (Area of Slit/Area of Aperture)} \qquad (4.10)$$

The recorded values for the current collected on each probe component are also presented in Table IV.4. It should be noted that secondary electrons can be generated, due to the impact of incoming electrons on the tungsten grid meshes. This would cause a redistribution of the net electron current between the probe components. However, the total electron current would remain constant.

Table IV.4: Collected Currents during Electron Transmission Test

Component	Bias (Volts)	Current (nA)
Grid 1	50.6	-9.3
Grid 2	55.5	-12.8
Grid 3	60.0	-11.5
RF Plates	64.6	-4.0
End Collector	70.3	-39.9
		Total: -77.5

Before a transmission can be calculated from this data a compensation must be made for ions that may have been collected. If a perfect electron transmission is assumed, this implies that ~0.0076 x $I_{max\text{-}ion}$ is the available number of ions that could be collected, which is ~16 nA; this is the possible error in the value of the total electron current above. The value of the electron transmission through the slit, α, is then computed as a range from,

$$\alpha = (I_{meas} + I_{error})/I_{max\text{-}electron} \rightarrow (I_{meas})/I_{max\text{-}electron} \qquad (4.11)$$

which yields a value of α ranging from 0.91 to 0.75. This gives a corresponding range of values on β of 0.0069 to 0.0057.

Unfortunately, performing a similar test with the probe in an ion transmission mode yields inconclusive results in attempting to calculate an independent value for the ion transmission, β. While the bias on the slit is

positive going, the probe remains mostly in an ion space charge limited condition, and, beyond the floating potential point, the electron contribution to the collected current becomes space charge limited, and therefore at an unknown level. A further complication is, due to the different space charge conditions in the probe, the apparent transmission appears to be a function of the slit bias voltage. Repeating the same process as above at V = -25 Volts and V = -15 Volts, gives a rough estimate of the electron transmission, α, of ~1.0 and ~0.67, respectively.

Due to the presence of space charge in the analyzer, it is very difficult to calculate a definite result for the absolute ion and electron slit transmissions for the Omegatron probe. However, enough information is available to place an upper limit of approximately $\beta_{max} \approx 0.007$ on the ion transmission through the slit of the Omegatron probe.

IV.4 "Advanced" Omegatron Tests

The final test performed with the Omegatron probe was of a more advanced nature; it was an attempt to measure the temperature of a resonant ion species as described by the Omegatron theoretical model. For this experiment, the probe was set up in Omegatron mode, as described previously, but the frequency was held fixed, to observe a single ion species, in this case, the H^+ signal. The bias on the RF plates was then ramped to obtain an current vs. voltage (I-V) trace. In Table IV.5, below, is a list of the operating conditions for this experiment.

Table IV.5: "Advanced" Omegatron Mode Operating Parameters

Component	Bias (Volts)
Slit	Grounded
Grid 1	-15.7
Grid 2	-15.7
Grid 3	-15.7
RF Plates	Swept
End Collector	V_{RF} - 6.8 V
RF Amplitude	4.0 V p-p (2.6 V @ 2.0 MHz)
RF Frequency	Fixed @ 2.0 MHz
Magnetic Field	~ 1350 Gauss

Before the I-V trace could be compared to the theoretical model of the Omegatron, a proper scaling had to made between the experimental conditions and the theoretical results. First, the Omegatron model that included plasma potential fluctuations (whose level is represented by γ) was used, since the slit was held at a fixed potential. Second, all biases are measured relative to the plasma potential, whereas the data taken is with respect to the lab ground. Therefore, when matching the two sets of results, the plasma potential is another variable. Third, the collected current is a function of two potential differences, $\Delta\phi_{max}$ and $\Delta\phi_{coll}$ (refer to equations 2.12 and 2.13). However, by operating in a mode in which $\Delta\phi_{coll}$ is the most positive potential in the system, then $\Delta\phi_{max} = \Delta\phi_{coll}$. In performing this experiment, it was decided to operate in this mode, so that the quantity, $V_{RF} - V_{plasma}$, would correspond to $\Delta\phi_{max}$. Another variable is the transmission of the ions through the probe. As discussed above, this is a difficult issue to address, but, with an upper bound on the transmission, it serves at a good starting point for the model. The last variable is the ion temperature, which is one of the parameters of interest.

A first guess at the ion temperature can be obtained by looking at the collected current at large positive biases. The last part of equation 2.12 is,

$$\Gamma = \left(\frac{kT_i}{2\pi m}\right)^{\frac{1}{2}} \left[1 - e^{-\frac{mv_{\parallel}^2}{2kT_i}}\right] e^{-\left(\frac{qZ\Delta\phi}{kT_i}\right)}$$

whose derivative (with respect to $\Delta\phi$) yields,

$$\frac{\partial\Gamma}{\partial(\Delta\phi)} = -\left(\frac{qZ}{kT_i}\right)\Gamma \quad \text{which can be rewritten as,} \quad \frac{d\Gamma}{\Gamma} = -\left(\frac{qZ}{kT_i}\right)d(\Delta\phi).$$

Integrating the above equation yields a model for the current versus voltage (I-V) characteristic from which an ion temperature can be deduced,

$$\ln\left(\frac{\Gamma_{max}}{\Gamma}\right) = \left(\frac{qZ}{kT_i}\right)\Delta\phi + \text{Constant} \qquad (4.12)$$

This temperature is then used as a starting point to get an initial fit to the measured I-V trace.

An important consideration is the range of the RF bias over which the analysis will be valid. As seen in the space charge analysis in the preceding sections, space charge effects dominate much of the Omegatron probe's operating regime. In the RF Cavity, there are indications that below -5 V to 0 V, some limit causes a preferential drawing of ions to the RF/Collector plates is achieved in the analyzer cavity. Therefore, it implies that the model be restricted to RF plate biases above 0 V.

In Figure IV.20, a curve is shown of the data taken for this experimental run. The data curve shown has the typical shape for an I-V trace of an ideal Omegatron RF signal with some fluctuation level (refer to Figure II.10). From data taken with the Slit - Langmuir Probe, it is known that the floating potential is near -5 V, and that T_e is around 5 eV. This gives a plasma potential, V_P, of approximately 10 V. Note that the maximum signal occurs around 3 Volts, which is consistent with the fluctuation model results that the maximum signal could shift from the plasma potential ~ 5 to 10 Volts. Additionally, since the model assumes that there are no space charge limits in the analyzer, only the "positive going" biases will be considered since, for negative going biases, the current collected will be due to some space charge current limit.

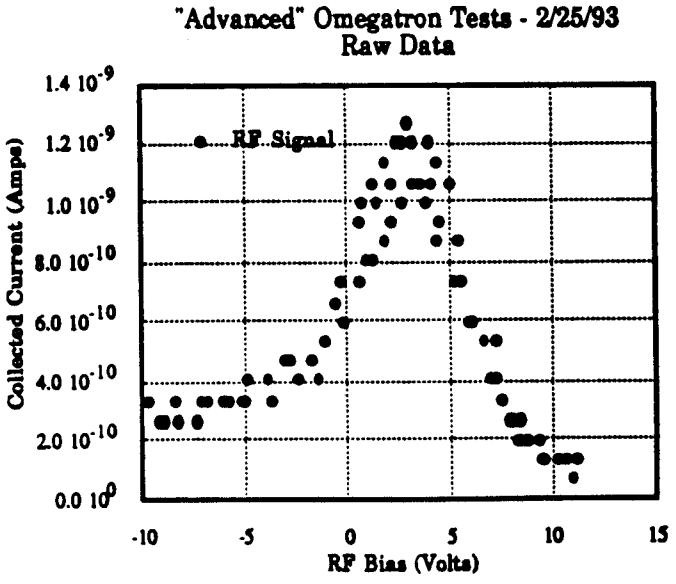

Figure IV.20 (a): Initial "Advanced" Omegatron Mode I-V Trace

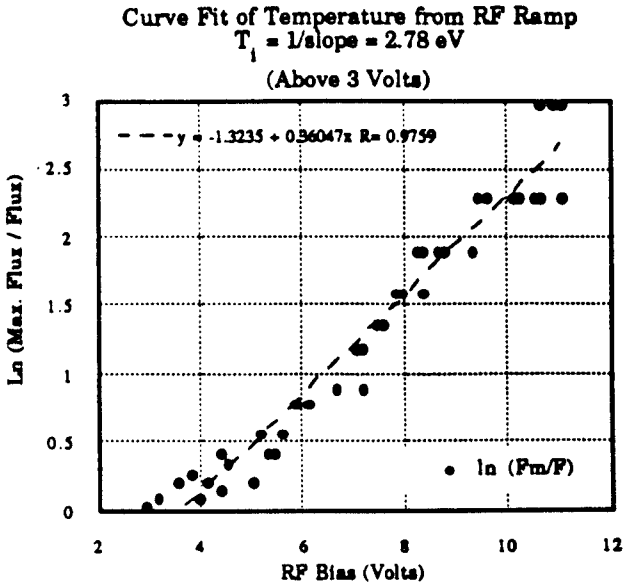

Figure IV.20 (b): Initial Temperature Measurement

With the proper conditions established, a comparison was made between the experimental results and the theoretical results. After many iterations using different combinations of T_i, V_p, ion transmission, β, and fluctuation level, γ, the two sets of results converged to a small range of values for the chosen variables; the resultant fit is shown in Figure IV.21.

The final results for the variables are,

$T_i \approx 2.0 \pm 0.2$ eV
$\beta \approx 0.006 \pm 0.001$
$\gamma \approx 0.50 \pm 0.05$
$V_p \sim 5$ V to 10 V, but maximum current is matched at $V_{max} \sim 2.8$ V

which are all very reasonable results for operations on the HCD. Furthermore, these results are consistent with the previous estimates of $\beta_{max} \approx 0.007$ [see section IV.3.3.2] and $T_i \approx 2.78$ eV [see Figure IV.20 (b)]. Although, with more effort, a better match may be achieved, the fit shown here provides reasonable values for each of the above parameters. This

gives some degree of confidence in both the theoretical model and our understanding of how the actual Omegatron functions.

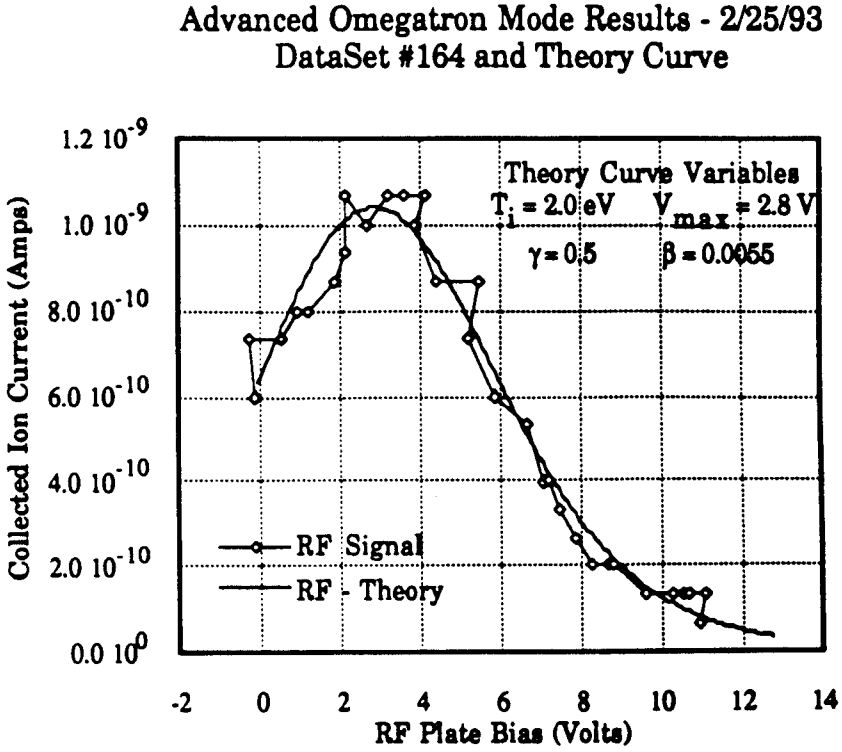

Figure IV.21: Comparison of Experimental and Theoretical "Advanced" Omegatron Results

With this result, it is clear that despite some difficulties, the Omegatron probe is fully functional and gives experimental results that follow theoretical expectations. Additionally, the experimental results show that the Omegatron is indeed capable of measuring (or at least, placing a limit on) the temperature of individual ion species in a plasma.

[1] Hsu, T.C., "The NED Hollow Cathode Discharge Machine", Course Notes for Plasma Laboratory Course 22.69, Nuclear Engineering Department, Massachusetts Institute of Technology, 1992.

[2] Hewlett-Packard, Instruction Manual for Data Collection Package, PC Instruments, 1985.

[3] Wang, E.Y., et. al., "An Omegatron Mass Spectrometer for Plasma Ion Species Analysis", Review of Scientific Instruments, Vol. 61, No. 8, (1990).

[4] Jones, B.K., Electronics for Experimentation and Research, Prentice/Hall International, 1986.

[5] Lorrain, P. and D. Corson, Electromagnetic Fields and Waves, W. H. Freeman and Company, New York, 1970.

[6] Hutchinson, I.H., Principles of Plasma Diagnostics, Cambridge University Press, 1987.

[7] Green, T.S., "Space Charge Effects in Plasma Particle Analyzers", Plasma Physics, Vol. 12, (1970).

[8] LaBombard, B., Private Communications on Omegatron Electronics and Omegatron Probe Theory, 1991-1993.

[9] Chen, F.F., Introduction to Plasma Physics, Plenum Press, New York, 1974.

[10] Wan, A.S. "Ion and Electron Parameters in the Alcator C Tokamak Scrape-Off Region", Ph.D. Thesis, Massachusetts Institute of Technology, 1986.

[11] Matthews, G.F., "The Measurement of Ion Temperature in Tokamak Edge Plasma", Ph.d. Thesis, University of Oxford, 1985.

[12] Hutchinson, I.H., Principles of Plasma Diagnostics, Cambridge University Press, 1987.

[13] Lipschultz, B., et. al., "Electric Probes in Plasmas", Journal of Vacuum Science and Technology A, Vol. 4, No. 3, 1986.

Chapter V: Results and Conclusions

A summary is made of the key results of the first Omegatron experiment. These results cover the Omegatron mode and the Omegatron probe characterization experiments and includes scalings to operation on Alcator C-Mod. Additionally, suggestions are made for improving the Omegatron Probe's performance on C-Mod.

V.1 Omegatron Mode Measurements

The Omegatron performance in the HCD experiment yielded extremely promising results. Although the probe was designed to operate in a vastly different plasma environment, the Omegatron probe was still able to successfully produce "Z/m" spectra of the HCD plasma and produce scalings that were consistent with theoretical predictions.

When the probe operated in Omegatron Mode, it was configured to take data that would produce a "Z/m" spectrum of the plasma. It was discovered that there is a fairly restricted regime of biases on the probe components in which to achieve this mode of operation; however, once this regime was established, it became almost trivial to obtain experimental data in Omegatron mode. The ability to reliably achieve this mode of operation aided in determining the validity of the various models used to describe the probe's performance.

Table V.1: Operating Regime for Omegatron Mode

1) $V_{slit} > V_{floating}$ (Slit bias greater than the floating potential.)
2) $V_{slit} > V_{Grids} = V_{G1} = V_{G2} = V_{G3}$ (Grid biases less that slit bias.)
3) $V_{Plasma} > V_{RF} > V_{slit}$ (RF plates bias greater than slit but less than or equal to plasma potential.)
4) $V_{RF} > V_{C/R}$ (End Collector bias less than that of RF plates)

V.1.1 Experimental Scalings

A typical Omegatron mode data set appears similar to the curve shown in Figure V.1. In this case, the applied RF signal is being ramped in frequency so as to obtain a spectrum of the species in the plasma; in this case,

the H^+ (at ~ 2 MHz) is observed.

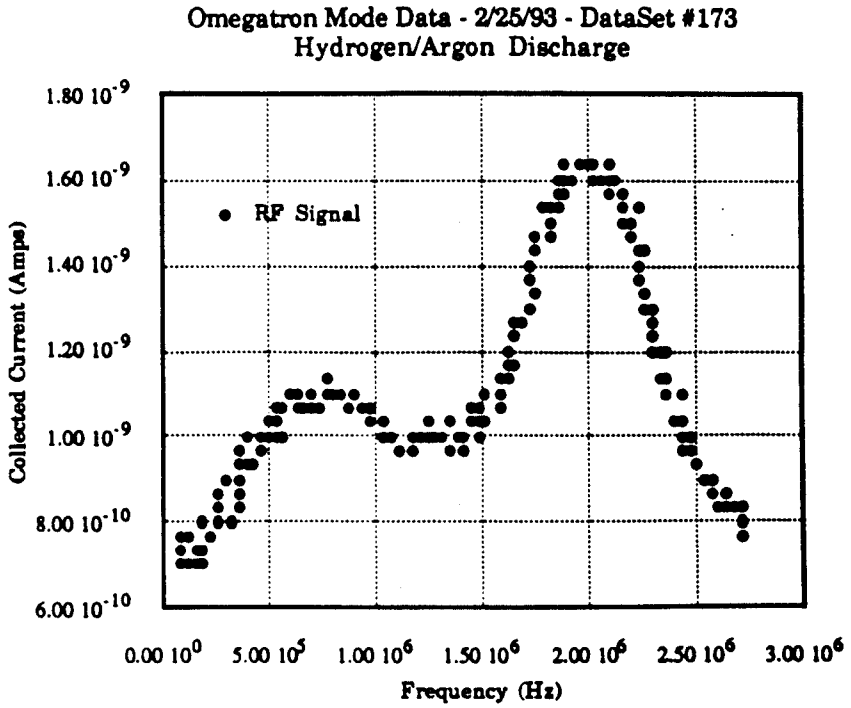

Figure V.1: Typical Omegatron Mode Dataset

Of particular importance is the scaling of the frequency width, Δf, of the collected signal with applied RF amplitude and magnetic field strength (see sections II.1.4, IV.2.3 and IV.2.4 for specific details on the definition of Δf and the measurements taken). The experimental results showed that, in both cases, the measured value of Δf did scale properly, but with an offset from the theoretical prediction (see Figures IV.7 and IV.9); i.e., the absolute level of the measured Δf was larger than the theoretical value by a factor of ~ 2.5 to 3.

V.1.2 Plasma Measurements

Another important result from the HCD experiment was the use of the Omegatron probe to measure plasma conditions in the HCD. As demonstrated by the model developed for the Omegatron's operation, it is possible to obtain data on both the density fluctuation level of the plasma and the temperature of individual ion species. In an "Advanced" Omegatron mode

experiment performed to explore this, it was indeed possible to obtain an upper bound on the fluctuation level, $\gamma \sim 0.50 \pm 0.05$, and the temperature of the H^+ component of the plasma, $T_i \sim 2.0 \pm 0.2$ eV (refer to Figures IV.19 and IV.20). As stated in section IV.4, with more data taken to characterize the value of γ, and the transmission of the probe, a more precise estimate could be made. However, these first results are very reasonable for the HCD.

This particular result is very promising as it satisfies one of the primary objectives for designing the Omegatron probe: the ability to directly measure the temperature of individual ion species in a plasma. In Alcator C-Mod, it should be possible, in principle, to choose several interesting ion species (such as the Molybdenum or Nitrogen ions) for a particular discharge and to measure their temperatures.

V.2 Probe Performance

The measurements made to evaluate the Omegatron probe's operational performance led to several interesting results. In general, the probe performed adequately in obtaining a resonance signal and analyzing the plasma parameters. In this respect, the Omegatron probe was successful. However, there were several other effects that acted to limit the probe's operation.

V.2.1 Space Charge Current Limits

The dominant effect that hindered the Omegatron's performance was space charge. The presence of space charge limitations acted to degrade the level of collected currents and to complicate the data analysis. Additionally, the space charge problems made it difficult to compute a well-defined ion and electron transmission factor for the probe.

Two space charge limits were found to be present in the Omegatron. The first space charge limit exists between the Entrance Slit and Grid 1 and becomes an ion or electron limit depending upon the slit bias. This limit gates the number of particles that enter the analyzer; in the HCD, the total ion current was limited to ~30 nA.

The second space charge limit appears as an ion space charge limit

that exists between Grid 3 and the RF/Collector plates. This space charge limit acts to reduce the number of particles that make it into the RF Cavity. However, those particles that do make it past the space charge cloud will drift with low parallel velocities and remain in the analyzer cavity for a long time; increasing the likelihood that those resonant particles will be collected.

Unfortunately, there is no quantitative statement that can be made about the space charge problems. Since space charge results from self-potentials that are generated by a group of charged particles, there is no easy manner in which to model it. Therefore, any scaling to the C-Mod environment can, at best, be an educated guess. Although others, such as Matthews[1] and Wan,[2] have tried to model these effects for their gridded analyzer probe systems, they have not been able to develop a completely satisfactory picture to model the space charge effects. Further investigation may yield additional insight to the space charge limits that are present while operating the Omegatron on the HCD, but, eventually, the only way to assess the problem in the C-Mod environment, apart from developing a full, three-dimensional, self-consistent model, will be to operate on Alcator C-Mod.

V.2.2 Transmission Results

The results of the transmission experiments were somewhat more quantitative than the space charge results, but there are still unresolved issues. The first result was that electrons and ions have different transmissions through the Entrance Slit. It was determined that the relative ion (β) to electron (α) transmission ratio, $\beta/\alpha \approx 0.0076$ as measured from the floating potential of the internal probe components (V_f^C). Along with this measurement, it was also shown that V_f^C is approximately the same for all the probe components, consequently the ions and electrons have roughly the same transmission through all other remaining components. However, there some difficulty in establishing the absolute values for β and α.

As presented in section IV.3.3, the difficulties in measuring the absolute transmission level for the ions and electrons arose primarily as a consequence of the space charge limited conditions in the analyzer. However, it

was possible to place a bound on the electron and ion transmissions, $\alpha \sim 0.8 \pm 0.1$, and $\beta \sim 0.006 \pm 0.001$, respectively. The result indicated that the transmission through the slit was not necessarily a constant, but rather a function of the bias potential on the slit.

In scaling to C-Mod, it is likely that the transmission through the Entrance Slit will become a much weaker function of both the species and the slit potential. This is due to the much higher magnetic field that will be present in Alcator C-Mod. The Larmor (or gyro-) radius of a charged particle in a magnetic field is,[3]

$$r_L = \frac{\sqrt{2mT}}{qB} . \qquad (5.1)$$

For the plasma conditions in the HCD, with $T_i \sim 2.0$ eV, $T_e \sim 5.0$ eV and magnetic field, B ~ 1400 Gauss, the Larmor radius for Hydrogen is ~ 0.146 cm and the electron gyroradius is ~ 0.0034 cm; these are both larger than the slit width of ~ 0.0025 cm. Therefore, it is expected that the slit transmission on the HCD be fairly poor. For conditions in C-Mod, with $T_i \sim 10$ to 50 eV, $T_e \sim 10$ to 50 eV and magnetic field, B ~ 5 to 7 Tesla, a typical result for r_L ($T_i = 20$ eV, Hydrogen, $T_e \sim 30$ eV, B ~ 6 Tesla) will be, $r_{L\text{-ion}} \sim 0.0107$ cm and $r_{L\text{-electron}} \sim 0.0002$ cm. While the ion gyroradius may still be larger than the slit, due to the smaller radius, a much larger fraction of ions should make it through the slit, and unquestionably, all of the electrons should make it past the Entrance Slit. It is known from similar slit and grid arrangements in the Janus probe that the ion transmission through the slit should improve to ~ 5 percent [see Reference 2]. This effect, combined with densities ~ 10^{18} to 10^{19} m^{-3} on C-Mod (as compared to 10^{15} to 10^{16} m^{-3} in the HCD) could perhaps boost the collected signals by as much as 10^3 to 10^4, giving signal levels ~ 1 μA on the RF/Collector plates.

The unknown is the effect of space charge on the C-Mod results. The increased density and transmission characteristics could increase the space charge problems in the analyzer, while the higher ion and electron temperatures and stronger fields may nullify those effects. Ultimately, only operation on Alcator C-Mod that will determine the extent to which space charge will play a role in probe operations.

V.3 Scaling Results to Alcator C-Mod

Throughout this thesis, many references are made to operating the Omegatron probe in the Alcator C-Mod edge plasma environment. Arguments have been presented to justify the experiments performed on the HCD and the results and conclusions of those experiments are assessed based upon the necessity of operating the probe on C-Mod. As discussed at the outset of this thesis, the Omegatron probe used for this experiment is the actual hardware that is destined for use on Alcator C-Mod; this was to remove any geometrical factors that may have affected a scaling of results from the HCD to C-Mod. The differences in the two plasma experiments are primarily due to differences in magnetic field strengths and plasma ion conditions.

In this section, the final results of the scalings from the Hollow Cathode Discharge experiments to Alcator C-Mod are presented. This is followed by a brief discussion of modifications that could be made to the Omegatron to improve the operating conditions and the signal to noise ratio in the analyzer.

V.3.1 Operating Parameters

In Table V.2, a list is presented of the relevant operating parameters that were used for the HCD experiment and the suggested values for operations on Alcator C-Mod. This table is a compilation of the results that were obtained while running the Omegatron probe on the HCD. As can be seen in Table V.2, the various operating conditions as described for all modes of Omegatron probe operation have been listed. Additionally, a comparison is made between the Alcator C-Mod plasma conditions and the HCD plasma conditions. Of particular interest is the fact that the Hydrogen and Helium signals on the HCD are comparable to the predicted Molybdenum signal on C-Mod. The Molybdenum ion signal is expected to be the most difficult to detect on C-Mod, especially since Molybdenum can occupy a large number of charge states. The tests on the HCD indicate that the Omegatron is quite capable of detecting signals ~1 nA, so there is a good chance that Molybdenum studies can be successfully performed with the Omegatron.

Table V.2: Scaling Omegatron Operation to Alcator C-Mod

Condition	HCD	Alcator C-Mod
Operating Ranges		
Magnetic Field	1300-1400 Gauss	5 to 7 Tesla
"Z/m" Range	H^+ to He^+	H^+ to Mo^+
Frequency Range	2.5 to 0.5 MHz	100 to 0.90 MHz
RF Amplitude	1.5 V/cm	90 V/cm
Δf Theory	165 kHz	120 kHz
Δf Experiment (x3)	~ 500 kHz	~ 350 kHz
Best Resolution (for above)	20 to 4	550 to 8
Signal Level	~ 1 to 3 nA	~ 100 nA to 1 μA
Ion Transmission, β	~ 0.006 to ~0.008	~ 0.05 to 0.1
Electron Transmission, α	~0.8 to 1.0	~ 1.0
Plasma Conditions		
Ion Temperature	~ 2 to 3 eV	~ 10 to 50 eV
Electron Temperature	~ 3 to 5 eV	~ 10 to 50 eV
Density	~ 10^{15} to 10^{16} m^{-3}	~ 10^{17} to 10^{19} m^{-3}
Base Pressure	8 x 10^{-6} Torr	~ 10^{-9} Torr
Fill Pressure	~ 10^{-3} Torr	~ 10^{-5} to 10^{-4} Torr
Omegatron Settings (for both cases)		
Slit	Fixed Bias: $V_{slit} < V_{plasma}$	
Grids	Fixed, equal Biases: $V_{G1}=V_{G2}=V_{G3} < V_{slit}$	
RF/Collector Plates	(Spectrum) Fixed Bias: $V_{slit} < V_{RF} < V_{plasma}$ (Temperature) Swept Bias: $V_{Grids} \leq V_{RF}$	
End Collector	Linked to RF Plates: $V_{C/R} < V_{RF}$	
Limiting Conditions		
Probe Temperature	20 °C (maximum) steady state	Max Rise ~ 20 to 50 °C for a 3 to 5 second discharge
Probe Cooling	Water	Dry Nitrogen Gas
Space Charge	Ion/Electron	Ion/Electron

V.3.2 Hardware Modifications

In the course of performing the Omegatron tests, several ideas for modifying the probe were discussed as a means to improve the overall performance of the device and to facilitate data analysis. These ideas are presented along with the expected benefits from each of these modifications.

V.3.2.1 Grids

The primary motivation in redesigning the grids is to reduce the buildup of space charge between the grids and the slit. The space charge limited current condition gets worse the further apart the two biased electrodes are. By reducing the space charge, it should be possible to obtain a large increase in the signal to noise ratio. Two possibilities have been discussed for modifying the grid structure. The first idea is to use only a single grid that is placed close to the slit. In this way, there is only one gate that allows particles to enter the RF Cavity. Despite the simplicity of this system, its main drawback is that there is no mechanism to handle secondary electron production; which can seriously perturb the detected signal should the probe be operated in gridded-energy analyzer mode.

The second idea is to maintain the three-grid arrangement, but to tightly pack the grids together, reducing the overall size of the grid region. In this way, a mechanism to reduce the secondary electrons is available, but with highly biased electrical components in close contact, there is the possibility of arcing across the components. Additionally, reducing the grid spacing may enhance the stray capacitive coupling among the grids and between the grids and the entrance slit.

Despite the possible problems, both approaches should reduce the space charge effects in the Omegatron probe. Because of this, serious thought will be given to making some sort of modification to the grid arrangement prior to operating the Omegatron in Alcator C-Mod.

V.3.2.2 RF/Collector Plates

If there is a modification to the grids, it becomes necessary to modify the RF/Collector Plates. Since both ideas for the modification of the grids call for a more tightly packed arrangement, the RF plates would then have

to be extended further into the Grid Cavity. The objective would be to force the ions to experience the oscillating RF electric field as soon as possible after passing through the grids.

V.3.2.3 Probe Maintenance

Although not strictly a modification to the Omegatron probe, there are routine operations that can be used to enhance the probe's performance. While operating on the HCD, a buildup of hydrocarbons, primarily diffusion pump oil, was deposited all over the probe, particularly near the Entrance Slit. This layer of material reduced the number of ions that made it into the analyzer cavity and, over a period of several days, a general reduction of collected signal was noted. It was discovered that biasing the probe very negatively, ~ -75 V, allowed the plasma ions to sputter clean the slit and Langmuir probe surfaces and, hence increase the signal collected by the probe. Although the environment of Alcator C-Mod is expected to be much cleaner than the HCD, a periodic cleaning of the slit would ensure that the maximum possible signal would be collected by the Omegatron at all times.

V.4 Conclusions

The Omegatron probe experiments were successful in characterizing the probe's performance. Although designed for a completely different environment, the Omegatron yielded excellent results in obtaining "Z/m" spectra and measuring the plasma conditions (n_0, T_i, T_e) in the Hollow Cathode Discharge plasma. Also, the experiments showed that the probe operation follows theoretical scalings. A value was obtained for the relative ion to electron transmission and limits were placed on the values of the individual ion and electron transmissions through the slit.

The most important result is the characterization space charge effects in the Omegatron probe. A detailed examination of the space charge data was performed and a qualitative model was developed to explain the causes and the dependencies of the space charge conditions. Ideas for modifying the probe hardware to reduce these effects are already under consideration.

The degree to which the performance of the Omegatron probe has been

examined for the HCD experiment will undoubtedly simplify its operation, and the analysis and interpretation of its results, on Alcator C-Mod. I believe that the Omegatron, with a few minor modifications, will be able to operate completely successfully on Alcator C-Mod.

[1] Matthews, G.F., "The Measurement of Ion Temperature in Tokamak Edge Plasma", Ph.d. Thesis, University of Oxford, 1985.

[2] Wan, A.S. "Ion and Electron Parameters in the Alcator C Tokamak Scrape-Off Region", Ph.D. Thesis, Massachusetts Institute of Technology, 1986.

[3] Sears, F.W., M.W. Zemansky, H.D. Young, University Physics, 6th Edition, Addison-Wesley Publishing, Reading, MA, 1984.

APPENDIX A

Omegatron Probe Electronics

Omegatron Circuit Diagram

On the following page is a schematic of the primary Omegatron data collection circuit. It functions primarily as a fast time-response, low-current ($\leq$ 1 nA) ammeter. The circuit was designed to be fairly insensitive to high frequency plasma potential fluctuations (via multiple stage filtering) and has a nominal 5 kHz bandwidth. Additionally, this circuit is designed to reject common mode voltages in excess of 100 Volts. In laboratory tests, the circuit was capable of resolving currents as low as ~ 800 pA and has a maximum detectable current of ~ 10 μA. (At this current, the output of the Omegatron boards is 5 V, which is the limit set by the CAMAC data collection system.) In the HCD experiment, a 10 millisecond "pre-filter" was added to the data collection electronics; this allowed the detection of signals as low as ~ 500 pA, but also reduced the bandwidth. In Figure A.1, is a reproduction (from Chapter III) of the Omegatron data collection circuit block diagram.

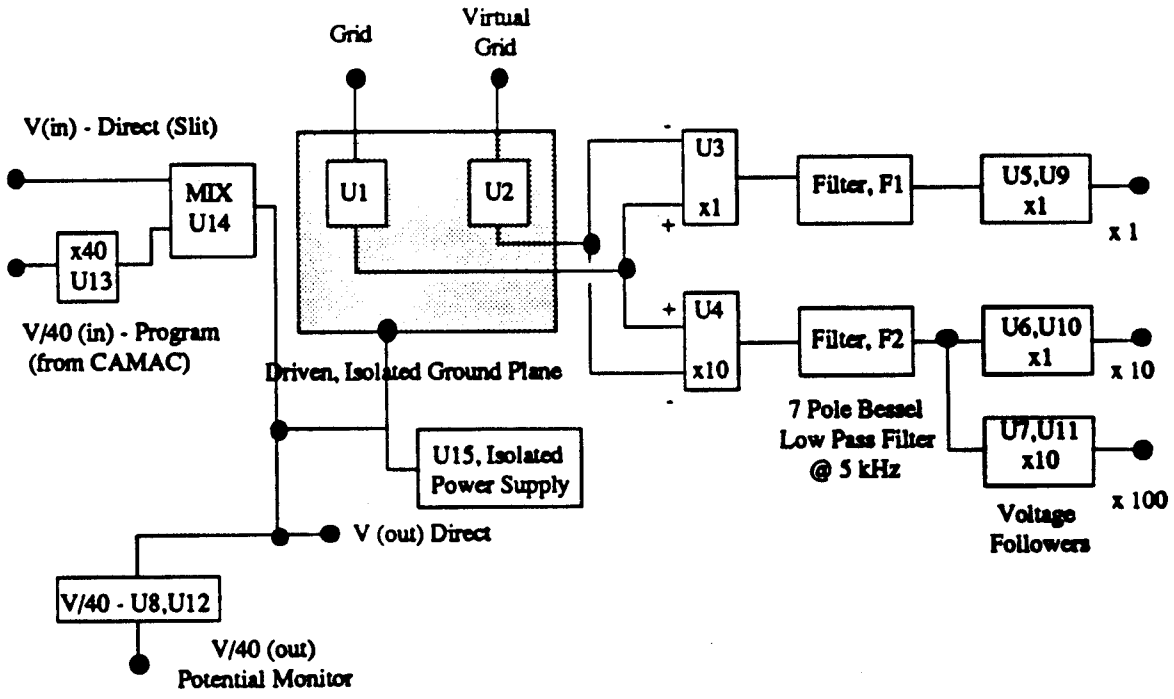

Figure A.1: Omegatron Circuit Block Diagram

For detailed Omegatron Probe Electronics Schematic, please contact,

Dr. Brian LaBombard
MIT Plasma Fusion Center
NW17-109
175 Albany Street
Cambridge, MA 02139

Langmuir Probe Circuit Diagram

On the following page is a schematic of the Langmuir Probe circuit. This circuit was designed by Dr. Brian LaBombard for use on the Alcator C-Mod Flush Mount Probe array; a series of Langmuir probes that look at the heat and particle flux to the first wall. This circuit is designed to have a large bandwidth ~ 1 MHz. Additionally, through a series of relays and TTL control lines, the circuit is flexible enough to measure ion saturation currents of a few microamperes, to electron saturation currents of up to 10 A. The block diagram, below (from Chapter III), shows the basic layout of the Langmuir Probe circuit.

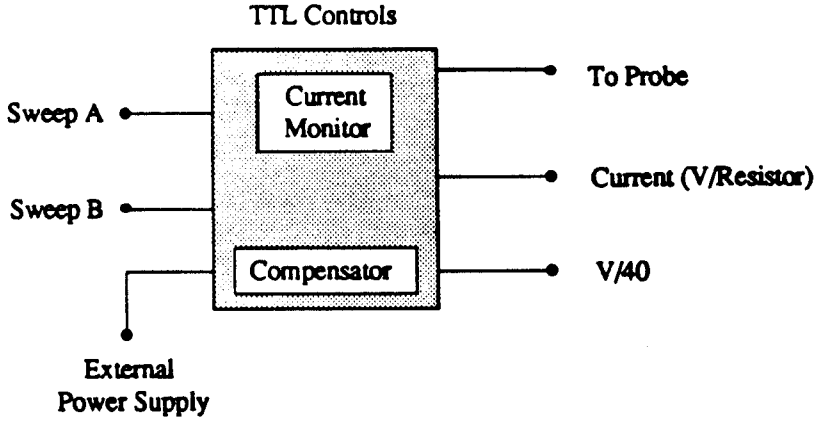

Figure A.2: Langmuir Probe Schematic

For detailed Langmuir Probe Electronics Schematic, please contact,

Dr. Brian LaBombard
MIT Plasma Fusion Center
NW17-109
175 Albany Street
Cambridge, MA 02139

APPENDIX B

Works Cited

Works Cited

Averina, et. al., "Omegatron Mass-Spectrometer for Analysis of the Composition of Residual Gases in High-Vacuum Systems", Translated from Pribory i Tekhnika Ékspermenta, No. 2, March-April, (1964).

Batrakov, B.P. and P.M. Kobzev, "Omegatron for High-Vacuum", Translated from Pribory i Tekhnika Ékspermenta, No. 4, July-August, (1963).

Berry, C., "Ion Trajectories in the Omegatron", Journal of Applied Physics, Vol. 25, No. 1 (1954).

Brillouin, L., "A Theorem of Larmor and Its Importance for Electrons in Magnetic Fields", Physical Review, Vol. 67, No. 7/8 (1945).

Brubaker, W. and G.D. Perkins, "Influence of Magnetic and Electric Field Distribution on the Operation of the Omegatron", Review of Scientific Instruments, Vol. 27, No. 9 (1956).

Chen, F.F., Introduction to Plasma Physics, Plenum Press, New York, 1974.

Cordey, J.G., R.J. Goldston, and R.R. Parker, "Progress Towards a Tokamak Fusion Reactor", Physics Today, Vol. 45, No. 1, (1992).

Freidberg, J.P., Ideal Magnetohydrodynamics, Plenum Press, New York, 1987.

Fussmann, G., et. al., "Sputtering Flux Measurements in the ASDEX Divertor", Max Planck Institute for Plasma Physics Report, IPP III/153, October, 1989.

Green, T.S., "Space Charge Effects in Plasma Particle Analyzers", Plasma Physics, Vol. 12, (1970).

Hakkarainen, P., "Standard MHD Equilibria Code for Alcator C-Mod", M.I.T. Plasma Fusion Center, 1990.

Hewlett-Packard, Instruction Manual for Data Collection Package, PC Instruments, 1985.

Hsu, T.C., "The NED Hollow Cathode Discharge Machine", Course Notes for Plasma Laboratory Course 22.69, Nuclear Engineering Department, Massachusetts Institute of Technology, 1992.

Hutchinson, I.H., Principles of Plasma Diagnostics, Cambridge University Press, 1987.

Hutchinson, I.H. "The Physics and Engineering of Alcator C-Mod", M.I.T. Plasma Fusion Center Research Report, PFC/RR-88-11, August, 1988.

Jones, B.K., Electronics for Experimentation and Research, Prentice/Hall International, 1986.

LaBombard, B., Private Communications on Omegatron Electronics and Omegatron Probe Theory, 1991-1993.

Lipschultz, B., et. al., "Electric Probes in Plasmas", Journal of Vacuum Science and Technology A, Vol. 4, No. 3, 1986.

Lorrain, P. and D. Corson, Electromagnetic Fields and Waves, W. H. Freeman and Compay, New York, 1970.

Marmar, E.S., et. al., "Impurity Injection Experiments on the Alcator C Tokamak", Nuclear Fusion, Vol. 22, No. 12, (1982).

Matthews, G.F., "The Measurement of Ion Temperature in Tokamak Edge Plasma", Ph.d. Thesis, University of Oxford, 1985.

Matthews, G.F., "Plasma Ion Mass Spectrometry in the Boundary of the DITE Tokamak", Plasma Physics and Controlled Fusion, Vol. 31, No. 5, (1989).

McCracken, G.M., and P.E. Stott, "Review Paper: Plasma-Surface Interactions in Tokamaks", Nuclear Fusion, Vol. 19, No. 7, (1979).

Pitts, R.A., "Ion Energy, Sheath Potential, and Secondary Electron Emission in the Tokamak Edge", PH.D. Thesis, University of London, 1990.

Sanford Process Corporation, Company Literature, "Technical Bulletin No. 102", Natick, MA.

Sears, F.W., M.W. Zemansky, H.D. Young, University Physics, 6th Edition, Addison-Wesley Publishing, Reading, MA, 1984.

Sommer, H., H.A. Thomas, and J.A. Hipple, "A Precise Method of Determining the Faraday by Magnetic Resonance", Physical Review, Vol. 76 (1949).

Sommer, H., H.A. Thomas, and J.A. Hipple, "The Measurement of e/M by Cyclotron Resonance", Physical Review, Vol. 82, No. 5, (1951).

Stamp, M.F., et. al., "Particle Influx Measurements in JET Helium Plasmas using a Multichannel Visible Spectrometer", Journal of Nuclear Materials, 162-164, (1989).

Stangeby, P.C. and G.M. McCracken, "Review Paper: Plasma Boundary Phenomena in Tokamaks", Nuclear Fusion, Vol. 30, No. 7, (1990).

Stott, P.E., "Measurements at the Plasma Edge", Proceedings of Diagnostics for Contemporary Fusion Experiments, Bologna, 1991.

Wagener, J.S., and P.T. Marth, "Analysis of Gases at Very Low Pressures by Using the Omegatron Spectrometer", Journal of Applied Physics, Vol. 28, No. 9, (1957).

Wan, A.S. "Ion and Electron Parameters in the Alcator C Tokamak Scrape-Off Region", Ph.D. Thesis, Massachusetts Institute of Technology, 1986.

Wan, A.S., et.al. "Janus, a Bidirectional, Multifunctional Plasma Diagnostic", Review of Scientific Instruments, Vol. 57, No. 8, (1986).

Wan, A.S., Private Communications on Gridded Energy Analyzer Designs, 1992.

Wang, E.Y., et. al., "An Omegatron Mass Spectrometer for Plasma Ion Species Analysis", Review of Scientific Instruments, Vol. 61, No. 8, (1990).

Watkins, J.G., et. al., "Scrape-Off Layer Measurements in DIII-D", Journal of Nuclear Materials, 196-198, (1992).

Weast, R., ed., CRC Handbook of Chemistry and Physics, 70th Edition, 1989-1990, CRC Press, Boca Raton, FL, 1990.

Weaver, J. , " The Development of a Reciprocating Langmuir Probe System for Alcator C-Mod", B.S. Thesis, Massachusetts Institute of Technology, 1992.

Wesson, J., Tokamaks, Oxford University Press, New York, 1987.

Wooten, A.J., et.al.,"Fluctuations and Anomalous Transport in Tokamaks", Fusion Research Center Report, #340, The University of Texas at Austin, 1989.